COLLISION-INDUCED ABSORPTION SPECTRA OF BINARY MIXTURES OF H_2 WITH D_2 AND Ar AND OF PURE HD

CHANG-TSANG WILLIAM HSIEH

COLLISION-INDUCED ABSORPTION SPECTRA OF BINARY MIXTURES OF H_2 WITH D_2 AND Ar AND OF PURE HD

by

©Chang-Tsang William Hsieh, M. Sc.

A thesis submitted to the School of Graduate

Studies in partial fulfilment of the

requirements for the degree of

Doctor of Philosophy

Department of Physics

Memorial University of Newfoundland

December 1992

St. John's Newfoundland Canada

ISBN 0-315-82651-7

Abstract

In the present research project a systematic study of the collision-induced infrared absorption (CIA) spectra of the binary mixtures of $H_2 - D_2$ in the region of the double fundamental vibrations of H_2 and D_2, and $H_2 - Ar$ in the fundamental band of H_2, and of pure HD in its fundamental and first overtone regions was undertaken. The experiments were carried out with a 2.0 m high-pressure low-temperature transmission-type absorption cell at 77, 201 and 296 K at total gas densities up to 550 amagat. Infrared prism and grating spectrometers equipped with a microprocessor-controlled stepping motor were used to record the spectra. All the experimental results obtained represent first-time observations in collision-induced absorption.

Collision-induced infrared absorption spectra of the double transitions of $H_2(v = 1 \leftarrow 0)$ and $D_2(v = 1 \leftarrow 0)$ have been observed at 77 and 201 K in the spectral region 7000-8000 cm^{-1} for total gas densities up to 550 amagat with a partial gas density ratio of 1:1 of H_2 and D_2. The observed spectra are interpreted in terms of the transitions, $Q_1(J)$ of H_2 + $Q_1(J)$ of D_2, $Q_1(J)$ of H_2 + $S_1(J)$ of D_2, $S_1(J)$ of H_2 + $Q_1(J)$ of D_2, and $S_1(J)$ of H_2 + $S_1(J)$ of D_2 for J=0 and 1 for H_2 and J=0, 1, and 2 for D_2. Analysis of the experimental absorption profiles was carried out using appropriate lineshape functions. The absorption coefficients, lineshape parameters, etc., are obtained from the analysis.

Collision-induced enhancement absorption spectra of the fundamental band of H_2 in $H_2 - Ar$ mixtures were recorded at room temperature for a base density of 72 amagat of H_2 for several partial densities of Ar up to 440 amagat. Hexadecapole-induced U transitions, $U_1(1)$, $U_1(2)$, $Q_1(0) + U_0(1)$, and $Q_1(1) + U_0(1)$ have been

identified in the spectral region 5400–6200 cm^{-1}. A "cage" model has been proposed to account for the double transitions of $H_2 - H_2$ in the $H_2 - Ar$ enhancement spectra. From the analysis of the absorption profiles, the lineshape parameters and the absorption coefficients have been determined.

The collision-induced absorption spectrum of the first overtone band of HD in the pure gas was observed at 77 K for gas densities up to 320 amagat. In addition to the allowed transitions $P_2(1)$, $R_2(0)$, and $R_2(1)$, the CIA transitions $Q_2(J)+Q_0(J)$, $Q_1(J)+Q_1(J)$, $Q_2(J)+S_0(J)$, $S_2(J)+Q_0(J)$, $Q_1(J)+S_1(J)$, $S_2(J)+S_0(J)$, and $S_1(J)+S_1(J)$ have been observed. An analysis of the observed absorption profiles has been completed. It is found that the isotropic overlap induction mechanism does not contribute to the intensity of the band and that negative contribution to the intensity of the band comes from the mixed term $(2\sqrt{3}\lambda_{32}exp[-(R-\sigma)/\rho_{12}] < < vJ \mid \alpha \mid v'J' >< vJ \mid Q \mid v'J' > (R/a_0)^{-4}$. The fundamental band of HD has been investigated at 77 K for gas densities in the range 40–310 amagat. For the first time the collision-induced transitions of the type $T_1(1)+Q_0(J)$, $Q_1(J)+T_0(1)$, $U_1(0)+Q_0(J)$, $Q_1(J)+U_0(0)$, $V_1(0)+Q_0(J)$, and $Q_1(J)+V_0(0)$ for HD have been identified. Here T, U, and V transitions correspond to ΔJ=3, 4, and 5, respectively.

Acknowledgements

First of all, I express my deep gratitude to my supervisor, Professor S.P. Reddy, for his valuable guidance and encouragement throughout the progress of the entire research project.

My special thanks are due to Dr. P.G. Gillard for his assistance in the design of the microprocessor-controlled stepping motor control circuit and providing the microprocessor-controlled data acquisition system. I would like to thank Drs. J.C. Lewis, D.H. Rendell, and N.H. Rich, members of my supervisory committee, for their interest in this work.

I am grateful to Messrs. Terry White and Michael Ryan of the Physics Machine-Shop for their technical assistance and to Mr. Roger Guest for his assistance in drafting several figures for the thesis.

Finally, I wish to thank the Physics Department for the support I received for my graduate studies at Memorial University of Newfoundland.

Contents

List of Figures

List of Tables

Chapter 1

Introduction

1.1 Collision-Induced Absorption in H_2 and D_2

Isolated homonuclear diatomic molecules such as hydrogen, deuterium, nitrogen, and oxygen in their ground electronic states do not have permanent static or oscillatory electric dipole moments because of a center of symmetry of their charge configuration. Consequently they are inactive in vibrational and rotational electric dipole absorption. However, these molecules in their pure state or in their mixtures with other gases give rise to collision-induced absorption (CIA) as a result of transient electric dipole moments induced in them by intermolecular interactions which are operative during binary or higher-order collisions. Generally these induced dipoles in a binary collision arise because of several factors which include the overlap of the electron clouds of the colliding molecules and the quadrupolar, hexadecapolar, and tetrahexadecapolar inductions resulting from the polarization of one molecule by the corresponding multipole field of the other. The dipole moments thus induced depend on the intermolecular separation as well as on the relative orientation and internuclear separation of the individual molecules taking part in a collision. The in-

duced dipole moments interact with the electromagnetic radiation and the colliding molecules absorb the radiation in the spectral regions corresponding to their relative translation, rotation-translation, and vibration-rotation-translation. Normally forbidden transitions occur in the CIA spectra.

The phenomenon of CIA was discovered in compressed oxygen and nitrogen by Crawford et al. (1949) in the regions of their fundamental bands. In the same year Welsh et al. (1949) identified the CIA spectra of the fundamental vibrational band of gaseous hydrogen. In the past forty-three years the CIA spectra of the fundamental and overtone bands of H_2 in the pure gas and its binary mixtures with inert gases and some simple gases such as N_2 and O_2 have been studied under a variety of experimental conditions in considerable detail. To a somewhat lesser extent those of the fundamental and first overtone bands of D_2 have also been studied after the first study of the CIA spectra of the fundamental band of D_2 by Reddy and Cho (1965).

1.2 Allowed Transitions in the Infrared Spectra of HD

Although the HD molecule, just as the H_2 and D_2 molecules, has no electric dipole moment in the equilibrium position in its ground electronic state, a weak oscillating electric dipole moment occurs in a molecular vibration because the displacement of the proton in H is larger than that of the deuteron in D and the negative charge center of the electrons lags behind the positive charge center of the nuclei. An allowed vibration-rotation spectrum of HD due to this oscillating dipole moment was predicted by Wick (1935), and weak absorption of the 3-0 and 4-0 vibration-

rotation bands was first observed by Herzberg (1950). An experimental investigation of the 1-0, 2-0, 3-0, and 4-0 bands was made in detail by Durie and Herzberg (1960). McKellar (1973, 1974) made a quantitative measurement of the intensity of 13 electric dipole P ($\Delta J = -1$) and R ($\Delta J = +1$) transitions of these four vibration-rotation bands including one electric quadrupole transition ($\Delta J = 0, \pm 2$). Bejar and Gush (1974) also measured the intensities of 5 electric dipole transitions of the 1-0 band of HD.

The allowed pure rotational spectrum of HD was first measured by Trefler and Gush (1968) and its dipole moment was determined from a measurement of the integrated intensities of four R lines.

1.3 Collision-Induced Spectra of HD

McKellar (1973) observed the collision-induced fundamental band of HD in the gaseous phase at 77 K. Crane and Gush (1966) studied the fundamental band of HD in the solid phase. Holleman and Ewing (1966) studied the same band in HD dissolved in liquid Ar and these authors (1967) also studied the pure rotational band of HD dissolved in liquid Ar. The CIA spectra of the fundamental band of HD in the pure gas at densities up to 50 amagat at 77, 196, and 298 K have been studied in our laboratory by Reddy and Prasad (1977). From the profile analysis these authors separated the overlap contribution to the intensity of the band and determined the overlap parameters of the overlap induced dipole moment $\mu_{overlap}$, of HD. Prior to the present work, the observed collision-induced transitions in HD correspond to the selection rule ΔJ=-2 (O branch), 0 (Q branch), and +2 (S branch).

1.4 Background Information on the Collision-Induced Spectra

There has been great interest in the study of the spectra of hydrogen and its isotopomers because of several reasons which include the following: molecules such as H_2 and HD are the simplest of all diatomic molecules; they can be treated more rigorously by theoretical calculations; the rotational components of the bands are somewhat separate in spite of the broad nature of their collision-induced spectra because of their small moments of inertia; and H_2 in particular is present in large quantities in the atmospheres of the major planets in the solar system and in certain cool stellar atmospheres. The collision-induced absorption spectra of H_2 are important in the understanding of the processes involved and in verifying the results of theoretical calculations as well as in promoting new theoretical studies. Welsh (1972) has given a comprehensive review of the experimental work done prior to 1971 and Reddy (1985) has reviewed exhaustively the collision-induced vibrational absorption of H_2, D_2, and HD in the gaseous phase. The reader is referred to these two review articles and the theses of van Nostrand (1983), Gillard (1983), and Xiang (1992), all from our laboratory for further information. Rich and McKellar (1976) and Hunt and Poll (1986) have compiled comprehensive bibliographies on the subject of CIA. Van Kranendonk (1974), Poll (1980), and Birnbaum et al. (1982) have reviewed the theoretical aspects of CIA.

The so-called "exponential-4" model for the induced-dipole moment in a binary collision was first given by Van Kranendonk (1957, 1958). Poll and Van Kranendonk (1961) and Poll and Hunt (1976) gave new expressions for the induced-

dipole moment μ_{ind}, taking into account its angular dependence. On the basis of the exponential-4 model, μ_{ind} consists of two additive parts $\mu_{ov}(R)$ arising from the overlap of the electron clouds of the colliding molecules and $\mu_{quad}(R)$ resulting from the polarization of one molecule by the quadrupole field of the other, R being the intermolecular separation. The isotropic (i.e., angle-independent) short-range overlap-induced dipole moment $\mu_{ov}(R)$ generally gives rise to the broad $Q_{ov}(J)$ ($\Delta J = 0$) transitions. The quadrupole-induced dipole moment μ_{quad} is dependent on the matrix elements of the quadrupole moment and the polarizability of the colliding molecules. The isotropic component of the polarizability of a colliding molecule contributes to the absorption intensity of the transitions O ($\Delta J = -2$), Q ($\Delta J = 0$), and S ($\Delta J = +2$). It gives rise to several double transitions of the type $O_{\Delta v}(J_1) + Q_0(J_2)$, $Q_{\Delta v}(J_1) + Q_0(J_2)$, $S_{\Delta v}(J_1) + Q_0(J_2)$, $Q_{\Delta v}(J_1) + Q_{\Delta v}(J_2)$, $Q_{\Delta v}(J_1) + S_{\Delta v}(J_2)$, and $S_{\Delta v}(J_1) + Q_{\Delta v}(J_2)$. The subscripts Δv ($= v' - v''$) represent the change in the vibrational quantum number and take values 0,1,2,$\cdots$,etc., and subscripts 1 and 2 refer to molecules 1 and 2 in a binary collision. The anisotropic component of the polarizability, on the other hand, contributes a small amount to the transitions given above and to the double transitions $S_{\Delta v}(J_1) + S_{\Delta v}(J_2)$. In a "single" transition, only one molecule of the colliding pair makes a vibration or a vibration-rotation transition while the other molecule makes an orientational transition denoted by $Q_0(J)$ with no change in internal energy. In a "double" transition, both molecules of the colliding pair simultaneously absorb a single photon and change their internal energies.

In addition to the components $\mu_{ov}(R)$ and $\mu_{quad}(R)$, the induced-dipole moment consists of two more components $\mu_{hexa}(R)$ and $\mu_{tetra-hexa}(R)$. Of these two, $\mu_{hexa}(R)$

results from the polarization of one molecule by the hexadecapole field of its collision partner and gives rise to weaker transitions given by $\Delta J = 0, \pm 2, \pm 4$. The transitions corresponding to $\Delta J = +4$ are known as U transitions. In the CIA spectra of the fundamental band of H_2, U transitions, first observed by Gibbs et al. (1974), have been studied and analyzed by Reddy et al. (1980). The $\mu_{tetra-hexa}(R)$ component comes from the polarization of a molecule by the tetra-hexadecapole field of its collision partner. This gives rise to very weak transitions corresponding to $\Delta J = 0, \pm 2, \pm 4$, and ± 6. Okumura et al. (1989) reported the pure rotational transition $W_0(J)$ corresponding to $\Delta J = +6$ in solid H_2.

Although the isotropic overlap induction mechanism contributes considerably to the intensity of the fundamental bands of H_2 (see, for example, Reddy et al., 1977), D_2 (see, for example, Penney et al., 1982), and HD (Reddy and Prasad, 1977), it does not appear to contribute to the first overtone bands of H_2 (see, for example, McKellar and Welsh, 1971; van Nostrand, 1983; Varghese et al., 1987; and McKellar, 1988) and D_2 (Gillard, 1983).

De Remigis et al. (1971) observed a decrease in the half-width of the quadrupole-induced transitions in the fundamental band of H_2 in $H_2 - Ar$ mixtures for gas densities above 300 amagat. Zaidi and Van Kranendonk (1971) explained the pressure-narrowing in terms of a diffusional effect in which the linewidth is proportional to the diffusion constant and thus its decrease is roughly proportional to the density of the gas mixture. Subsequently, Mactaggart et al. (1973) studied this effect in the fundamental band of H_2 in $H_2 - Ar$, $H_2 - Kr$, and $H_2 - Xe$. It is shown by Lewis and Tjon (1978) that the simple explanation given by Zaidi and Van Kranendonk for the narrowing of the lines is sometimes inapplicable.

1.5 The Present Work

Prior to the present work, no clear studies of the collision-induced vibrational spectra of the double transitions of the $H_2 - D_2$ mixtures have been reported. Although U (ΔJ=4) transitions in the pure hydrogen in its fundamental band have been reported earlier, no such transitions have yet been reported in the enhancement absorption spectra of H_2 with inert gases. Considerable experimental data is available on the CIA spectra of the first overtone bands of H_2 and D_2. However, no experiments have been carried out on the CIA spectra of HD in its first overtone region. The only collision-induced transitions reported in the fundamental band of HD are of the O, Q, and S type corresponding to ΔJ=-2, 0, and +2. However, just as one observes U (ΔJ=+4) and W (ΔJ=+6) transitions in H_2, transitions corresponding to ΔJ=3 (T transition), 4 (U transition), and 5 (V transition) are expected to occur in the collision-induced spectra of HD under suitable experimental conditions.

It is the aim of the present research project to make a systematic study of the previously unexplored aspects of CIA spectra of the binary mixtures $H_2 - D_2$ and $H_2 - Ar$ and of pure HD in its fundamental and first overtone regions. A summary of the work done is briefly described in the following paragraphs:

Although the H_2 gas is reasonably inexpensive, the D_2 gas is expensive and the HD gas is more expensive. The atmospheric water vapor has considerable absorption in the spectral regions of interest. The experiments were carried out carefully with a 2.0 m high-pressure low-temperature transmission-type absorption cell at 77, 201, and 296 K at gas densities up to 550 amagat. Spectrometers equipped with both prism and gratings as well as microprocessor-controlled stepping motor were

used. Background water vapor absorption was removed by flushing the entire path of the radiation with dry nitrogen gas continuously. The apparatus and experimental procedure are described in Chapter 2.

The theoretical aspects including models used for the collision-induced absorption processes and lineshape functions used in the profile analysis of the observed spectra are discussed in detail in Chapter 3.

Collision-induced infrared absorption spectra of the double transitions of $H_2(v = 1 \leftarrow 0)$ and $D_2(v = 1 \leftarrow 0)$ have been observed at 77 and 201 K for the first time in the spectral region 7000-8000 cm^{-1} for total gas densities up to 550 amagat with partial gas density ratio of 1:1 of H_2 and D_2. The observed spectra are interpreted in terms of the transitions, $Q_1(J)$ of H_2 + $Q_1(J)$ of D_2, $Q_1(J)$ of H_2 + $S_1(J)$ of D_2 and $S_1(J)$ of H_2 + $Q_1(J)$ of D_2 for J=0 and 1 for H_2 and J=0, 1, and 2 for D_2. Analysis of the experimental absorption profiles was carried out using appropriate lineshape functions. The absorption coefficients, lineshape parameters, etc., are obtained from the analysis. The details of all these are described in Chapter 4.

Collision-induced enhancement absorption spectra of the fundamental band of H_2 in $H_2 - Ar$ mixtures were recorded at room temperature for a base density of 72 amagat of H_2 for several partial densities of Ar up to 440 amagat. Hexadecapole-induced U transitions, $U_1(1)$, $U_1(2)$, $Q_1(0) + U_0(1)$, and $Q_1(1) + U_0(1)$ have been identified in the spectral region 5400-6200 cm^{-1}. A "cage" model has been proposed to account for the double transitions of $H_2 - H_2$ in the $H_2 - Ar$ enhancement spectra. From the analysis of the absorption profiles, the lineshape parameters and the absorption coefficients have been determined. Chapter 5 presents the experimental enhancement absorption profiles and the results of the analysis.

The collision-induced absorption spectrum of the first overtone band of HD in the pure gas was observed at 77 K for gas densities up to 320 amagat. In addition to the allowed transitions $P_2(1)$, $R_2(0)$, and $R_2(1)$, the CIA transitions $Q_2(J)+Q_0(J)$, $Q_1(J)+Q_1(J)$, $Q_2(J)-S_0(J)$, $S_2(J)+Q_0(J)$, $Q_1(J)+S_1(J)$, $S_2(J)+S_0(J)$, and $S_1(J)+S_1(J)$ have been observed. An analysis of the observed absorption profiles has been completed. It is found that isotropic overlap induction mechanism does not contribute to the intensity of the band and that negative contribution to the intensity of the band comes from the mixed term $(2\sqrt{3}\lambda_{32}exp[-(R-\sigma)/\rho_{32}]\times <vJ \mid \alpha \mid v'J' >< vJ \mid Q \mid v'J' > (R/a_0)^{-4}$ (for definitions of the symbol used here the reader is referred to Chapter 3). The results of this work are presented in Chapter 6.

The fundamental band of HD has been investigated at 77 K for gas densities in the range 40–310 amagat. For the first time the collision-induced transitions of the type $T_1(1)+Q_0(J)$, $Q_1(J)+T_0(1)$, $U_1(0)+Q_0(J)$, $Q_1(J)+U_0(0)$, $V_1(0)+Q_0(J)$, and $Q_1(J)+V_0(0)$ for HD have been identified. Here T, U, and V transitions correspond to ΔJ=3, 4, and 5, respectively. These results are presented in Chapter 7.

Chapter 2

Apparatus and Experimental Techniques

Collision-induced infrared absorption spectra of the binary mixtures of hydrogen with deuterium and argon and of the pure hydrogen deuteride gas were recorded at different temperatures in the range 77 to 298 K. The absorption cell used in this work was a 2 m high- pressure, low-temperature stainless steel cell. A description of the apparatus and the experimental techniques will be presented in this chapter.

2.1 The 2 m Absorption Cell

The 2 m transmission-type absorption cell was originally designed for observations at room temperature (Reddy and Kuo, 1971) and later modified for work at low temperatures (Chang, 1974, Prasad, 1976). In the early stages of the present work a further modification was made to the cell which improved its performance at low temperatures. A schematic diagram of one cross-section of the cell is shown in Fig. 2.1. The absorption tube T was made from type 303 stainless steel tube, 2 m long, 7.62 cm in outer diameter and 2.54 cm central bore. The polished light guide L,

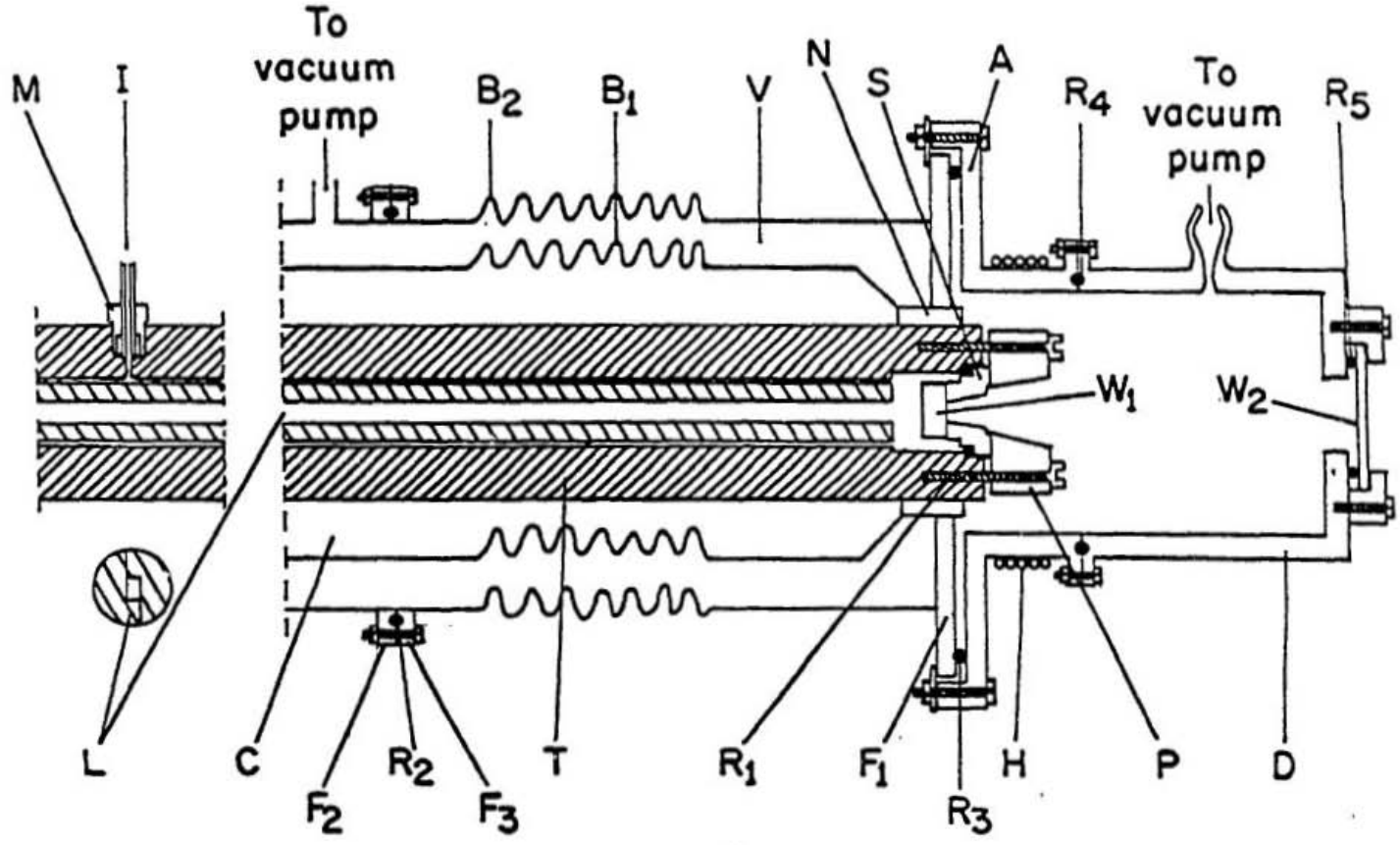

Figure 2.1: A cross-sectional view of one end of the 2 m absorption cell.

made in five sections from stainless steel, has a rectangular aperture of 1.00 *cm* × 0.50 *cm*. A synthetic sapphire window W_1, 2.54 *cm* in diameter and 1.00 *cm* thick, was attached to the polished stainless steel window seat S, having a circular aperture of 1.00 *cm*, with General Electric Silicone Sealant. The invar O-ring R_1 was placed between the window seat and the absorption cell. The retaining stainless steel end piece P was tightened against the cell body by means of eight Allen-head bolts to secure a pressure-tight seal. The gas inlet I consists of a stainless steel capillary tube, 0.64 *cm* in diameter, which was connected to the cell body by means of a 1.27 *cm* Aminco fitting M.

A 1.50 *cm* long stainless steel nut N, 7.62 *cm* in internal diameter, was threaded onto the end of the cell and welded to it. A stainless-steel flange F_1 and a stainless steel bellows B_1, 10.16 *cm* in diameter, was welded to the stainless steel cone. The outer jacket end piece consisted mainly of flanges F_2 and F_3 and bellows B_2, 16.51 *cm* in diameter, all of stainless steel. These two bellows allow for relative expansion and contraction of the absorption cell and the vacuum jacket V. A neoprene O-ring R_2 between F_2 and F_3 provides the vacuum seal. Chamber C was filled with the coolant (liquid nitrogen or dry ice-ethyl alcohol mixture) for low temperature experiments. Flange F_1, an aluminum end cap A, and a Delrin end cap D form a vacuum chamber 10.0 *cm* long and 10.5 *cm* in diameter. A vacuum-tight seal was provided by the silicone rubber O-ring R_3 between the flange F_1 and the aluminum end cap A and a neoprene O-ring R_4 between the aluminum end cap A and the Delrin end cap D. A sapphire window W_2, 0.30 *cm* thick and 5.08 *cm* in diameter, was sealed to the Delrin end cap with a neoprene O-ring R_5 between them. The vacuum chamber prevents frosting on the cell window W_1. Heating tape H wound

around the aluminum end cap A prevents freezing of the O-rings R_3 and R_4.

2.2 The Optical System

The optical system used in the experiments is schematically shown in Fig. 2.2. The light source L is a 600 W General Electric FFJ Quartzline lamp housed in a water-cooled brass jacket. The lamp was operated at a voltage of 90 V controlled by a Variac autotransformer connected to an AC voltage regulator. Radiation from the light source was focused onto the entrance window of the cell by a front coated concave spherical mirror M_1. Radiation which passed through the absorption cell was focused by another spherical mirror M_2 onto the entrance slit of the spectrometer S.

Two different spectrometers were used for the present work. For the H_2-Ar mixture experiments, a Perkin-Elmer model 112 double pass prism spectrometer was used. For the rest of the experiments, a Perkin-Elmer model 112G double-pass grating spectrometer was used. The model 112 prism spectrometer is equipped with a lithium fluoride (LiF) prism. Two different gratings were used for the grating spectrometer depending on the spectral region of interest. One grating blazed at 3.0 μm at an angle of 26°45′ has 300 grooves/mm. The other grating blazed at 1.2 μm at an angle of 10°25′ has also 300 grooves/mm. Both the spectrometers were equipped with an uncooled lead sulphide (PbS) detector and a 260 Hz tuning-fork chopper which chopped the focused radiation after the first pass in the spectrometer. The linear response of the PbS detector with the intensity of the incident radiation was satisfactorily tested by earlier researchers in this laboratory.

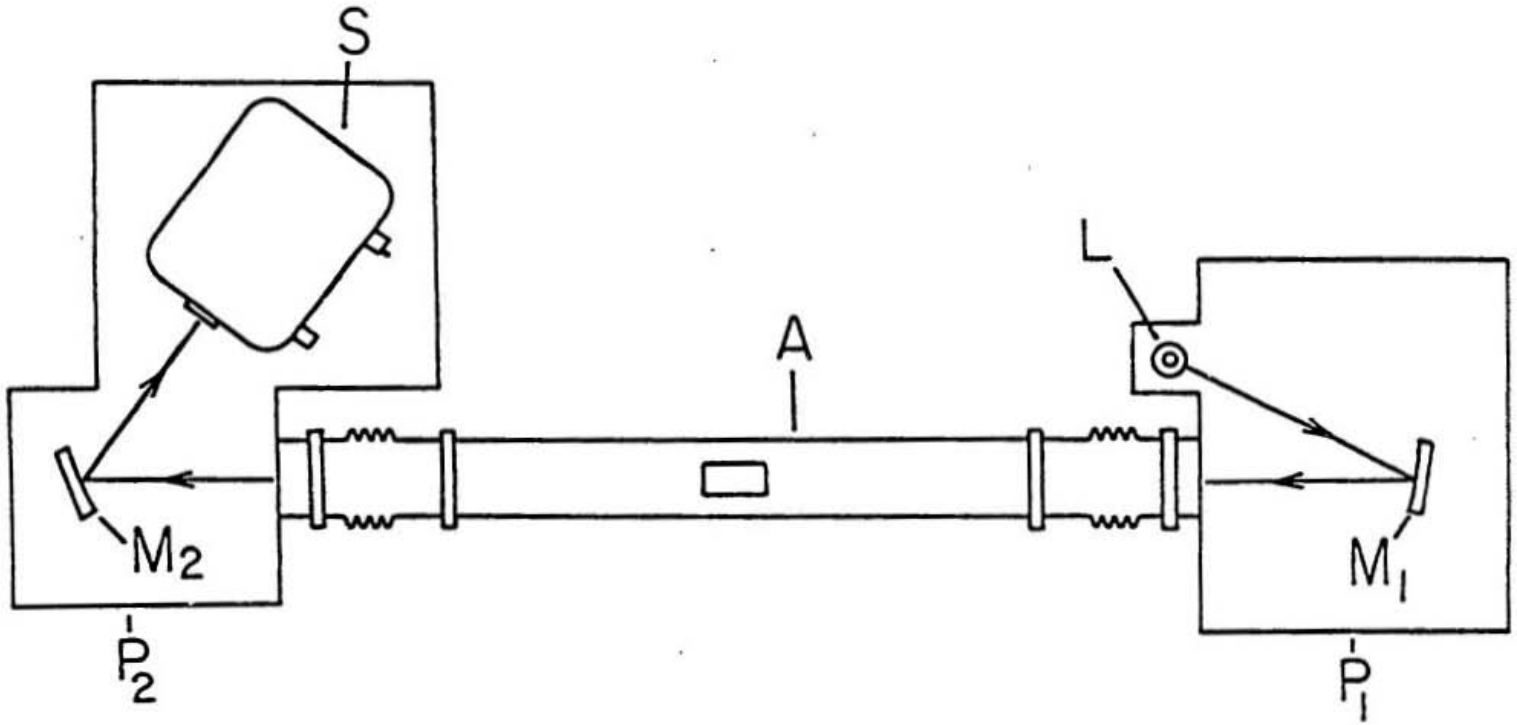

Figure 2.2: The optical arrangement: A - absorption cell, L - light source, M_1 and M_2 - spherical mirrors, S - spectrometer, P_1 and P_2 - plexiglas boxes.

2.3 Microprocessor-Controlled DC Stepping Motor

A model M091 - FD 03 dc stepping motor supplied by Superior Electric Company, Connecticut, U.S.A. was used to drive the wavenumber drum of the spectrometer for the H_2-Ar mixture experiments. It can be used in full step mode of 1.8° step angle or half step mode of 0.9° step angle. A 2:1 gear system was inserted between the stepping motor and the wavenumber drum. The stepping motor was operated in the half step mode and the wavenumber drum was rotated at a speed corresponding to a step angle of 0.45°. The pulses for driving the stepping motor were generated by an Intel 8255 parallel peripheral interface (PPI) controlled by a microprocessor. The stepping-motor control circuit is shown schematically in Fig. 2.3 and Fig. 2.4. Pulses generated by the PPI were first fed into a Schmitt trigger (74LS14) for pulse shaping and then into a 4-bit up/down binary counter (74LS191). The output from this counter was then decoded by a decimal decoder (74LS42). Two 3-input NAND gates (74LS10) and four optical isolators (4N25) were placed between the decoder and the power amplifier circuit as shown in Fig. 2.4. The electrical grounds of the stepping motor and the microcomputer were separated by the use of the optical isolators. The signal noise was reduced to a minimum by the use of the optical isolators. The full-step or half-step mode of the stepping motor was selected by the switch between the counter and the decoder. The direction of rotation of the motor was controlled by the up/down input of the counter.

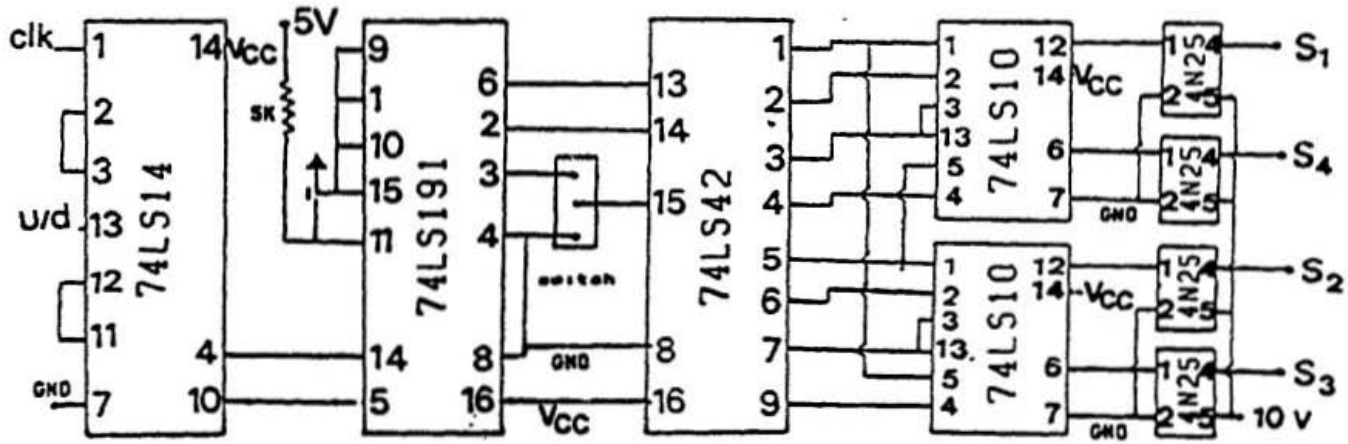

Figure 2.3: The stepping motor control circuit diagram: clk - clock input, u/d - up/down input of the counter, S_1 to S_4 - outputs (inputs to Fig. 2.4).

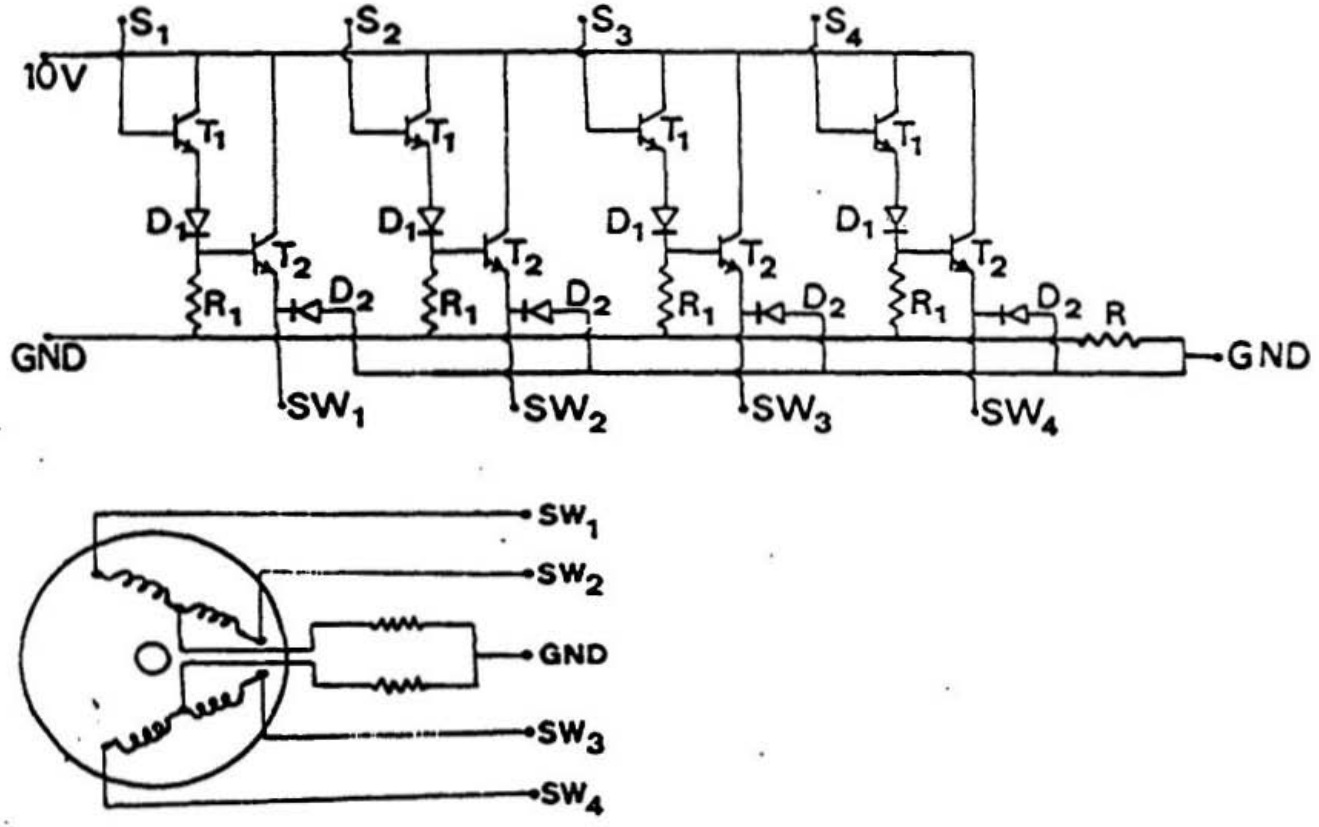

Figure 2.4: The stepping motor control circuit diagram: S_1 to S_4 - the inputs from Fig. 2.3, D_1 - diode (1N5402), T_1 - transistor (ECG123A), T_2 - transistor (2N3055), R - resistor (10 kΩ).

2.4 The Signal Detection System

Figure. 2.5 shows a block diagram of the signal detection and recording system used in the present experiments. The radiation transmitted by the absorption cell was focused on the entrance slit of the spectrometer. It was then dispersed by either a prism or a grating. This radiation focused after the first pass was chopped by a 260 Hz tuning fork chopper and was then reflected back to the dispersing element , and was finally focused on the exit slit of the spectrometer. The radiation was then focused on a PbS detector by a paraboloid mirror. The detector gave rise to an output signal proportional to the intensity of the radiation falling on it. This signal was first amplified by a Brower Laboratories model 261 preamplifier and then by a Brower model LI-100 lock-in voltmeter. A 260 Hz signal from the power supply for the tuning fork chopper was sent to the lock-in voltmeter where it was matched only with the chopped radiation, thus discarding the unchopped first-pass radiation. The ac signal was full-wave rectified and the random noise was reduced with an RC filter. As the dc signal leaving the lock-in voltmeter was in the range 0 to 10 volts while the acceptable range of the analog-to-digital converter (ADC) was only 0 to 2 volts, a model DV-412 decade divider supplied by Electro-Measurement Inc. was used to attenuate the signal. This attenuated dc signal was then fed to a 3711 ADC controlled by the microprocessor and then to a Hewlett Packard model 7132A strip chart recorder.

A block diagram of the microprocessor-controlled data-acquisition system is shown in Fig. 2.6. This system was originally designed by Gillard (1983) and was modified in the present work to accommodate a stepping motor control unit.

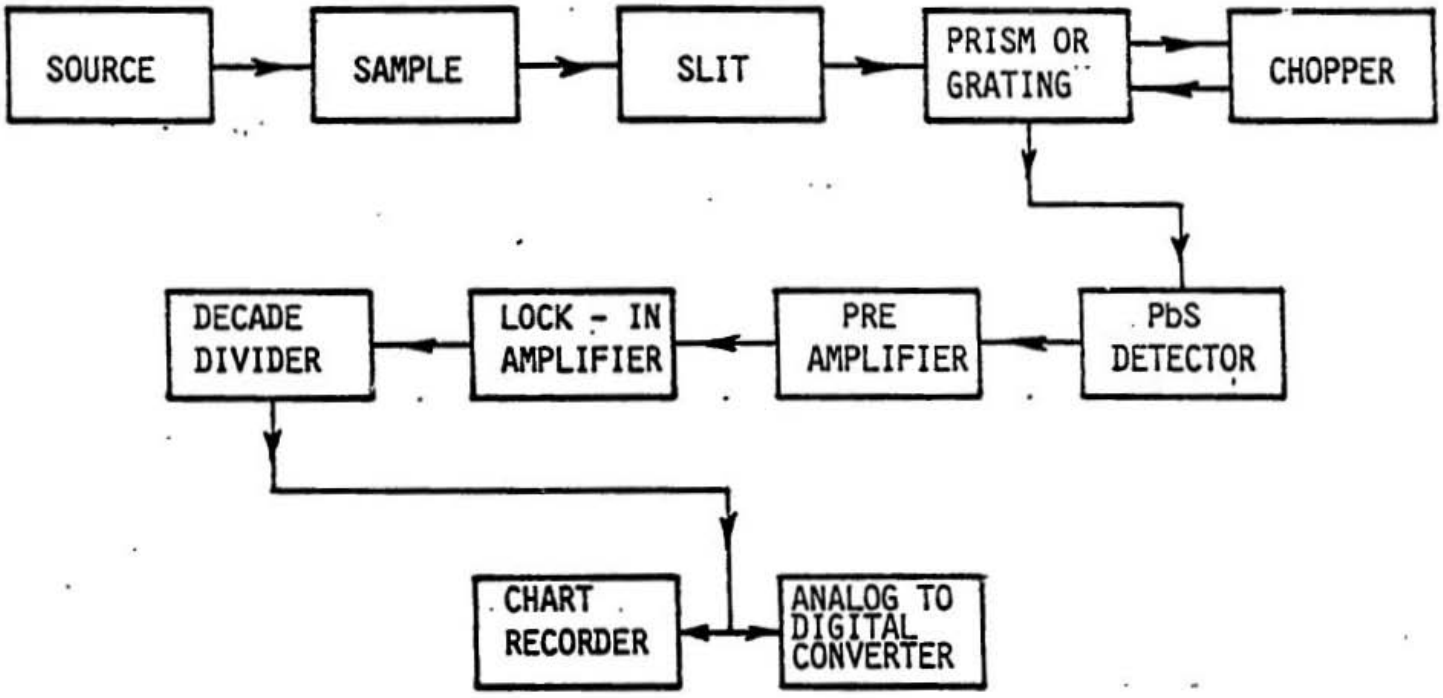

Figure 2.5: A block diagram of the signal detection and recording system.

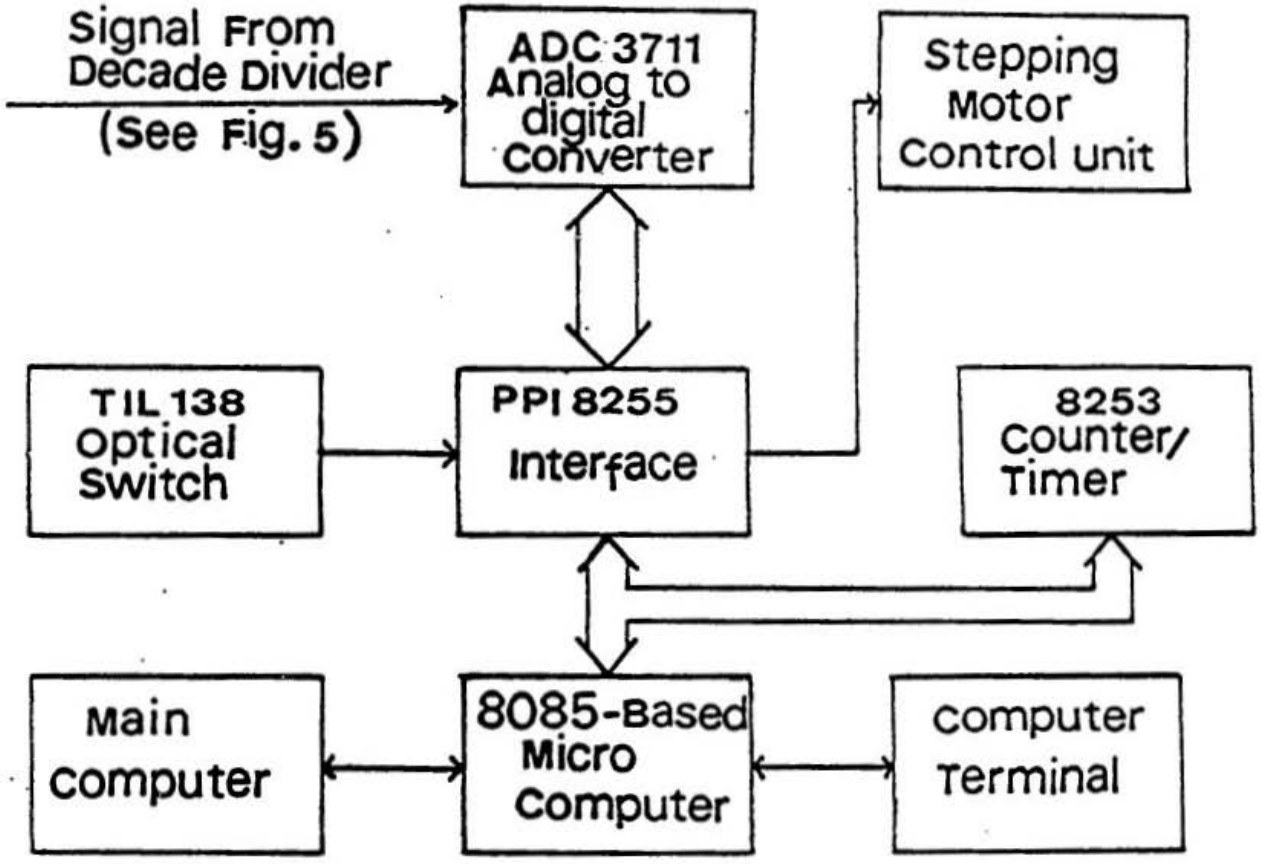

Figure 2.6: A block diagram of the microprocessor-controlled data acquisition system.

The microcomputer is based on the Intel 8085 micro-processor and was supplied in kit form by Netronics R & D Ltd. It incorporates a standard S-100 microcomputer bus and an interpreter for the BASIC language. The Intel 8255 PPI has three individually programmable input/output ports and was used to control the operation of the ADC, stepping motor control unit, and the optical switches. The Intel 8253 is a programmable counter/timer chip which provides the critical timing signals for the data acquisition system and counts the number of pulses in a given trace. The ADC converts the input dc signal into a 4 digit decimal number in the range 0 - 3999. The microcomputer reads the data from the ADC and sends the result to the main computer. The optical switches assist the positioning of the wavenumber drum of the monochromator. For a detailed description of the data acquisition system the reader is referred to Gillard (1983).

2.5 The Gas-Handling System

The high-pressure gas-handling system used in the present work is shown schematically in Fig. 2.7. Thermal compressors T_1, T_2, and T_3 were made from stainless steel. Gas pressure can be raised to about 15,000 psi from 1,500 psi by cooling the gas with liquid nitrogen and warming it up in these compressors repeatedly. Gas from a cylinder was first allowed to enter a copper coil which was immersed in liquid nitrogen. This copper coil kept at 77 K acted as a trap for the impurities such as water vapour and CO_2, etc., in the gas. The purified gas from the cold trap was then admitted into the thermal compressors for developing high pressures and finally to the absorption cell. In Fig. 2.7, G_1, G_2, and G_3 were Ashcroft-type Bourdon tube pressure gauges manufactured by Dresser Industries Inc. They were calibrated

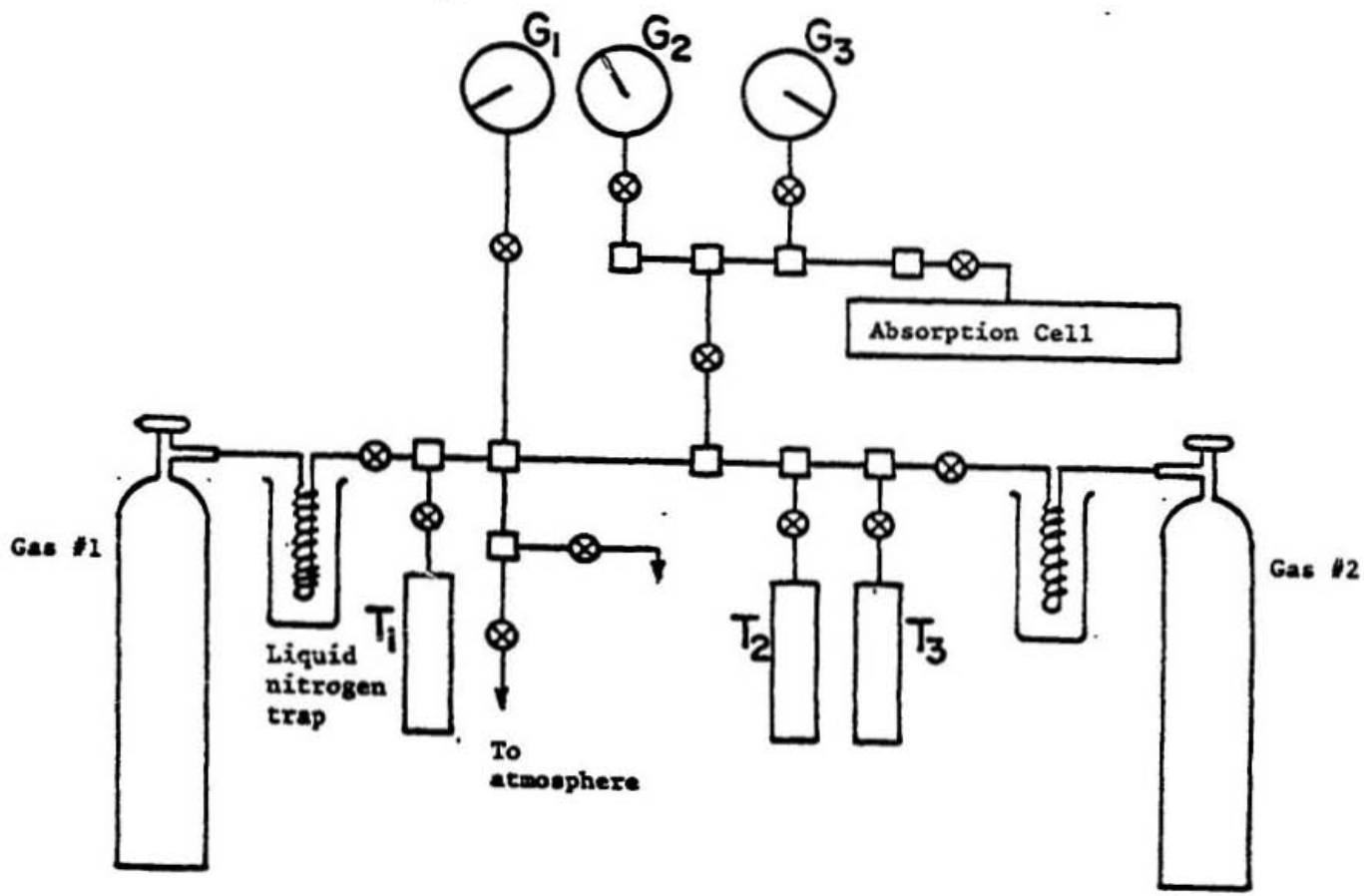

Figure 2.7: The high-pressure gas handling system.

against test gauges, which in turn were calibrated against an Ashcroft dead-weight pressure balance having an accuracy of 0.1%. Gauges G_1, G_2, and G_3 were usually in the ranges 0 - 20,000 psi, 0 - 5,000 psi, and 0 - 1,000 psi, respectively. All fittings in the system except those of the copper coil and the gas cylinders were Aminco stainless steel high-pressure fittings rated for pressures up to 60,000 psi. Except for the section containing the copper tubing, the assembled system was tested for pressures up to 15,000 psi.

The ultra high purity grade hydrogen, C.P. grade deuterium and ultra high purity grade argon used in the experiments were supplied by Matheson Gas Products Canada. The hydrogen deuteride (HD) gas was supplied by Merck, Sharp & Dohme Isotopes. There is a small amount of H_2 impurity in HD and this has been taken into account in the analysis of the data. At high pressures the argon gas showed small absorption in the spectral region around 5700 cm^{-1}. Hence in the experiments on the fundamental band of H_2 in H_2-Ar mixtures, the absorption due to the impurities in the argon gas was subtracted from the observed enhancement absorption profiles.

2.6 Removal of Water Vapor from the Optical Path

The atmospheric water vapor has strong absorption in the spectral regions 3500 - 3900 cm^{-1} and 5200 - 5500 cm^{-1}. It was therefore necessary to remove the atmospheric water vapor from the optical path of the radiation from the source to the detector. The source and the spherical mirror M_1 were enclosed in a Plexiglas box which was sealed to one end cap of the absorption cell with a rubber tube, and the monochromator and the spherical mirror M_2 were placed in another Plexiglas box

which was sealed to the other end cap of the absorption cell (see Fig. 2.2). Both boxes were airtight and equipped with side windows fitted with neoprene gloves so that the monochromator and the mirror could be adjusted without breaking the airtight seal. The system was flushed continuously with dry nitrogen gas produced by evaporating liquid nitrogen in a 200 litre dewar with a small electric heater (a 100 Ω, 25 W resistor worked satisfactorily). The outlets of the two Plexiglas boxes were fitted with one-way valves to prevent any outside air from entering the boxes. Initially it took about four to five days of continuous flushing with dry nitrogen to reduce the water vapor absorption to a negligible and stable level. Flushing with dry nitrogen was continued during the entire experiment.

2.7 Isothermal Data and Density Calculation

The density of a gas is expressed in units of amagat, which is the ratio of the density of the gas at a given temperature and pressure to the density of an ideal gas at the standard temperature and pressure (S.T.P.). If the density of the gas is ρ amagat, then ρn_0 represents the number of gas molecules per cm^3, n_0 being the Loschmidt's number (number density of an ideal gas at S.T.P $=2.687\times10^{19}cm^{-3}$).

The isothermal data required to calculate densities of hydrogen at various temperatures were obtained by linear interpolation and by a nonlinear least-squares fit of the PVT data tabulated by McCarty et al. (1981). The pressure-density data of deuterium were derived from the corresponding data of hydrogen by using a procedure outlined by Woolley et al. (1948). The pressure-density data for HD at a given temperature were obtained from the isothermal data for H_2 and D_2 at the same temperature by direct interpolation (i.e., by taking the average). The densi-

ties of argon were obtained by nonlinear least-squares fit of the PVT data given by Michels et al. (1949; 1958).

In the experiments of the H_2-D_2 mixtures, the partial densities of H_2 and D_2 were kept equal for all individual binary mixtures of H_2 and D_2. The procedure of calculating the partial pressures of H_2 and D_2 for the desired partial densities is described below. In a binary mixture of gases a and b, if the first gas admitted to the cell is gas a at density ρ_a, the partial density ρ_b of gas b can be determined from the approximate formula (Reddy and Cho, 1965)

$$\rho_b = (1/1 + \beta')[(\rho_a)_P + \beta'(\rho_b)_P] - \rho_a \,, \tag{2.1}$$

where $(\rho_a)_P$ and $(\rho_b)_P$ are the densities of the pure gases at the total pressure P of the mixture, and $\beta' = \rho_b'/\rho_a$, ρ_b' being the approximate partial density of the gas b obtained from the known isothermal data at the given partial pressure P_b. The partial pressure P_a of gas a for the first density ρ_1 $(=\rho_a = \rho_b)$ of the binary mixture was obtained directly from the isothermal data of gas a. To find the partial pressure P_b of gas b and the total pressure P $(=P_a = P_b)$ for the mixture such that $\rho_b = \rho_a = \rho_1$, a value P_b was assumed which was obtained from the isothermal data of gas b corresponding to the density ρ_b $(=\rho_1)$ of the pure gas b. Then $P = P_a + P_b$ and Eq.(2.1) was used to calculate the actual ρ_b in the mixture. If the actual value of ρ_b was lower (or higher) than the desired value ρ_1, then a new higher (or lower) value of partial pressure P_b was assumed and the procedure was repeated until the actual partial density ρ_b was equal to the desired value ρ_1. To raise the density of the mixture to $\rho_2(a) + \rho_2(b)$, two steps were followed. The first step was to raise the density of gas b to ρ_2 while the density of gas a was kept at ρ_1. The above

Table 2.1: The total pressures P for the binary mixtures of H_2-D_2 for various partial densities of H_2 and D_2 at 77 K and 201 K.

77 K			201 K		
Partial Density (amagat)		Total Pressure (atmosphere)	Partial Density (amagat)		Total Pressure (atmosphere)
H_2	D_2		H_2	D_2	
100	0	27.3	150	0	120.5
100	100	53.3	150	150	270.1
100	125	60.1	150	165	287.4
125	125	67.2	165	165	305.6
150	125	74.5	180	165	324.1
150	150	81.8	180	180	342.7
150	175	89.4	180	195	362.2
175	175	97.8	195	195	382.8
200	175	106.6	210	195	403.8
200	200	115.3	210	210	424.7
200	225	124.8	210	225	446.7
225	225	135.9	225	225	470.5
250	225	147.6	240	225	494.4
250	250	159.0	240	240	517.9
250	275	172.1	240	255	543.0
275	275	188.7	255	255	570.6

described procedure was performed for this step such that $\rho_a = \rho_1$ and $\rho_b = \rho_2$. The second step was to raise the density of gas a from ρ_1 to ρ_2. This procedure was repeated by interchanging gases a and b. Table 2.1 lists the total pressure P for the binary mixture of H_2-D_2 for various densities at 77 K and 201 K. The procedure described here made it possible to conserve the experimental gases H_2 and D_2. This is particularly valuable in the case of the D_2 gas as it is very expensive.

For each of the $H_2 - Ar$ mixture experiments, only one base pressure of H_2 and a number of partial pressures of Ar were used. The base density of H_2 was directly

obtained from the isothermal data of H_2. The partial densities of Ar in the mixtures were obtained from the isothermal data of Ar and Eq. (2.1).

2.8 Calibration of the Spectral Region and Calculation of the Absorption Coefficients

The spectral region which covers the absorption of the fundamental bands of H_2 and HD, the double vibrational transitions of $H_2 - D_2$, and the first overtone band of HD ranges from 3000 to 8200 cm^{-1}. This region was calibrated with mercury emission lines (Zaidel et al. 1970) from a General Electric model H100A4/T mercury lamp and the absorption peaks of the atmospheric water vapor (Humphreys, 1953 and Plyler et al., 1955). For each specific spectral region of interest, a polynomial least-squares fit of the standard wavenumbers against position on the recorder chart was performed. For the prism spectrometer in which a stepping motor was used, the wavenumber ν was expressed in terms of the pulse number n of the stepping motor as $\nu = a_0 + a_1 n + a_2 n^2 + a_3 n^3 + a_4 n^4$. In fact, the pulse number n is directly proportional to the chart position d (the distance on the chart from a selected reference mercury emission line). For the grating spectrometer, two different polynomials were used in the calibration of the spectral regions of interest. For the grating blazed at 1.2 μm, the chart position d was expressed in terms of a polynomial of the reciprocal of the wavenumber ν as $d = a_0 + a_1\nu^{-1} + a_2\nu^{-2} + a_3\nu^{-3} + a_4\nu^{-4}$. For the grating blazed at 3.0 μm, the wavenumber ν was expressed in terms of the polynomial $\nu = a_0 + a_1 d + a_2 d^2 + a_3 d^3 + a_4 d^4$. In both polynomials d is the chart position from a reference line. A calibration chart of positions of wavenumber at 10 cm^{-1} intervals in each case was then made using the coefficients of the polynomial.

The absorption coefficient $\alpha(\nu)$ is given by

$$\alpha(\nu) = l^{-1} \ln[I_0(\nu)/I(\nu)] \,, \tag{2.2}$$

where $I_0(\nu)$ and $I(\nu)$ are the intensities of radiation at wavenumber ν transmitted by the evacuated cell and the cell filled with the experimental gas, respectively, and l is the sample path length.

In the enhancement absorption of gas a (e.g., H_2) due to the presence of a foreign gas b (e.g., Ar), the enhancement absorption coefficient $\alpha_{en}(\nu)$ is given by

$$\alpha_{en} = l^{-1} \ln[I_1(\nu)/I_2(\nu)] \,, \tag{2.3}$$

where $I_1(\nu)$ and $I_2(\nu)$ are the intensities of radiation at wavenumber ν transmitted by the cell filled with gas a and with a mixture of gases a and b, respectively. In the case of the chart recorder used with the grating spectrometer, the quantity $\log_{10}[I_0(\nu)/I(\nu)]$ or $\log_{10}[I_1(\nu)/I_2(\nu)]$ was measured using a standard logarithmic scale by superimposing on the chart recorder trace the calibration chart with lines at intervals of 10 cm^{-1}. In the case of the microprocessor-controlled stepping motor used with the prism spectrometer, the intensities $I_0(\nu)$, $I(\nu)$, $I_1(\nu)$, and $I_2(\nu)$ stored in the main computer (see Section 2.4) were used to calculate $\log_{10}[I_0(\nu)/I(\nu)]$ or $\log_{10}[I_1(\nu)/I_2(\nu)]$. The integrated absorption coefficient of the band $\int \alpha(\nu)d\nu$ or $\int \alpha_{en}(\nu)d\nu$ was then obtained from measurement of the area under the experimental profile of $\log_{10}[I_0(\nu)/I(\nu)]$ vs. ν or $\log_{10}[I_1(\nu)/I_2(\nu)]$ vs. ν.

Chapter 3

Theoretical Aspects

3.1 Absorption Coefficients in the Collision-Induced Absorption Spectra

The absorption coefficient $\alpha(\nu)$ at a given wavenumber ν (in cm^{-1}) of an absorbing gas at density ρ_a is expressed in terms of the intensities $I_0(\nu)$ and $I(\nu)$ and the sample path length l (see Section 2.8 for definitions of $I_0(\nu)$ and $I(\nu)$) as

$$I(\nu) = I_0(\nu)e^{-\alpha(\nu)l} , \tag{3.1}$$

or

$$\alpha(\nu) = (1/l)ln[I_0(\nu)/I(\nu)] . \tag{3.2}$$

For a binary mixture of gases of species a at density ρ_a and species b at density ρ_b, the enhancement absorption coefficient $\alpha_{en}(\nu)$ is expressed in terms of $I_1(\nu)$, $I_2(\nu)$, (see also Section 2.8) and l as

$$I_2(\nu) = I_1(\nu)e^{-\alpha_{en}(\nu)l} , \tag{3.3}$$

or

$$\alpha_{en}(\nu) = (1/l)ln[I_1(\nu)/I_2(\nu)] . \tag{3.4}$$

In the literature on CIA, related absorption coefficients $\tilde{\alpha}(\nu) \equiv \alpha(\nu)/\nu$, and $\tilde{\alpha}_{en}(\nu) \equiv \alpha_{en}(\nu)/\nu$ are also used (see for example, Reddy, 1985). The integrated absorption coefficient $\int \tilde{\alpha}(\nu)d\nu$ of a single line or a band is more theoretically tractable than the frequency-dependent absorption coefficient $\alpha(\nu)$. The integrated absorption coefficient can be conveniently expressed as a power series in densities (expressed in amagat units). Thus for the pure gas

$$\int \alpha(\nu)d\nu = \alpha_{1a}\rho_a^2 + \alpha_{2a}\rho_a^3 + \cdots , \tag{3.5}$$

and for a binary mixture of type $H_2 - X$ where X is an inert gas,

$$\int \alpha_{en}(\nu)d\nu = \alpha_{1b}\rho_a\rho_b + \alpha_{2b}\rho_a\rho_b^2 + \cdots . \tag{3.6}$$

The quantities α_{1a} and α_{1b} (in $cm^{-2}amagat^{-2}$) are the binary absorption coefficients and α_{2a} and α_{2b} (in $cm^{-2}amagat^{-3}$) are the ternary absorption coefficients. Analogous quantities $\tilde{\alpha}_{1a}$ and $\tilde{\alpha}_{1b}$ (in cm^6s^{-1}), and $\tilde{\alpha}_{2a}$ and $\tilde{\alpha}_{2b}$ (in cm^3s^{-1}) are defined from the following equations:

$$c\int \tilde{\alpha}(\nu)d\nu = \tilde{\alpha}_{1a}n_0^2\rho_a^2 + \tilde{\alpha}_{2a}n_0^3\rho_a^3 + \cdots \tag{3.7}$$

and

$$c\int \tilde{\alpha}_{en}(\nu)d\nu = \tilde{\alpha}_{1b}n_0^2\rho_a\rho_b + \tilde{\alpha}_{2b}n_0^3\rho_a\rho_b^2 + \cdots , \tag{3.8}$$

where c is the speed of light and n_0 is the Loschmidt's number. The new binary and ternary absorption coefficients $\tilde{\alpha}_{1a}$ (and $\tilde{\alpha}_{1b}$) and $\tilde{\alpha}_{2a}$ (and $\tilde{\alpha}_{2b}$) are related to the previous coefficients by the following relations:

$$\tilde{\alpha}_{1a} = (c/n_0^2)\alpha_{1a}/\overline{\nu} \tag{3.9}$$

$$\tilde{\alpha}_{1b} = (c/n_0^2)\alpha_{1b}/\overline{\nu} \tag{3.10}$$

$$\tilde{\alpha}_{2a} = (c/n_0^3)\alpha_{2a}/\overline{\nu} \tag{3.11}$$

and

$$\tilde{\alpha}_{2b} = (c/n_0^3)\alpha_{2b}/\bar{\nu} \ , \tag{3.12}$$

where the band center $\bar{\nu}$ is given by

$$\bar{\nu} = \frac{\int \alpha(\nu)d\nu}{\int \alpha(\nu)\nu^{-1}d\nu} \tag{3.13}$$

and

$$\bar{\nu}_{en} = \frac{\int \alpha_{en}(\nu)d\nu}{\int \alpha_{en}(\nu)\nu^{-1}d\nu} \ . \tag{3.14}$$

However, for a mixture of two absorbing gases such as $H_2 + D_2$, we can express the integrated absorption coefficient as

$$\int \alpha(\nu)d\nu = \alpha_1\rho_a\rho_b + \alpha_{2ab}\rho_a^2\rho_b + \alpha_{a2b}\rho_a\rho_b^2 + \cdots \ . \tag{3.15}$$

In a special case where the partial densities of the two gases in a mixture are equal, i.e., $\rho_a = \rho_b = \rho$, Eq.(3.15) simplifies to

$$\int \alpha(\nu)d\nu = \alpha_1\rho^2 + (\alpha_{2ab} + \alpha_{a2b})\rho^3 + \cdots \ , \tag{3.16}$$

where α_1 is the binary absorption coefficient and α_{2ab} and α_{a2b} are the ternary absorption coefficients.

3.2 Collision-Induced Vibration-Rotation Bands

(a) Theoretical Expressions for the Expansion Coefficients in Collision-Induced Absorption

The theory of the integrated absorption coefficients for collision-induced vibration-rotation bands has been developed by Van Kranendonk (1951 a,b; 1957, 1958, 1959) who introduced the "exponential-4" model for the induced dipole moment μ in a

collision pair of molecules. In this model, μ contains two terms, one representing the short-range electron overlap induced dipole moment which decreases exponentially with the intermolecular separation R, and the second term representing the long-range quadrupole induced dipole moment which varies as R^{-4}. Poll and Van Kranendonk (1961) expressed the spherical components of the induced dipole moment in terms of the expansion coefficients $A(\lambda_1\lambda_2\Lambda\mathcal{L};\mathcal{R})$. Here the coefficients A are independent of the coordinate system and give an invariant classification of the induction effects in terms of the parameters $\lambda_1, \lambda_2, \Lambda$, and L. Further expressions for the integrated binary absorption coefficients have been given by Poll (1971) and Karl et al. (1975). Subsequently Poll and Hunt (1976) and Hunt and Poll (1978) introduced the matrix elements $B_\Lambda(\lambda_1\lambda_2\mathcal{L};\mathcal{R})$ (also called the coefficients B) which are related to the expansion coefficients A (see Eq. 3.19 in this chapter). Meyer et al. (1989) obtained theoretical expressions for the induced dipole moment in an $H_2 - H_2$ collision pair by treating the pair as a single supermolecule in self-consistent-field and size-consistent, coupled electron pair approximations. From the induced dipole moments these authors have calculated the induced absorption spectra arising from the binary collisions for the rotation-translation and the fundamental band of H_2 using the vibrationally averaged isotropic potential from *abinitio* calculations. In a review article, Reddy (1985) summarized the theoretical aspects of the collision-induced vibrational bands. A brief account of the essentials of the theory is presented in the following paragraphs.

When two molecules 1 and 2 collide with each other, the intermolecular interaction induces an electric dipole moment $\vec{\mu}$. This dipole moment is a function of the separation of the centers of mass of the molecules, $\vec{R}(R,\Omega)$, and the internuclear

separations and orientations, $\vec{r}_1(r_1,\omega_1)$ and $\vec{r}_2(r_2,\omega_2)$, with respect to a space fixed coordinate system. A spherical component μ_ν of the induced dipole moment $\vec{\mu}$ in a pair of diatomic molecules (e.g., H_2-H_2) can be expanded as a sum of components, each with a definite angular dependence (Poll and Van Kranendonk, 1961; Poll and Hunt, 1976),

$$\mu_\nu(r_1 r_2 \omega_1 \omega_2 R\Omega) = \frac{(4\pi)^{3/2}}{\sqrt{3}} \sum_{\lambda_1\lambda_2\Lambda\mathcal{L}} A_\Lambda(\lambda_1\lambda_2\mathcal{L}; r_1 r_2 R) \sum_{\mu M} C(\lambda_1\lambda_2\Lambda; \nu - M - \mu, \mu) \times C(\Lambda\mathcal{L}1; \nu - M, M) Y_{\lambda_1,\nu-M-\mu}(\omega_1) Y_{\lambda_2\mu}(\omega_2) Y_{\mathcal{L}M}(\Omega) \ . \quad (3.17)$$

Here the coefficient $A_\Lambda(\lambda_1\lambda_2\mathcal{L}; r_1 r_2 R)$ describes the r_1, r_2, R dependence of a particular component of the dipole moment characterized by the angular dependence $\lambda_1, \lambda_2, \Lambda, \mathcal{L}$. Also the following five relations must hold: (i) $\lambda_1 + \lambda_2 + \mathcal{L}$ is odd, (ii) λ_1, λ_2, and $\mathcal{L}$ satisfy the triangle relations $\Delta(\lambda_1\lambda_2\Lambda)$ and $\Delta(\Lambda\mathcal{L}1)$(Rose, 1957); (iii) A_Λ are real for all values of λ and $\mathcal{L}$; (iv) for homonuclear diatomic molecules only even λ's occur, thus $\mathcal{L}$ is odd from relation (i); (v) for two identical diatomic molecules, $A_\Lambda(\lambda_1\lambda_2\mathcal{L}; r_1 r_2 R) = (-1)^{\lambda_1+\lambda_2-\Lambda+1} A_\Lambda(\lambda_2\lambda_1\mathcal{L}; r_2 r_1 R)$. The quantities $C(\lambda_1\lambda_2\Lambda; \nu - M - \mu, \mu)$ and $C(\Lambda\mathcal{L}1; \nu - M, M)$ are Clebsch-Gordan coefficients and $Y's$ are spherical harmonics (see Rose, 1957).

In the case of the induced fundamental band arising from collisions between molecules 1 and 2, we are interested in the vibrational-rotational matrix elements of the induced dipole moment operator. These matrix elements are

$$< v_1 = 0, v_2 = 0, J_1 m_1 J_2 m_2 \mid \mu_\nu \mid v_1 = 1, v_2 = 0, J_1' m_1' J_2' m_2' >$$
$$= \frac{(4\pi)^{3/2}}{\sqrt{3}} \sum_{\lambda_1\lambda_2\Lambda\mathcal{L}} \sum_M B_\Lambda(\lambda_1\lambda_2\mathcal{L}; R) C(\lambda_1\lambda_2\Lambda; \nu - M - \mu, \mu) C(\Lambda\mathcal{L}1; \nu - M, M)$$
$$\times < J_1 m_1 \mid \lambda_1 \nu - M - \mu \mid J_1' m_1' >< J_2 m_2 \mid \lambda_2 \mu \mid J_2' m_2' > Y_{\mathcal{L}M}(\Omega) \ , \quad (3.18)$$

where

$$B_\Lambda(\lambda_1\lambda_2\mathcal{L};R) = < v_1 = 0, v_2 = 0 \mid A_\Lambda(\lambda_1\lambda_2\mathcal{L};r_1r_2R) \mid v_1' = 1, v_2' = 0 > \quad (3.19)$$

is the matrix element of $A_\Lambda(\lambda_1\lambda_2\mathcal{L};r_1r_2R)$ between the 0 and 1 vibrational states of molecule 1. A similar expression is valid if we interchange subscripts 1 and 2. We represent the matrix element $B_\Lambda(\lambda_1\lambda_2\mathcal{L};\ R)$ in the concise form $B_{\mathcal{L}\Lambda}(R)$ where $\mathcal{L}$ takes odd values as Λ takes even values for H_2-H_2 collisions (see Poll et al., 1976). An approximate model for the B matrix elements in terms of ea_0 units (e:electronic charge; a_0:first Bohr radius) are represented by the following expressions:

$$B_{10}(R)/ea_0 = \lambda_{10}exp[-(R-\sigma)/\rho_{10}] \quad (3.20)$$

$$B_{12}(R)/ea_0 = \lambda_{12}exp[-(R-\sigma)/\rho_{12}] \quad (3.21)$$

$$B_{32}(R)/ea_0 = \lambda_{32}exp[-(R-\sigma)/\rho_{32}] + \sqrt{3} < vJ \mid \alpha \mid v'J' >< vJ \mid Q \mid v'J' > (R/a_0)^{-4} \quad (3.22)$$

where $B_{10}(R)$ is the isotropic overlap component of the radial part of the induced dipole moment and contributes to the intensity of the Q branch, $B_{12}(R)$ is the $\mathcal{L}$=1 anisotropic overlap component, and $B_{32}(R)$ is the $\mathcal{L}$=3 anisotropic overlap and anisotropic quadrupolar component. Both $B_{12}(R)$ and $B_{32}(R)$ contribute in principle to the intensity of the O, Q, and S branches. The intensity is proportional to the square of $B_{\mathcal{L}\Lambda}(R)$. Thus the intensity arising from the $[B_{32}(R)/ea_0]^2$ term comprises the sum of three terms as given below:

$$[B_{32}(R)/ea_0]^2 = \lambda_{32}^2 exp[-2(R-\sigma)/\rho_{32}] + 3 < vJ \mid \alpha \mid v'J' >^2 < vJ \mid Q \mid v'J' >^2 (R/a_0)^{-8}$$

$$+2\sqrt{3}\lambda_{32}exp[-(R-\sigma)/\rho_{32}]$$
$$\times < vJ \mid \alpha \mid v'J' >< vJ \mid Q \mid v'J' > (R/a_0)^{-4} . \quad (3.23)$$

(b) The Overlap Binary Absorption Coefficient

For the fundamental band, the overlap binary absorption coefficient can be expressed as

$$\tilde{\alpha}_{1,ov} = (8\pi^3/3h) \int B_0(001; R)^2 g_0(R) d^3R , \quad (3.24)$$

where $g_0(R)$ is the low density limit of the pair distribution funtion, and $B_0(001; R)$ is assumed to have the form

$$B_0(001; R) = \lambda e k_1 exp[-(R-\sigma)/\rho] . \quad (3.25)$$

Here σ is the intermolecular separation corresponding to zero intermolecular potential (i.e., $V(R) \mid_{R=\sigma} = 0$), λ and ρ are parameters representing the magnitude and range, respectively, of the dipole transition moment,and k_1 is the $1 \leftarrow 0$ transition element of the internuclear separation r with respect to its equilibrium value r_0. The quantity k_1 is represented by

$$k_1 = < v = 0 \mid r - r_0 \mid v' = 1 > . \quad (3.26)$$

By substituting Eqs. (3.25) and (3.26) in Eq. (3.24), $\tilde{\alpha}_{1,ov}$ can be written as

$$\tilde{\alpha}_{1,ov} = (8\pi^3/3h)(\lambda e)^2 < 0 \mid r - r_0 \mid 1 >^2 \int exp[-2(R-\sigma)/\rho] g_0(R) 4\pi R^2 dR , \quad (3.27)$$

or

$$\tilde{\alpha}_{1,ov} = \lambda^2 I \tilde{\gamma} . \quad (3.28)$$

Here

$$\tilde{\gamma} = (8\pi^3/3h) e^2 \sigma^3 < 0 \mid r - r_0 \mid 1 >^2 \quad (3.29)$$

and has the dimensions of the binary absorption coefficient, $cm^6 s^{-1}$, and

$$I = 4\pi \int_0^\infty exp[-2(x-1)\sigma/\rho] g_0(x) x^2 dx \ , \tag{3.30}$$

is a dimensionless temperature-dependent integral representing the average R-dependence of $B_0(001; R)^2$. The reduced quantity x is defined as R/σ. The classical value I_{cl} of the integral I can be calculated from Eq. (3.30) by using the low density limit of the classical pair distribution function,

$$g_0(x) = exp[-V^*(x)/T^*] \ , \tag{3.31}$$

where $V^*(x) = V(x)/\epsilon$ and $T^* = kT/\epsilon$ are the reduced quantities, ϵ being the depth of the potential well in the Lennard-Jones (L-J) intermolecular potential,

$$V(x) = 4\epsilon(x^{-12} - x^{-6}) \ . \tag{3.32}$$

One must note that the L-J potential is a rough approximation to the true intermolecular potential. At high temperatures, the integral I can be approximated by its classical value I_{cl}. At intermediate temperatures, quantum effects should be included and I can be expressed as (Van Kranendonk, 1958),

$$I = I_{cl} - \Lambda^{*2} I^{(2)} + \Lambda^{*4} I^{(4)} + \cdots \tag{3.33}$$

where $\Lambda^* = [h^2/2m_r\epsilon\sigma^2]^{1/2}$ is the quantum mechanical wavelength (de Boer, 1949), m_r being the reduced mass of the two molecules.

(c) *Lth* Order Multipole-Induced Binary Absorption Coefficient

The expansion coefficients $B_\Lambda(\lambda_1\lambda_2\mathcal{L}; R)$ for the multipole-induced dipole moments are dependent on the matrix elements of the quadrupole moment or other

higher order multipole moment and of the polarizability of the molecules. These matrix elements of the quadrupole moment and the polarizability for the hydrogens H_2, D_2, HD, etc., have been numerically evaluated (see, for example, Hunt et al., 1984 and the references therein). The matrix elements of the hexadecapole moment of H_2 and HD have been similarly calculated by Karl et al. (1975). In the rest of this section, we give expressions for the integrated binary absorption coefficient arising from the multipole-induction mechanism from the existing literature. We note that in the form given below, the absorption coefficient is different by a factor c (speed of light) from the definition used earlier in this section.

The integrated binary absorption coefficient of a specific *Lth* order multipole-induced transition can be written as (Poll, 1971; Karl et al., 1975; Reddy, 1985)

$$\tilde{\alpha}_{Lm} = \frac{1}{\rho^2}\int \frac{\alpha_m(\nu)}{\nu} d\nu \tag{3.34}$$

$$= \frac{4\pi^3 e^2}{3hc} n_0^2 a_0^5 (a_0/\sigma)^{2L+1} \tilde{J}_L X_{Lm} \ , \tag{3.35}$$

where

$$\tilde{J}_L = 4\pi(L+1)\int_0^\infty x^{-2(L+2)} g_0(x) x^2 dx \tag{3.36}$$

$$\begin{aligned} X_{Lm} = \ & P_{J_1} P_{J_2} [C(J_1 L J_1'; 00)^2 < v_1 J_1 \mid Q_{L_1} \mid v_1' J_1' >^2 \\ & \times C(J_2 0 J_2'; 00)^2 < v_2 J_2 \mid \alpha_2 \mid v_2' J_2' >^2 \\ & + C(J_2 L J_2'; 00)^2 < v_2 J_2 \mid Q_{L_2} \mid v_2' J_2' >^2 \\ & \times C(J_1 0 J_1'; 00)^2 < v_1 J_1 \mid \alpha_1 \mid v_1' J_1' >^2] + Y_{Lm} \ , \end{aligned} \tag{3.37}$$

and

$$Y_{Lm} = P_{J_1} P_{J_2} [C(J_1 L J_1'; 00)^2 C(J_2 2 J_2'; 00)^2$$

$$\times \frac{2}{9} < v_1 J_1 \mid Q_{L_1} \mid v_1' J_1' >^2 < v_2 J_2 \mid \gamma_2 \mid v_2' J_2' >^2$$

$$+ C(J_1 2 J_1'; 00)^2 C(J_2 L J_2'; 00)^2$$

$$\times \frac{2}{9} < v_2 J_2 \mid Q_{L_2} \mid v_2' J_2' >^2 < v_1 J_1 \mid \gamma_1 \mid v_1' J_1' >^2$$

$$- \frac{4}{15} \delta_{L2} C(J_1 2 J_1'; 00)^2 C(J_2 2 J_2'; 00)^2$$

$$\times < v_1 J_1 \mid Q_{2_1} \mid v_1' J_1' >< v_2 J_2 \mid \gamma_2 \mid v_2' J_2' >$$

$$\times < v_2 J_2 \mid Q_{2_2} \mid v_2' J_2' >< v_1 J_1 \mid \gamma_1 \mid v_1' J_1' > \quad . \tag{3.38}$$

In these equations, L is the order of the multipole induction and takes values 2,4,6, etc., for quadrupole (2^2), hexadecapole (2^4), tetrahexadecapole (2^6) induction, etc., respectively; m represents all the quantum numbers characterizing the transition; a_0 is the first Bohr radius; and the $<| \alpha |>$ and $<| \gamma |>$ are the matrix elements of the isotropic and anisotropic polarizability, respectively. The quantity δ_{L2}=1 if $L = 2$, and 0 if $L \neq 2$. The normalized Boltzmann factors P_J are given by

$$P_J = \frac{g_T(2J+1)exp(-E_J/kT)}{\sum_J g_T(2J+1)exp(-E_J/kT)} \ , \tag{3.39}$$

where g_T is the nuclear statistical weight of the molecule in a given rotational state and E_J is the rotational energy. For H_2, g_i is 1 for even J and 3 for odd J. For D_2, g_T is 6 for even J and 3 for odd J. For normal H_2 or normal D_2, the conversion between the ortho and para species is not allowed. Therefore the expression for P_J should be modified to

$$P_J = \frac{g_T(2J+1)exp(-E_J/kT)}{\sum_J g_T(2J+1)exp(-E_J/kT)} \times F \ , \tag{3.40}$$

where F takes values $C_p/(C_p + C_o)$ and $C_o/(C_p + C_o)$, C_p and C_o being the concentrations of the para and ortho molecules. The values of F are 1/4 and 3/4 for the

even (para) and odd (ortho) J, respectively, for H_2, and 2/3 and 1/3 for the even (ortho) and odd (para) J, respectively, for D_2. It should be noted that in Eq. (3.40) the summation over J in the denominator should be performed for either even J or odd J only. The quantities $C(JLJ';00)$ are Clebsch-Gordan coefficients and their squares for various transitions are given by (Rose, 1957)

$$\begin{aligned} Q: C(J0J';00)^2 &= \delta_{JJ'} \\ O: C(J2J-2;00)^2 &= \frac{3J(J-1)}{2(2J-1)(2J+1)} \\ Q: C(J2J;00)^2 &= \frac{J(J+1)}{(2J-1)(2J+3)} \\ S: C(J2J+2;00)^2 &= \frac{3(J+1)(J+2)}{2(2J+1)(2J+3)} \\ U: C(J4J+4;00)^2 &= \frac{35(J+1)(J+2)(J+3)(J+4)}{8(2J+1)(2J+3)(2J+5)(2J+7)} . \end{aligned} \tag{3.41}$$

In the case of molecules like HD the following Clebsch-Gordan coefficients also apply.

$$\begin{aligned} P: \ C(J1J-1;00)^2 &= \frac{J}{2J+1} \\ R: \ C(J1J+1;00)^2 &= \frac{J+1}{2J+1} \\ T: \ C(J3J+3;00)^2 &= \frac{5(J+1)(J+2)(J+3)}{2(2J+1)(2J+3)(2J+5)} \\ V: \ C(J5J+5;00)^2 &= \frac{63(J+1)(J+2)(J+3)(J+4)(J+5)}{8(2J+1)(2J+3)(2J+5)(2J+7)(2J+9)} . \end{aligned} \tag{3.42}$$

3.3 Line Shape Functions

The absorption coefficient $\tilde{\alpha}(\nu)$ at a given wavenumber ν can be expressed as (Van Kranendonk, 1968; Mactaggart and Welsh, 1973, and Reddy et al., 1977).

$$\tilde{\alpha}(\nu) = \sum_{m,n} \frac{\tilde{\alpha}^0_{nm} W_n(\Delta\nu)}{1 + exp(-hc\Delta\nu/kT)} , \tag{3.43}$$

where n stands for the induction mechanism, m represents a specific transition, $\tilde{\alpha}^0_{nm}$ is a parameter representing twice the maximum absorption coefficient at the molecular frequency ν_m, $W_n(\Delta\nu)$ is the line shape function for type n and $\Delta\nu = \nu - \nu_m$. The factor $[1 + exp(-hc\Delta\nu/kT)]$ converts the symmetric line shape $W_n(\Delta\nu)$ into the observed asymmetric line shape. This Boltzmann symmetrization is an approximation for the vibration-rotation bands (see for example Meyer et al., 1989).

For overlap induction the line-shape function $W_{ov}(\Delta\nu)$ is

$$W_{ov}(\Delta\nu) = W^0_{ov}(\Delta\nu)D(\Delta\nu) \ , \tag{3.44}$$

where $W^0_{ov}(\Delta\nu)$ is the intracollisional line-shape function and is represented by the Levine-Birnbaum (1967) expression as

$$W^0_{ov}(\Delta\nu) = (2\Delta\nu/\delta_d)^2 K_2(2\Delta\nu/\delta_d) \ , \tag{3.45}$$

where $K_2(x)$ is a modified Bessel function of the second kind of order 2, and δ_d $(= 1/2\pi c\tau_d)$ is the intracollisional half-width at half-height,and τ_d is the duration of the collision. The function $D(\Delta\nu)$ is the intercollisional line shape function and is represented by (Van Kranendonk, 1968)

$$D(\Delta\nu) = 1 - \frac{\gamma}{1 + (\Delta\nu/\delta_c)^2} \ , \tag{3.46}$$

where γ is a constant which is usually assumed to be unity and δ_c $(= 1/2\pi c\tau_c)$ is the intercollisional half-width at half-height, and τ_c is the mean time between the collisions. Lewis and Van Kranendonk (1972) have taken into account the correlations between *all* collisions in the collision sequence and have shown that in such a case $\delta_c = (1 - \tilde{\Delta})/2\pi c\tau_c$ where $\tilde{\Delta}$ is the mean persistence-of-velocity and is 0.24 for

H_2-He, 0.02 for H_2-Ar and is even smaller for the case of heavier perturbers. Lewis (1985) discussed the asymmetry in $W_{ou}(\Delta\nu)$ resulting from phase shifts. For further details on the mechanism of inter-collisional interference the reader is referred to several papers by Lewis which are referenced in Lewis (1985).

For quadrupolar induction the line-shape function is usually represented by the Lorentz line-shape function as

$$W_q^L(\Delta\nu) = \frac{1}{1+(\Delta\nu/\delta_q)^2} , \tag{3.47}$$

where δ_q is the quadrupolar half-width at half-height. An improved line-shape function including a fourth power term in the denominator of the Lorentz line-shape function was found to give a better fit in the high wavenumber wing (Gillard et al., 1984).

$$W_q^{ML}(\Delta\nu) = \frac{1}{1+(\Delta\nu/\delta_{q2})^2+(\Delta\nu/\delta_{q4})^4} . \tag{3.48}$$

Another line-shape function for the quadrupolar induction in collision-induced absorption has been developed by Birnbaum and Cohen (1976), which can be expressed as

$$W_q^{BC}(\Delta\nu) = \frac{\tau_1}{\pi} exp(\tau_2/\tau_1) exp(hc\Delta\nu/2kT) \frac{zK_1(z)}{1+(2\pi c\Delta\nu\tau_1)^2} \tag{3.49}$$

where

$$z = [1+(2\pi c\Delta\nu\tau_1)^2]^{1/2}[(\tau_2/\tau_1)^2+(h/4\pi kT\tau_1)^2]^{1/2} . \tag{3.50}$$

Here $K_1(z)$ is a modified Bessel function of the second kind of order 1, and τ_1 and τ_2 are time parameters. One can also use wavenumber parameters δ_1 and δ_2 instead of τ_1 and τ_2 by defining $\delta_i = 1/2\pi c\tau_i$. Then $W_q^{BC}(\Delta\nu)$ and z become

$$W_q^{BC}(\Delta\nu) = \frac{1}{2\pi^2 c\delta_1} exp(\delta_1/\delta_2) exp(hc\Delta\nu/2kT) \frac{zK_1(z)}{1+(\Delta\nu/\delta_1)^2} \tag{3.51}$$

and

$$z = [1 + (\Delta\nu/\delta_1)^2]^{1/2}[(\delta_1/\delta_2)^2 + (hc\delta_1/2kT)^2]^{1/2} . \qquad (3.52)$$

Chapter 4

Collision-Induced Absorption Spectra of the Double Transitions $H_2(v=1\leftarrow0)+D_2(v=1\leftarrow0)$

Collision-induced infrared absorption spectra of the double transitions of H_2 (v=1←0) and D_2 (v=1←0) have been observed in the binary mixtures of H_2 and D_2 at 77 and 201 K in the spectral region 7000–8000 cm^{-1}. The spectra were recorded for a number of mixtures for total gas densities up to 550 amagat with partial gas density ratio of 1:1 of H_2 and D_2 with a 2 m absorption cell. Experimental procedure and details are given in Chapter 2. The absorption profiles are presented in Section 4.1. The analysis of the absorption profiles and the results obtained from it are described in Section 4.2. The absorption coefficients are given in Section 4.3.

4.1 Profiles of the Double Transitions

The experimental procedure and the calculation of the total pressures for the equal partial densities of H_2 and D_2 in their binary mixtures are described in detail in Section 2.7. The partial density of each of H_2 and D_2 ranged from 125 to 275 amagat

at 77 K and from 150 to 270 amagat at 201 K. Three representative absorption profiles at each temperature are shown in Figs. 4.1 and 4.2, respectively, by plotting $log_{10}[I_0(\nu)/I(\nu)]$ versus ν.

In these figures the positions of the double transitions of $H_2 + D_2$ of the types $Q_1(J)+Q_1(J), Q_1(J)+S_1(J), S_1(J)+Q_1(J)$, and $S_1(J)+S_1(J)$ calculated from the constants of the free H_2 and D_2 molecules (Bragg et al., 1982; McKellar and Oka, 1978) are marked along the wavenumber axis. The strong absorption peak around 8085 cm^{-1} is due to the collision-induced first overtone band of H_2 and is assigned to the double transitions $Q_2(J) + Q_0(J)$ arising from the $H_2 - H_2$ collisions. The measured wavenumbers of the absorption peaks due to $H_2 - D_2$ collisions and their assignments are given in Table 4.1 and Table 4.2 for 77 K and 201 K, respectively.

The most obvious feature of these absorption profiles is the absence of the dip in the Q branch. The Q branch dips are very prominent features of the collision-induced fundamental bands of H_2, D_2, HD, etc. As an example, an absorption profile of the collision-induced fundamental band of H_2 at 298 K (Reddy et al., 1977) is reproduced in Fig. 4.3. In this figure the dip in the Q branch is seen very clearly. The origin of this phenomenon has been explained by Van Kranendonk (1968) in terms of the destructive interference between the short-range induced dipoles of a molecule in successive collisions. This intercollisional interference effect is found to be dependent on the density of the gas mixture. The absence of the Q dip in the collision-induced double fundamental transitions in H_2-D_2 mixtures is similar to those in the collision-induced first overtone bands of H_2 (Van Nostrand, 1983; McKellar and Welsh, 1971; McKellar, 1988) and D_2 (Gillard, 1983). This implies that the overlap induction mechanism makes little or no contribution to

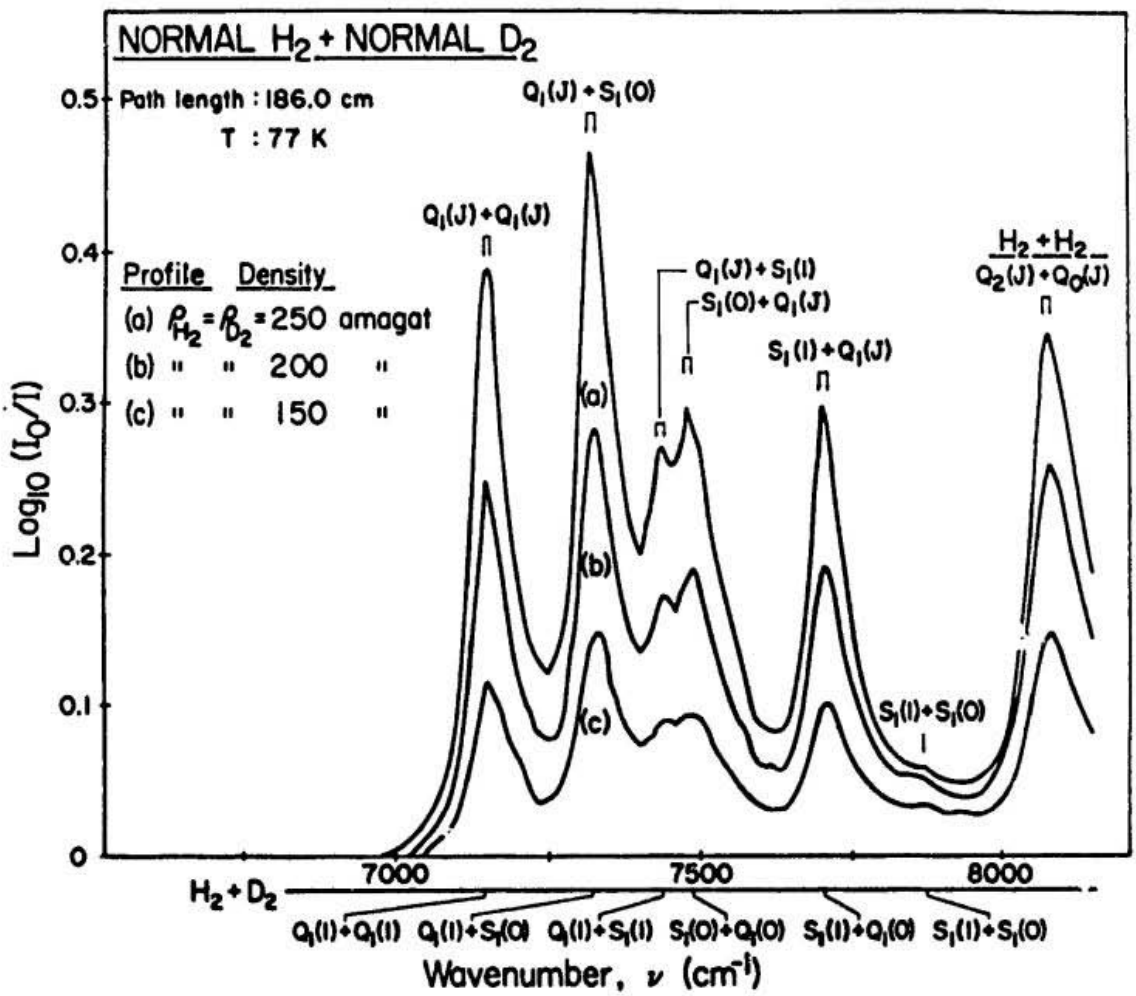

Figure 4.1: Collision-induced double fundamental absorption profiles of $H_2 + D_2$ at three different total densities of the mixture at 77 K. In the indicated double transitions, the first one refers to H_2 and the second one refers to D_2. For example, $Q_1(J) + S_1(0)$ is really $Q_1(J)$ of $H_2 + S_1(0)$ of D_2.

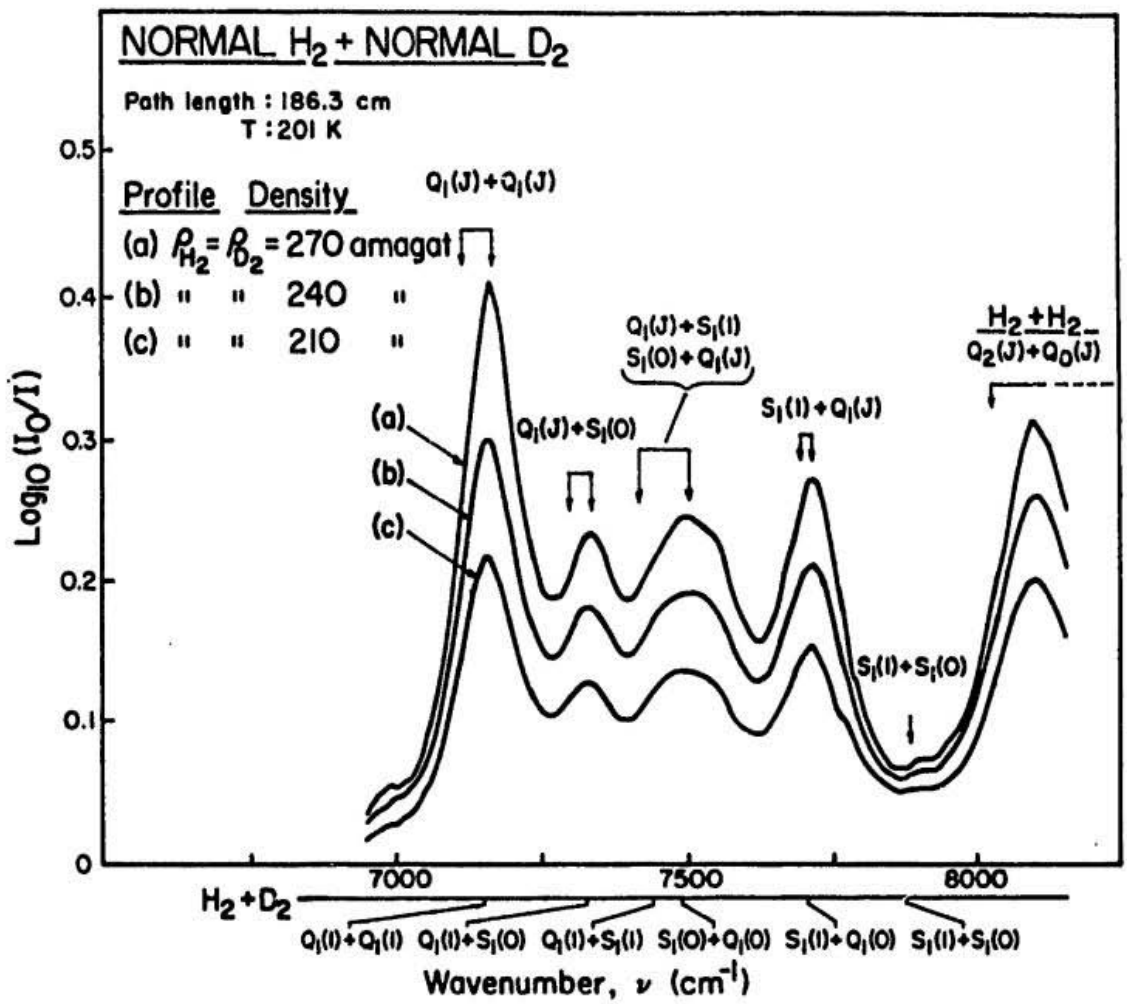

Figure 4.2: Collision-induced double fundamental absorption profiles of $H_2 + D_2$ at three different total densities of the mixture at 201 K. See caption of Figure 4.1 for other details.

Table 4.1: Assignments of the observed absorption peaks of the double fundamental transitions in H_2-D_2 mixtures at 77 K.

Transition $H_2 + D_2$	Calculated wavenumber (cm^{-1})	Measured wavenumber (cm^{-1})
$Q_1(1) + Q_1(2)$	7142.6	
$Q_1(1) + Q_1(1)$	7146.8	7147
$Q_1(0) + Q_1(2)$	7148.5	
$Q_1(1) + Q_1(0)$	7148.9	
$Q_1(0) + Q_1(1)$	7152.7	
$Q_1(1) + S_1(0)$	7321.6	
$Q_1(0) + S_1(0)$	7327.5	7326
$Q_1(1) + S_1(1)$	7433.8	7433
$Q_1(0) + S_1(1)$	7439.7	
$S_1(0) + Q_1(2)$	7485.1	7486
$S_1(0) + Q_1(1)$	7489.3	
$S_1(0) + Q_1(0)$	7491.5	
$Q_1(1) + S_1(2)$	7542.5	
$Q_1(0) + S_1(2)$	7548.4	
$S_1(0) + S_1(0)$	7664.2	
$S_1(1) + Q_1(2)$	7700.2	
$S_1(1) + Q_1(1)$	7704.4	7705
$S_1(1) + Q_1(0)$	7706.5	
$S_1(1) + S_1(0)$	7879.3	7880

Table 4.2: Assignments of the observed absorption peaks of the double fundamental transitions in H_2-D_2 mixtures at 201 K.

Transition $H_2 + D_2$	Calculated wavenumber (cm^{-1})	Measured wavenumber (cm^{-1})
$Q_1(2) + Q_1(2)$	7130.8	
$Q_1(2) + Q_1(1)$	7135.0	
$Q_1(1) + Q_1(3)$	7136.2	
$Q_1(1) + Q_1(2)$	7142.6	
$Q_1(1) + Q_1(1)$	7146.8	7145
$Q_1(0) + Q_1(2)$	7148.5	
$Q_1(1) + Q_1(0)$	7148.9	
$Q_1(0) + Q_1(1)$	7152.7	
$Q_1(2) + S_1(0)$	7309.8	
$Q_1(1) + S_1(0)$	7321.6	7324
$Q_1(0) + S_1(0)$	7327.5	
$Q_1(1) + S_1(1)$	7433.8	
$Q_1(0) + S_1(1)$	7439.7	
$S_1(0) + Q_1(3)$	7478.8	
$S_1(0) + Q_1(2)$	7485.1	7485
$S_1(0) + Q_1(1)$	7489.3	
$S_1(0) + Q_1(0)$	7491.5	
$Q_1(1) + S_1(2)$	7542.5	
$Q_1(0) + S_1(2)$	7548.4	
$Q_1(1) + S_1(3)$	7647.3	
$S_1(0) + S_1(0)$	7664.2	
$S_1(1) + Q_1(3)$	7693.9	
$S_1(1) + Q_1(2)$	7700.2	
$S_1(1) + Q_1(1)$	7704.4	7703
$S_1(1) + Q_1(0)$	7706.5	
$S_1(1) + S_1(0)$	7879.3	7880

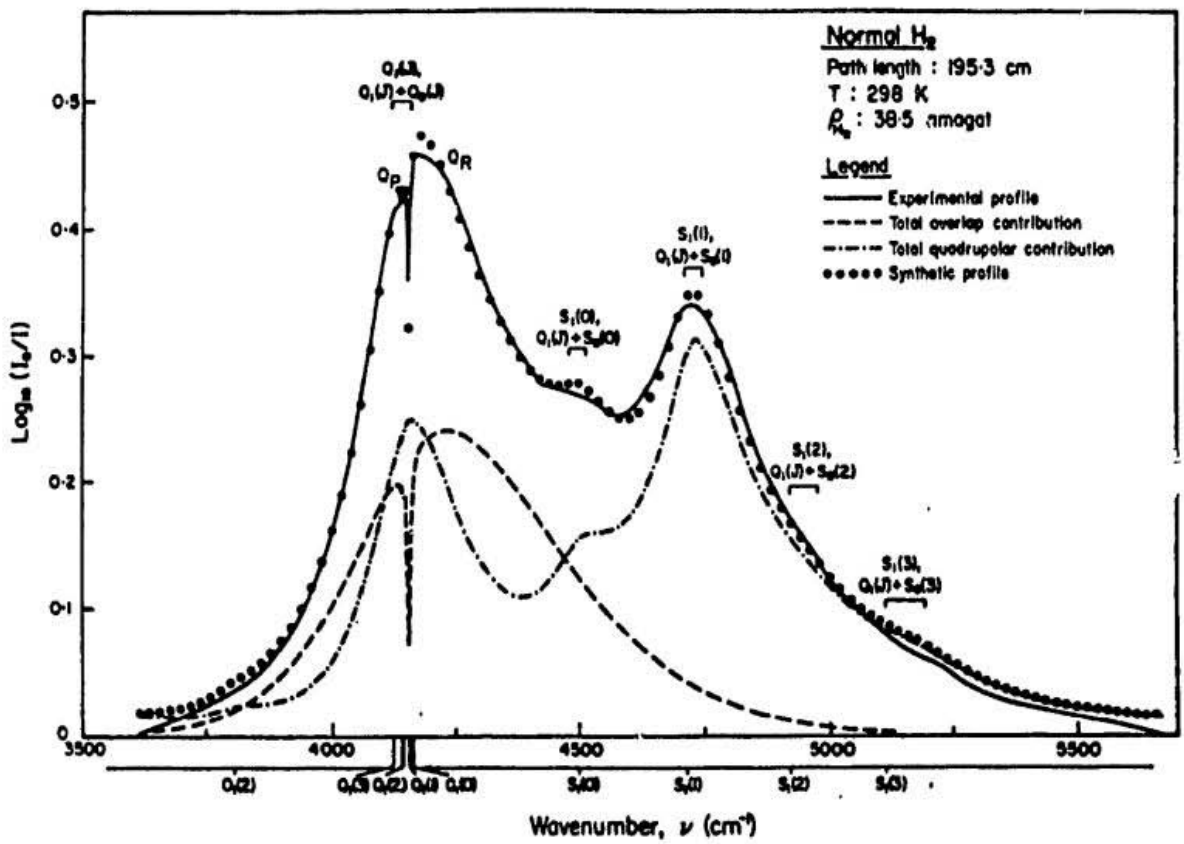

Figure 4.3: An absorption profile of the collision-induced fundamental band of H_2 at a density of 38.5 amagat at room temperature. The solid curve is the experimental profile. The dashed curve is the computed overlap-induced profile and the dot-dashed curve is the computed quadrupole-induced profile. The dots represent the sum of the computed overlap and quadrupolar components(adopted from Reddy et al., 1977).

the double fundamental transitions of H_2 and D_2. Thus it is justified to consider quadrupole induction mechanism only in the calculation of the transition intensities of the double fundamental transitions of H_2 and D_2. We mention here that McKellar (1990) studied the infrared spectra of $H_2 - D_2$ dimers using para H_2 and ortho D_2 at 20 K at very low gas densities and observed the following transitions: $Q_1(0)(H_2) + S_1(0)(D_2), S_1(0)(H_2) + Q_1(0)(D_2), Q_2(0)(H_2) + S_0(0)(D_2)$.

4.2 Profile Analysis

Collision-induced absorption spectra of H_2-D_2 gaseous mixtures in the spectral region 7000–8000 cm^{-1} consist of a superposition of double fundamental transitions of the type $Q_1(J) + Q_1(J), Q_1(J) + S_1(J), S_1(J) + Q_1(J)$, and $S_1(J) + S_1(J)$, where in each of the double transitions, the first one refers to H_2 and the second to D_2. The subscript 1 in these transitions indicates the change in the vibrational quantum number v; in particular, it is $v = 1 \leftarrow 0$ here.

(a) The line shapes

The absorption coefficient $\tilde{\alpha}(\nu)$ at a given wavenumber ν can be expressed as (Eq. (3.43)),

$$\tilde{\alpha}(\nu) = \sum_{m,n} \frac{\tilde{\alpha}^0_{nm} W_n(\Delta\nu)}{1 + exp(-hc\Delta\nu/kT)} . \tag{4.1}$$

The induction mechanism in the double fundamental transitions in the H_2-D_2 mixtures is considered to be entirely quadrupolar and thus the subscript n in Eq. (4.1) becomes only q and hence

$$\tilde{\alpha}(\nu) = \sum_{m} \frac{\tilde{\alpha}^0_{qm} W_q(\Delta\nu)}{1 + exp(-hc\Delta\nu/kT)} . \tag{4.2}$$

For the profile analysis of the double fundamental transitions in the H_2-D_2 mixtures,

the Lorentzian line-shape function $W_q^L(\Delta\nu)$ (Eq. (3.47)), the modified Lorentzian line-shape function $W_q^{ML}(\Delta\nu)$ (Eq. (3.48)), and the Birnbaum-Cohen line-shape function $W_q^{BC}(\Delta\nu)$ (Eqs. (3.51) and (3.52)) have been used. For convenience these four equations are listed below.

$$W_q^L(\Delta\nu) = \frac{1}{1+(\Delta\nu/\delta_q)^2} , \tag{4.3}$$

$$W_q^{ML}(\Delta\nu) = \frac{1}{1+(\Delta\nu/\delta_{q2})^2+(\Delta\nu/\delta_{q4})^4} . \tag{4.4}$$

$$W_q^{BC}(\Delta\nu) = \frac{1}{2\pi^2 c\delta_1} exp(\delta_1/\delta_2) exp(hc\Delta\nu/2kT) \frac{zK_1(z)}{1+(\Delta\nu/\delta_1)^2} \tag{4.5}$$

where

$$z = [1+(\Delta\nu/\delta_1)^2]^{1/2}[(\delta_1/\delta_2)^2+(hc\delta_1/2kT)^2]^{1/2} . \tag{4.6}$$

(b) Transition intensities

The integrated binary absorption coefficient of the mth quadrupole-induced double transitions of H_2+D_2 can be written readily using the general expression for the integrated binary absorption coefficient of the Lth order multipole-induced transition by letting $L=2$ in Eqs. (3.34) to (3.41).

$$\begin{aligned} \tilde{\alpha}_{2m} &= \frac{1}{\rho_a\rho_b}\int\frac{\alpha_m(\nu)}{\nu}d\nu \\ &= \frac{4\pi^3e^2}{3hc} n_0^2 a_0^5 (a_0/\sigma)^5 \tilde{J}_2 X_{2m} \end{aligned} \tag{4.7}$$

$$\begin{aligned} \tilde{J}_2 &= 12\pi\int_0^\infty x^{-8} g_0(x) x^2 dx \\ &= 12\pi J_8 \end{aligned} \tag{4.8}$$

The subscript 8 in Eq. (4.8) refers to the negative power of x above. When quantum corrections are included, J_8 is written as

$$J_8 = J_8^{cl} + (\Lambda^*)^2 J_8^{(1)} + (\Lambda^*)^4 J_8^{(2)} \tag{4.9}$$

Here J_s^{cl} occurs when $g_0^{cl}(x) = exp[-V(x)/kT]$. The absorption intensities of the quadrupole-induced double fundamental transitions of $H_2 + D_2$ at 77 K and 201 K were calculated by using these formulas and the matrix elements of the quadrupole moment $<|\ Q\ |>$ and the polarizability $<|\ \alpha\ |>$ of the H_2 and D_2 molecules available in the literature (see Hunt et al., 1984 and the references therein). The calculated intensities are presented in Table 4.3.

(c) Method of computation

The profiles of the collision-induced double fundamental transitions in the H_2-D_2 mixtures at 77 K and 201 K were analyzed using Eq. (4.2) and two computer programs, one for the modified Lorentzian line shape (which becomes the Lorentzian line shape when the fourth power term in the denominator is neglected) and the other for the Birnbaum-Cohen line shape. These two programs were written by the author and are presented in Appendix A and Appendix B. In the programs there are four adjustable parameters A_1, A_2, A_3, and A_4. For the modified Lorentzian line shape $A_1 = \delta_{q2}$ and $A_2 = \delta_{q4}$. For the Birnbaum-Cohen line shape $A_1 = \delta_1$ and $A_2 = \delta_2$. The parameter A_3 is a multiplication factor relating the theoretical quantity $\tilde{\alpha}(\nu)$ to the corresponding experimental factor $log_{10}(I_0(\nu)/I(\nu))$. The parameter A_4 accounts for any possible shift of the free molecular transition wavenumbers ν_m. A set of values for A_1, A_2, A_3, and A_4 was assumed in the beginning and the computer would calculate the variance. Then A_1, A_2, A_3, and A_4 were varied in turn until the best fit of the synthetic profile to the experimental profile was found. Note that the calculated absorption intensities $\tilde{\alpha}(cm^{-1})$ in Table 4.3 were used for the quantities $\tilde{\alpha}_m^0$ in Eq. (4.2). In the fitting of the synthetic profile to the experimental profile, it is necessary to take into account the contribution of the $Q_2(J) + Q_0(J)$ transitions

Table 4.3: Absorption intesities@ of the quadrupole-induced double fundamental transitions* in the H_2-D_2 mixtures at 77 K and 201 K.

Transition H_2+D_2	Wavenumber (cm^{-1})	$\tilde{\alpha}$ (77 K) (cm^{-1})	$\tilde{\alpha}$ (201 K) (cm^{-1})
$Q_1(1)+Q_1(2)$	7142.55	4.9024e-11	1.8592e-10
$Q_1(1)+Q_1(1)$	7146.76	1.8993e-10	1.5440e-10
$Q_1(0)+Q_1(2)$	7148.46	6.6754e-12	1.8895e-11
$Q_1(1)+Q_1(0)$	7148.87	1.5759e-10	7.6812e-11
$Q_1(0)+Q_1(1)$	7152.67	3.0890e-11	1.8743e-11
$Q_1(1)+S_1(0)$	7321.61	3.5942e-10	1.7291e-10
$Q_1(0)+S_1(0)$	7327.53	1.1316e-10	4.0635e-11
$Q_1(1)+S_1(1)$	7433.78	1.1263e-10	9.1557e-11
$Q_1(0)+S_1(1)$	7439.69	3.5419e-11	2.1491e-11
$S_1(0)+Q_1(2)$	7485.13	1.8952e-11	5.3642e-11
$S_1(0)+Q_1(1)$	7489.34	6.3438e-11	3.8491e-11
$S_1(0)+Q_1(0)$	7491.45	1.0345e-10	3.7148e-11
$Q_1(1)+S_1(2)$	7542.52	2.6005e-11	9.8613e-11
$Q_1(0)+S_1(2)$	7548.43	8.1653e-12	2.3262e-11
$S_1(0)+S_1(0)$	7664.20	1.1532e-11	4.1410e-12
$S_1(1)+Q_1(2)$	7700.20	2.9096e-11	1.1205e-10
$S_1(1)+Q_1(1)$	7704.41	9.7472e-11	7.9231e-11
$S_1(1)+Q_1(0)$	7706.52	1.5856e-10	7.6281e-11
$S_1(1)+S_1(0)$	7879.26	1.8505e-11	8.9022e-12

@ For the transitions at 201 K, calculations were made for J=0 to 3 of H_2 and J=0 to 4 of D_2; however, very low absorption intensities are omitted from this table.

* In each double transition, the first one refers to H_2 and the second one refers to D_2. For example, $Q_1(1)+Q_1(2)$ is really $Q_1(1)$ of H_2 + $Q_1(2)$ of D_2.

of $H_2 + H_2$ which occur on the high wavenumber wing of the $H_2 + D_2$ transitions. Hence the fitting was performed for the experimental profile up to $\sim 7800 cm^{-1}$ on the high wavenumber wing.

(d) Results of the profile analysis

Profiles of the collision-induced absorption spectra of H_2-D_2 mixtures at 77 K and 201 K were analyzed using the two computer programs mentioned above. It is found that the agreement between the experimental and the synthetic profiles at 77 K is remarkbly good for both the Lorentzian and the Birnbaum-Cohen lineshapes. For the profiles at 201 K, the agreement is also satisfactory. Two typical analyzed profiles at 77 K are shown in Figs. 4.4 and 4.5 for the Lorentzian and the Birnbaum-Cohen lineshapes, respectively. An analyzed profile at 201 K is shown in Fig. 4.6 for the Lorentzian lineshape. In Fig. 4.4 the contribution to the intensity of the synthetic profile from the intensities of the individual double transitions (except a few very weak ones) is also shown. The half-width δ_q obtained from the profile analysis is found to be density dependent. The wavenumber shift $\delta\nu$ from the free molecular transition wavenumber is also found to be density dependent. Table 4.4 lists the values of δ_q and $\delta\nu$ obtained from the absorption profiles at 77 K using the Lorentzian line-shape function. A plot of the half-width δ_q versus the total density of the mixture $\rho_a + \rho_b$ is shown in Fig. 4.7. Similarly a plot of the wavenumber shift $\delta\nu$ against $\rho_a + \rho_b$ is given in Fig. 4.8. In Fig. 4.7, the half-width δ_q seems to remain constant for total densities of the binary mixtures of $H_2 + D_2$ up to ~ 350 amagat, and then it decreases linearly with the total density. The decrease of the half-width with density of the gas (commonly known as the pressure narrowing) was first observed by De Remigis et al. (1971) in the $S_1(1)$ quadrupolar line of the

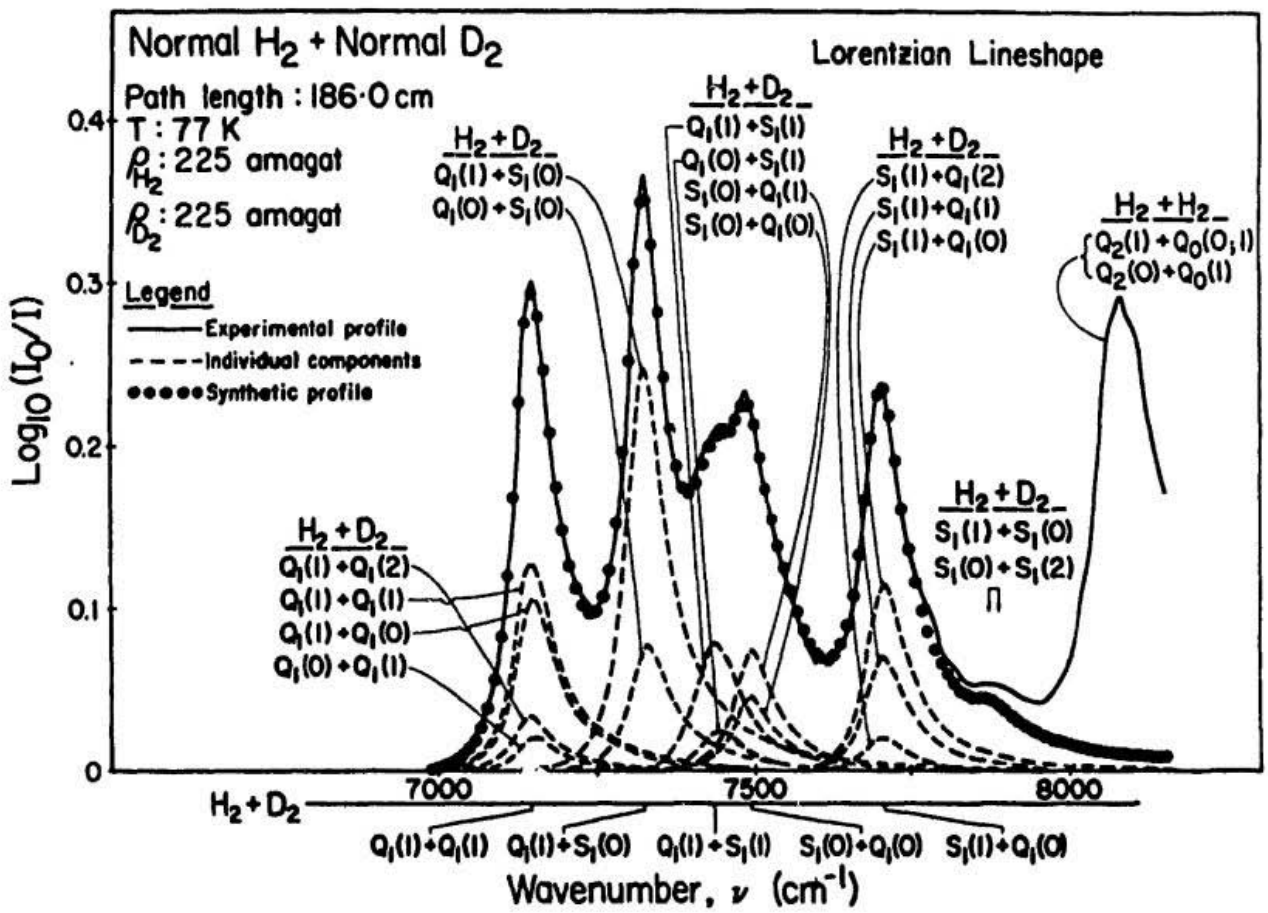

Figure 4.4: Analysis of an absorption profile of $H_2 + D_2$ at a total density of 450 amagat (with a partial density ratio of H_2:D_2=1:1) at 77 K using Lorentzian lineshape function for the individual components.

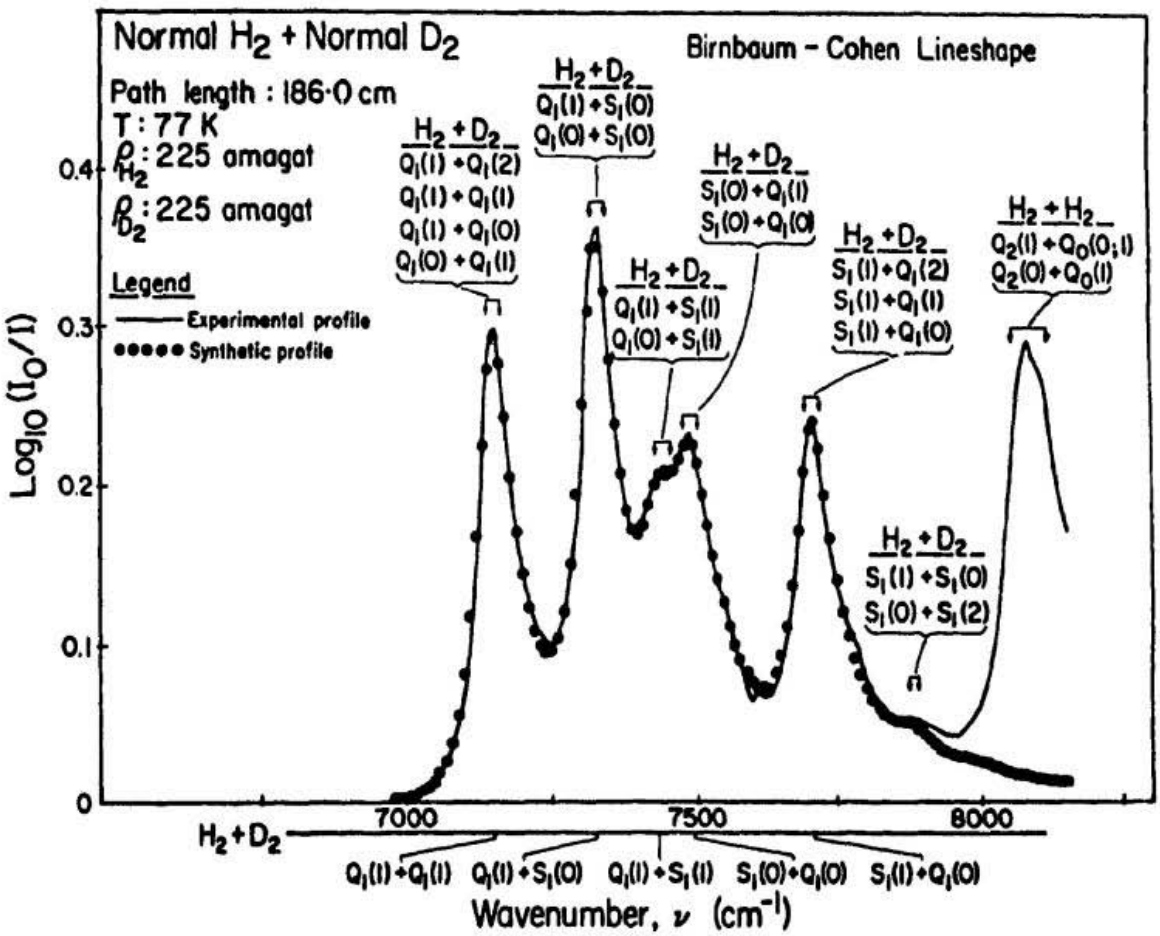

Figure 4.5: Analysis of an absorption profile of $H_2 + D_2$ at a total density of 450 amagat (with a partial density ratio of H_2:D_2=1:1) at 77 K using Birnbaum-Cohen lineshape function for the individual components.

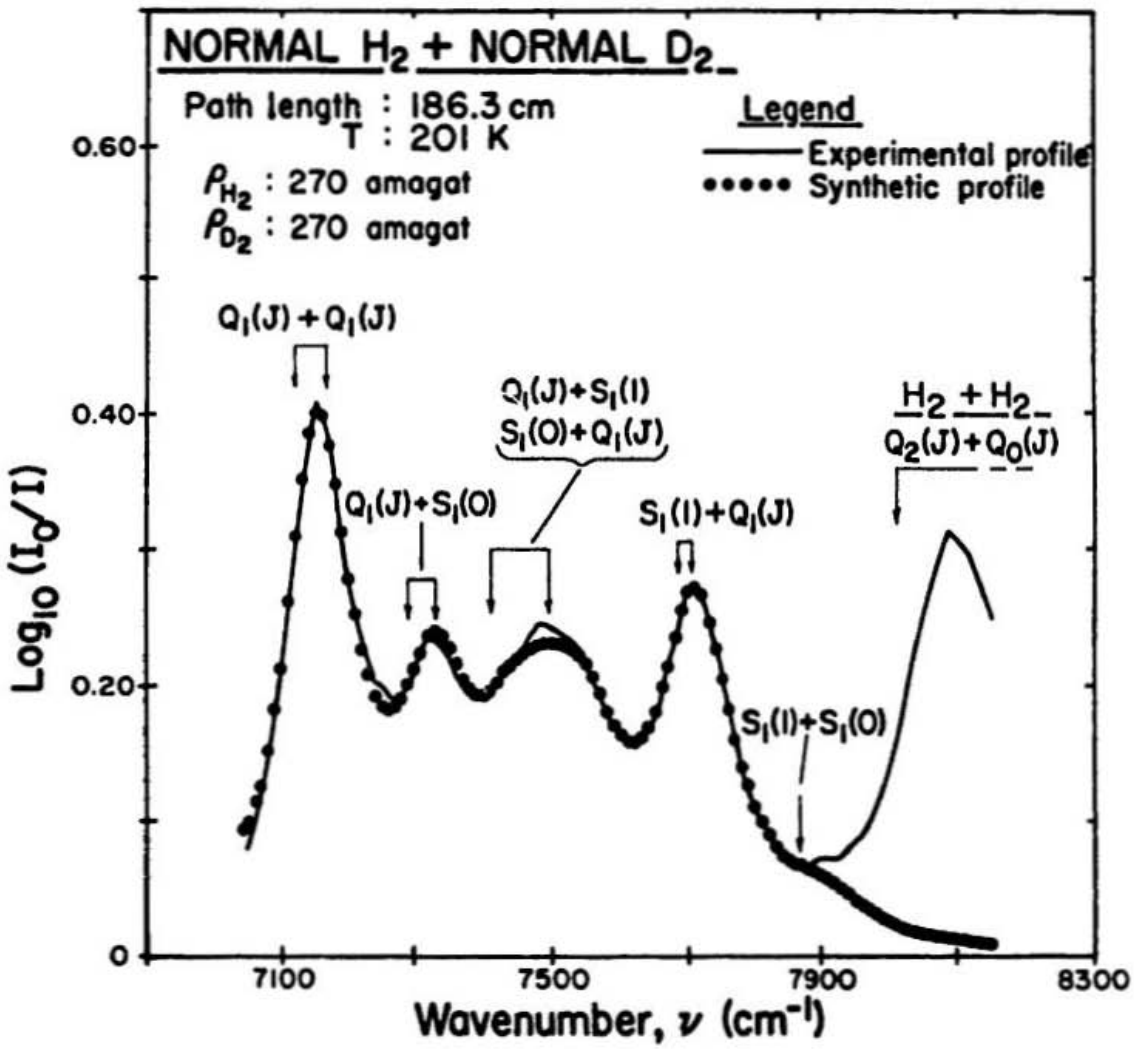

Figure 4.6: Analysis of an absorption profile of $H_2 + D_2$ at a total density of 540 amagat (with a partial density ratio of H_2:D_2=1:1) at 201 K using Lorentzian lineshape function for the individual components. For the explanation of double transitions, see caption of Figure 4.1.

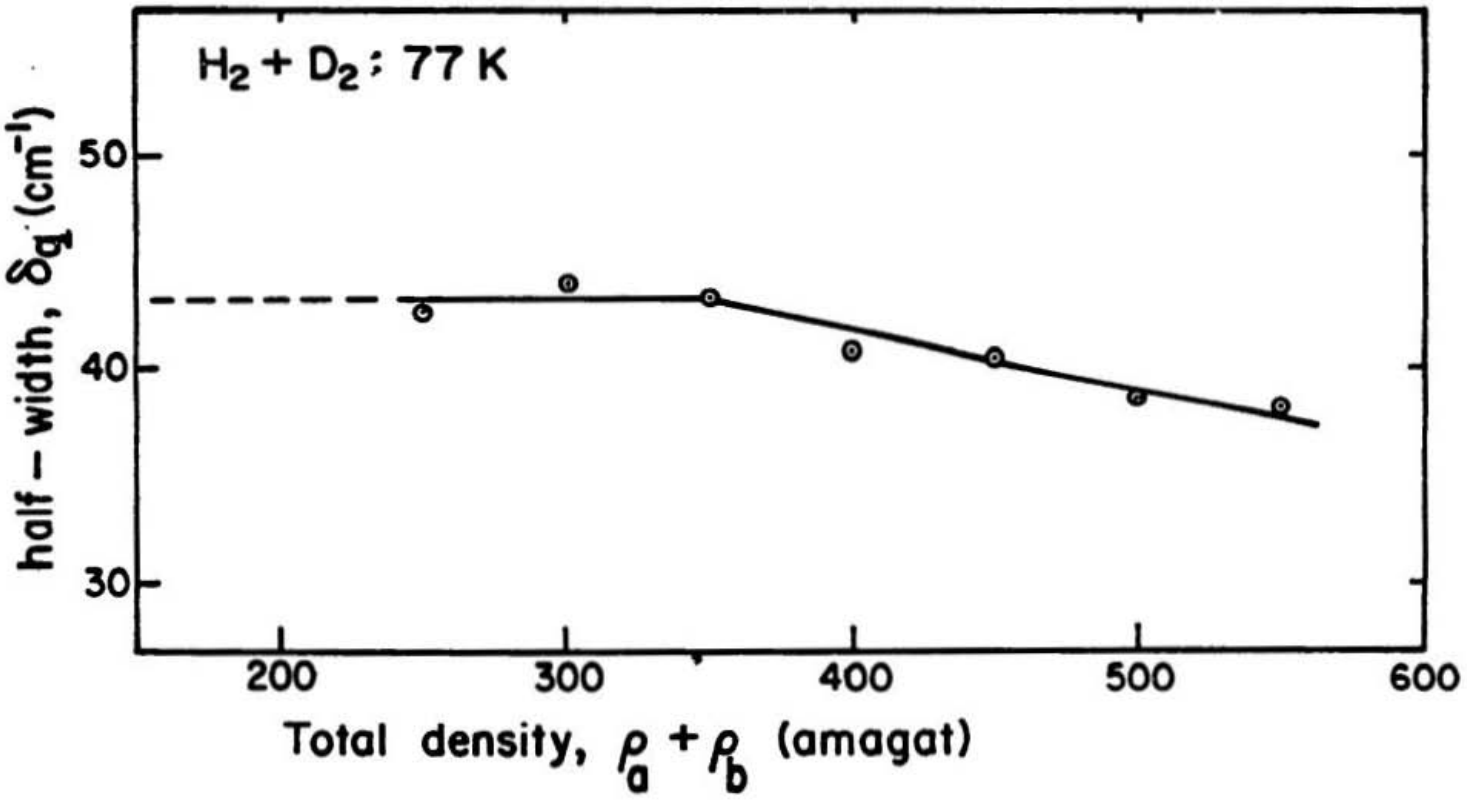

Figure 4.7: The quadrupolar half-width δ_q versus the total density of the binary mixture of H_2 and D_2.

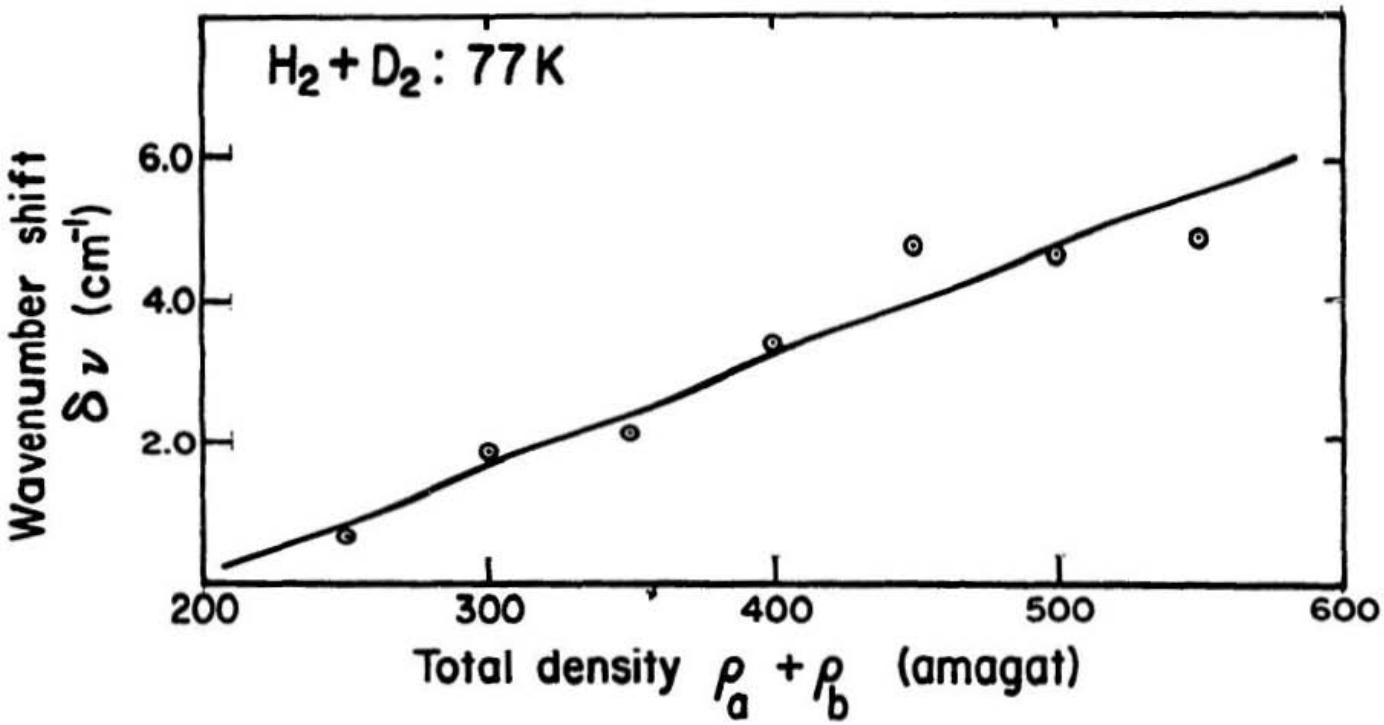

Figure 4.8: The wavenumber shift $\delta\nu$ versus the total density of the binary mixture of H_2 and D_2.

H_2 fundamental band in H_2-Ar mixtures. These authors found that the half-width at 152 K remained constant for Ar densities up to 300 amagat and then decreases approximately linearly from 55 cm^{-1} to 25 cm^{-1} at 820 amagat. Later Mactaggart et al. (1973) studied the pressure narrowing in several quadrupolar lines of the collision-induced fundamental band of H_2 in $H_2 - Ar$, $H_2 - Kr$, and $H_2 - Xe$ binary mixtures. In the double transitions of the type $S_{\Delta v}(J) + S_{\Delta v}(J)$ in H_2 first overtone region in the pure gas van Nostrand (1983) also observed the decrease of the half-width with the density of the gas in the density range 640–940 amagat. The theoretical explanation of the pressure narrowing effect at high gas densities was given by Zaidi and Van Kranendonk (1971) as due to the diffusion of H_2 molecules in the foreign gas. In fact the pressure narrowing effect can be understood from basic physics that at high Ar densities the H_2 molecules have longer effective collision duration because of multiple collisions with Ar atoms and thus the half-width decreases. In Fig. 4.8, the wavenumber shift $\delta\nu$ is seen to increase linearly with the total density of the mixture. For the absorption profile shown in Fig. 4.5 in which the Birnbaum-Cohen line-shape function was used to fit the synthetic profile to the experimental profile, the half-widths δ_1 and δ_2 were found to be 40.4 cm^{-1} and 371.6 cm^{-1}, respectively.

4.3 Absorption Coefficients

In collision-induced absorption the absorption coefficient $\alpha(\nu)$ at a given wavenumber ν (in cm^{-1}) is given by Eq.(3.2), (see Section 3.1). However, as explained in Chapter 2, the experimental profile of a collision-induced absorption spectrum is usually a plot of the quantity $log_{10}[I_0(\nu)/I(\nu)]$ versus the wavenumber ν. Therefore

Table 4.4: Results of profile analysis using Lorentzian lineshape. T = 77 K.

Total density (amagat)	Half-width δ_q (cm^{-1})	Wavenumber shift $\delta\nu$ (cm^{-1})
250	43.8	0.7
300	42.4	1.8
350	43.2	2.1
400	40.7	3.3
450	40.4	4.7
500	38.4	4.6
550	37.9	4.8

the following expression for $\alpha(\nu)$ is usually used instead,

$$\alpha(\nu) = (ln10/l)log_{10}[I_0(\nu)/I(\nu)] . \tag{4.10}$$

The integrated absorption coefficient $\int \alpha(\nu)d\nu$ can be written as

$$\int \alpha(\nu)d\nu = (ln10/l)\int log_{10}[I_0(\nu)/I(\nu)]d\nu . \tag{4.11}$$

Since the area under the profile of the plot of $log_{10}[I_0(\nu)/I(\nu)]$ versus ν is equal to $\int log_{10}[I_0(\nu)/I(\nu)]d\nu$, from Eq. (4.8) the integrated absorption coefficient can be expressed as

$$\int \alpha(\nu)d\nu = (ln_{10}/l)(area\ under\ the\ curve) \tag{4.12}$$

In the present study the partial densities of H_2 and D_2 in the mixture were always made equal and the integrated absorption coefficient can be expressed as a power series in densities (see Eq. (3.16)),

$$\int \alpha(\nu)d\nu = \alpha_1\rho^2 + (\alpha_{2ab} + \alpha_{a2b})\rho^3 + \cdots \tag{4.13}$$

Table 4.5: Absorption coefficients* for double fundamental transitions in the H_2-D_2 mixtures.

T (K)	Binary Absorption Coeff. α_1 $(10^{-5} cm^{-2} amagat^{-2})$	Ternary Absorption Coeff. α_2 $(10^{-8} cm^{-2} amagat^{-3})$
77	3.0± 0.1	1.2± 0.5
201	3.3± 0.5	0.1± 2.0

* The errors quoted are standard errors.

where ρ is the partial density of H_2 or D_2. Eq. (4.13) can be written in the following form,

$$(1/\rho^2) \int \alpha(\nu) d\nu = \alpha_1 + \alpha_2 \rho + \cdots , \tag{4.14}$$

where $\alpha_2 = \alpha_{2ab} + \alpha_{a2b}$ is the total ternary absorption coefficient.

If the densities of the gases are not too high then four-body and higher order collisions will be rare and terms in ρ^4 and higher can be neglected in Eq. (4.13). Plots of $(1/\rho^2) \int \alpha(\nu) d\nu$ against ρ are shown in Fig. 4.9 and are found to be straight lines. The ordinate-intercept α_1 and the slope α_2 were obtained from a linear least squares fit of the data. The binary and ternary absorption coefficients for double fundamental transitions in H_2-D_2 mixture at 77 K and 201 K are presented in Table 4.5.

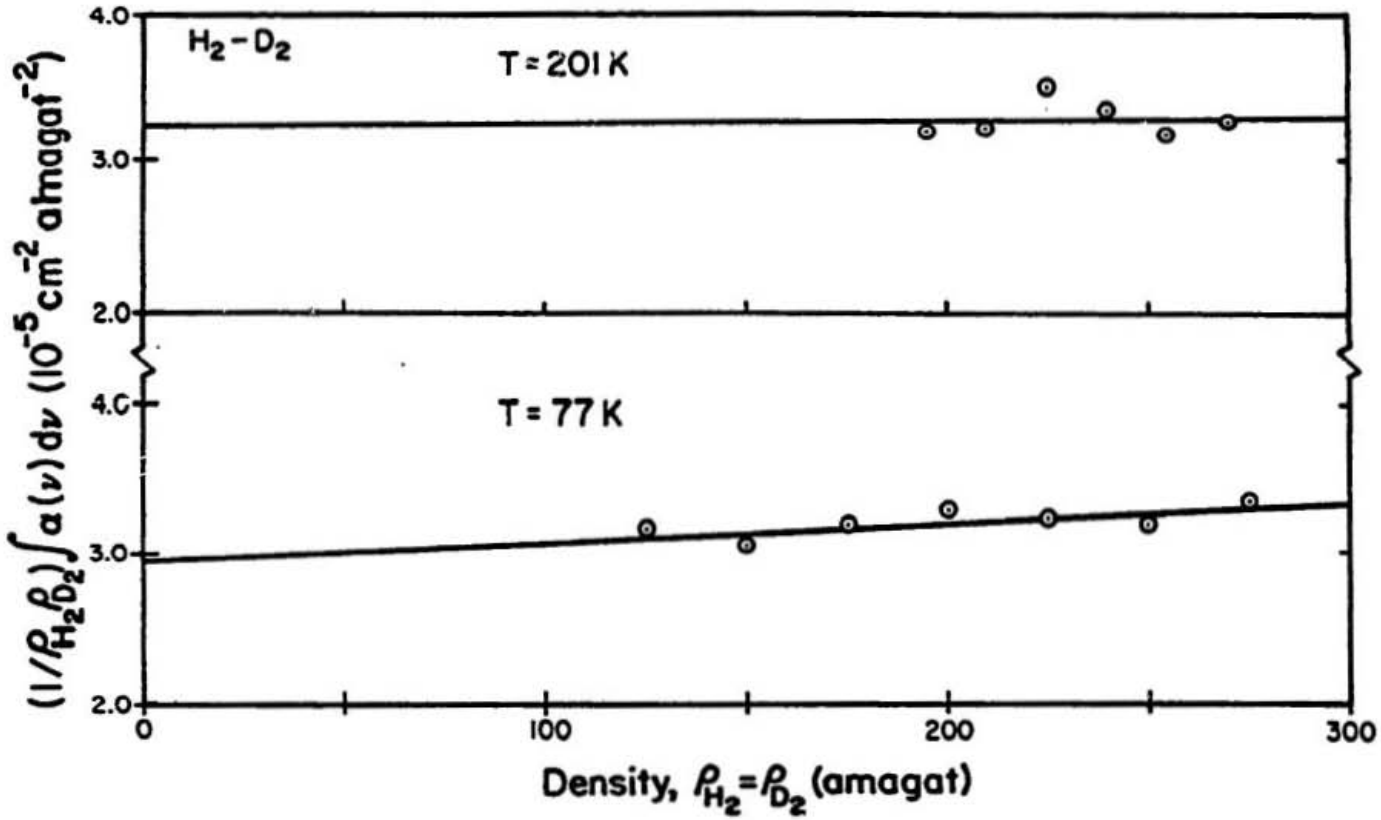

Figure 4.9: A plot of $(1/\rho_{H_2}\rho_{D_2})\int\alpha(\nu)d\nu$ versus $\rho_{H_2}(=\rho_{D_2})$ for the profiles of the double fundamental transitions of $H_2 + D_2$ at 77 K and 201 K.

Chapter 5

Hexadecapole-Induced U($\Delta J = +4$) Transitions in the Fundamental Band of H_2 in H_2-Ar Mixtures

5.1 Introduction

The hexadecapole-induced U transitions of the form $U_1(J)$ and $Q_1(J) + U_0(J)$ corresponding to the rotational selection rule $\Delta J = +4$ were first observed by Gibbs et al. (1974) in the fundamental band of H_2 in the gas phase at 195 K. Reddy et al. (1980) later studied these transitions in more detail at 77 K. Prasad et al. (1978) first observed the U transitions in the fundamental band of solid H_2 in this laboratory. In the present work the U transitions in the enhancement fundamental band of H_2 in the $H_2 - Ar$ mixtures at 296 K is reported for the first time.

5.2 Absorption Profiles

For the purpose of comparison, a collision-induced enhancement absorption profile (Babu, 1986) of the fundamental band of H_2 in an $H_2 - Ar$ mixture at ρ_{H_2}=4.3 amagat and ρ_{Ar}=151.7 amagat at 296 K is reproduced in Fig. 5.1. In this profile the transitions $O_1(2)$, $Q_1(J)$ for $J = 0$ to 3 and $S_1(J)$ for $J = 0$ to 3 are observed. The collision-induced enhancement absorption profiles of the U-branch transitions in the fundamental band of H_2 in $H_2 - Ar$ mixtures at 296 K were obtained using the apparatus and experimental techniques described in detail in Chapter 2. The U-branch occurs on the high wavenumber wing of the fundamental band. The spectrometer slit width maintained at 45 μm gave a spectral resolution of ~ 9 cm^{-1} at 5695 cm^{-1}, the calculated wavenumber of the $U_1(1)$ transition of H_2. The enhancement absorption spectra were recorded with a base density of 72.3 amagat of H_2 for several partial densities of Ar in the range 340-440 amagat. Three representative enhancement absorption profiles of the fundamental band of H_2 in the spectral region 5400-6200 cm^{-1} for Ar densities of 382, 422, and 440 amagat are shown in Fig. 5.2. The positions of the transitions $U_1(1)$ (5695.4 cm^{-1}), $Q_1(1) + U_0(1)$ (5776.9 cm^{-1}), $Q_1(0) + U_0(1)$ (5782.8 cm^{-1}), and $U_1(2)$ (6100.0 cm^{-1}), calculated from the constants of the free H_2 molecules (Bragg et al., 1982) are shown along the wavenumber axis. The transition $U_1(0)$ (5271.4 cm^{-1}) is completely masked by the strong absorption in the wings of the overlap and quadrupolar components of the fundamental band and therefore is not shown in this figure.

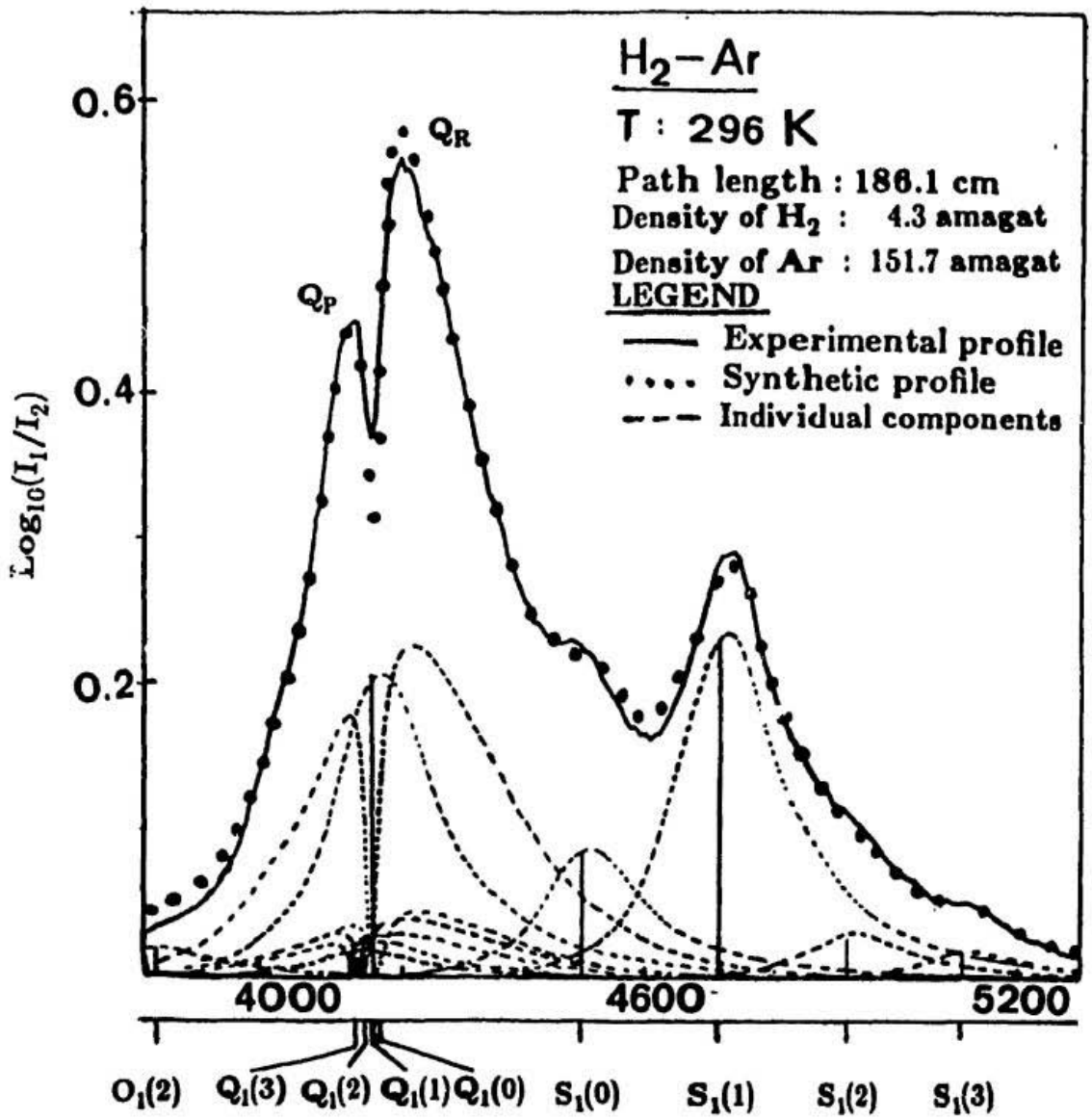

Figure 5.1: A collision-induced enhancement absorption profile of the fundamental band of H_2 in an $H_2 - Ar$ mixture of ρ_{H_2}=4.3 amagat and ρ_{Ar}=151.7 amagat at 296 K (adopted from Babu,1986).

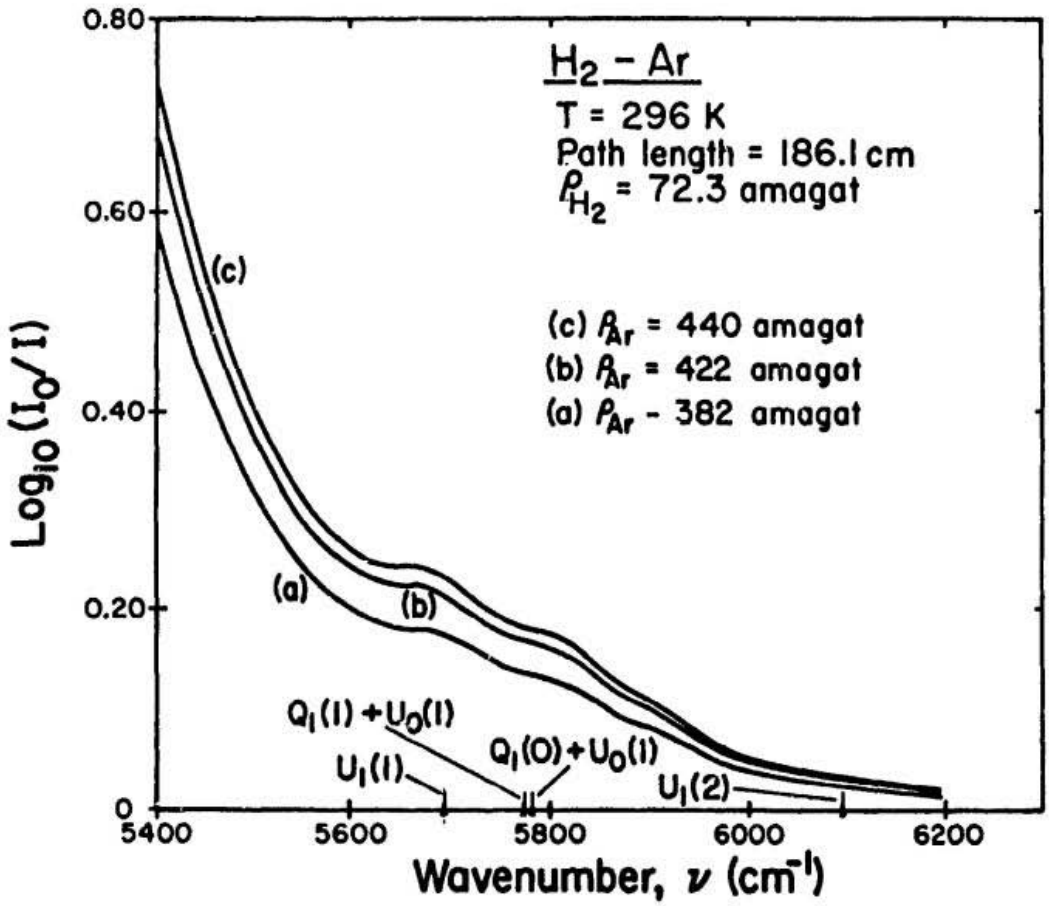

Figure 5.2: Collision-induced enhancement absorption profiles of the fundamental band of H_2 in $H_2 - Ar$ mixtures of ρ_{H_2}=72.3 amagat and ρ_{Ar}=382, 422, and 440 amagat at 296 K.

5.3 Profile Analysis

(a) The absorption coefficient and the line shapes

The absorption coefficient due to all possible U transitions at a given wavenumber ν of the fundamental band arising from the hexadecapolar induction can be written as (see Eq. (3.43))

$$\alpha(\nu)_{hexa} = \sum_m \left[\frac{\tilde{\alpha}^0_{3m}\nu}{1 + exp(-hc\Delta\nu/kT)} \right] W_3(\Delta\nu) \,, \tag{5.1}$$

where $\alpha(\nu)_{hexa} \equiv \tilde{\alpha}(\nu)_{hexa} \cdot \nu$, and the subscript 3 represents the hexadecapolar induction (the subscript 0, 1, and 2 represents the overlap induction, the quadrupolar induction with isotropic polarizability, and the quadrupolar induction with anisotropic polarizability, respectively). The line-shape function $W_3(\Delta\nu)$ is usually represented by the Lorentzian line-shape function (see Chapter 3) ,

$$W_3(\Delta\nu) = \frac{1}{1 + (\Delta\nu/\delta_u)^2} \,, \tag{5.2}$$

where δ_u is the half-width at half-height and $\Delta\nu = \nu - \nu_m$, ν_m being the molecular wavenumber of the mth transition.

The U transitions in the enhancement fundamental band of H_2 at 296 K in the spectral region $\sim 5700\ cm^{-1}$ lie on the strong high wavenumber tail of the $S_1(3)$ transition ($5108.4\ cm^{-1}$), where the overlap and the other quadrupolar transitions also make considerable contributions to the total absorption of the band. The absorption coefficient due to the total wing of the overlap and quadrupolar contributions in the spectral region 5400–6200 cm^{-1} can be expressed by

$$\alpha(\nu)_{wing} = \frac{a_1\nu}{1 + exp(-hc\delta\nu/kT)} \cdot \frac{1}{1 + (\delta\nu/a_2)^2 + (\delta\nu/a_3)^4} \,, \tag{5.3}$$

where a_1, a_2, and a_3 are adjustable parameters and $\delta\nu = \nu - \nu_s$, ν_s being the molecular wavenumber of $S_1(3)$. The line-shape function in the absorption coefficient of the overlap-quadrupolar wing has been expressed as a modified Lorentzian form which includes the additional term $(\delta\nu/a_3)^4$ in the denominator to account for the faster decrease of the absorption intensity with wavenumber in the observed wing than that given by the ordinary Lorentzian form.

(b) Transition intensities

The integrated binary absorption coefficient of the *mth* hexadecapole-induced transition of H_2 in $H_2 - Ar$ mixtures can be written readily using the general expression for the integrated binary absorption coefficient of the *Lth* order multipole-induced transition by letting $L = 4$ in Eqs. (3.34) to (3.41).

$$\begin{aligned}
\tilde{\alpha}_{4m} &= \frac{1}{\rho_a \rho_b} \int \frac{\alpha_m(\nu)}{\nu} d\nu \\
&= \frac{4\pi^3 e^2}{3hc} n_0^2 a_0^5 \left(\frac{a_0}{\sigma}\right)^9 \tilde{J}_4 X_{4m} \qquad (5.4) \\
\tilde{J}_4 &= 20\pi \int_0^\infty x^{-12} g_0(x) x^2 dx \\
&= 20\pi J_{12} \qquad (5.5) \\
J_{12} &= J_{12}^{CL} + (\Lambda^*)^2 J_{12}^{(1)} + (\Lambda^*)^4 J_{12}^{(2)} \qquad (5.6)
\end{aligned}$$

The absorption intensities of the hexadecapole-induced transitions of H_2 in $H_2 - Ar$ mixtures at 296 K were calculated by using these formulas and the matrix elements of the hexadecapole moment $<|\ H\ |>$ and the polarizability $<|\ \alpha\ |>$ of H_2 and Ar molecules, respectively, available in the literature (Karl et al., 1975). The relative intensities of these transitions were obtained from the absolute intensities by assigning a relative intensity of 1.0000 to the strongest transition ($U_1(1)$).

When the experimental profiles were analyzed (see next subsection) using the

Table 5.1: Theoretical enhancement absorption intensities of $U_1(J)$ transitions of H_2 by Ar at 296 K.

Transition	Wavenumber (cm^{-1})	Absolute Intensity $(10^{-10} cm^{-1} amagat^{-2})$	Relative Intensity
$U_1(0)$	5271.4	0.532	0.409
$U_1(1)$	5695.4	1.300	1.000
$U_1(2)$	6100.0	0.163	0.125
$U_1(3)$	6482.1	0.096	0.074

theoretical absorption intensities of Table 5.1, a large discrepancy between the experimental and the synthetic profiles was found. To account for this discrepancy, absorption intensities due to double transitions of the type $Q_1(1) + U_0(1)$ and $Q_1(0) + U_0(1)$ must be considered. In the enhancement spectra of the fundamental band of a diatomic gas such as H_2 in its binary mixtures with an inert gas such as Ar, if the density of the inert gas is not too high, then only single transitions such as $U_1(1)$ of H_2 will occur. A single transition will occur as a result of a binary collision between an H_2 molecule and an Ar molecule. The hexadecapole moment of the H_2 molecule induces an electric dipole moment in the Ar molecule which causes the absorption. When the densities of the inert gas become high enough, double transitions of the type $Q_1(1) + U_0(1)$ and $Q_1(0) + U_0(1)$ begin to appear in the spectra. The origin of these double transitions can be explained by the following argument (see, for example, Mactaggart, 1971). As the densities of the Ar gas become high enough, it is possible that two or more H_2 molecules are trapped in a temporary "cage" of Ar molecules. The interaction between pairs of H_2 molecules in the cage results in the double transitions. That is, one H_2 molecule makes a pure

vibrational transition while its collision partner makes a pure rotational transition. The relative intensities of the two double transitions $Q_1(1) + U_0(1)$ (5776.9 cm^{-1}) and $Q_1(0) + U_0(1)$ (5782.8 cm^{-1}) are assumed to be in the same ratio as that of the single transitions $Q_1(1)$ and $Q_1(0)$, i.e., 3:1 for H_2. Hence the relative intensities of $Q_1(1) + U_0(1)$ and $Q_1(0) + U_0(1)$ are 1.0000 and 0.3333, respectively.

In the profile analysis of the next subsection, the intensity ratio of the strongest double transition $Q_1(1) + U_0(1)$ to the strongest single transition $U_1(1)$ is taken as an additional adjustable parameter in the computer program.

(c) Method of profile analysis

The enhancement absorption profiles of H_2 in $H_2 - Ar$ mixtures in the spectral region 5400-6200 cm^{-1} have been analyzed using a computer program similar to the first program used in Chapter 3 (see Appendix A). There are ten adjustable parameters, $a_1, a_2, \cdots, a_{10}$ in the program. The first three parameters, a_1, a_2, and a_3 have been described previously in the expression of $\alpha(\nu)_{wing}$ (Eq. (5.3)). The remaining seven parameters represent intensity factors, half-widths, and possible shifts in the molecular wavenumber ν_m of the single and double U transitions and the possible shift of the molecular wavenumber ν_s of the quadrupolar transition $S_1(3)$ in the overlap-quadrupolar wing.

(d) Results

Five absorption profiles have been analyzed using the above mentioned computer program. A representative example of the analysis of an experimental profile with the synthetic profile resulting from the four individual components of the U group and the wing of overlap and quadrupolar components of the band is shown in Fig. 5.3. From this figure we see that the agreement between the experimental

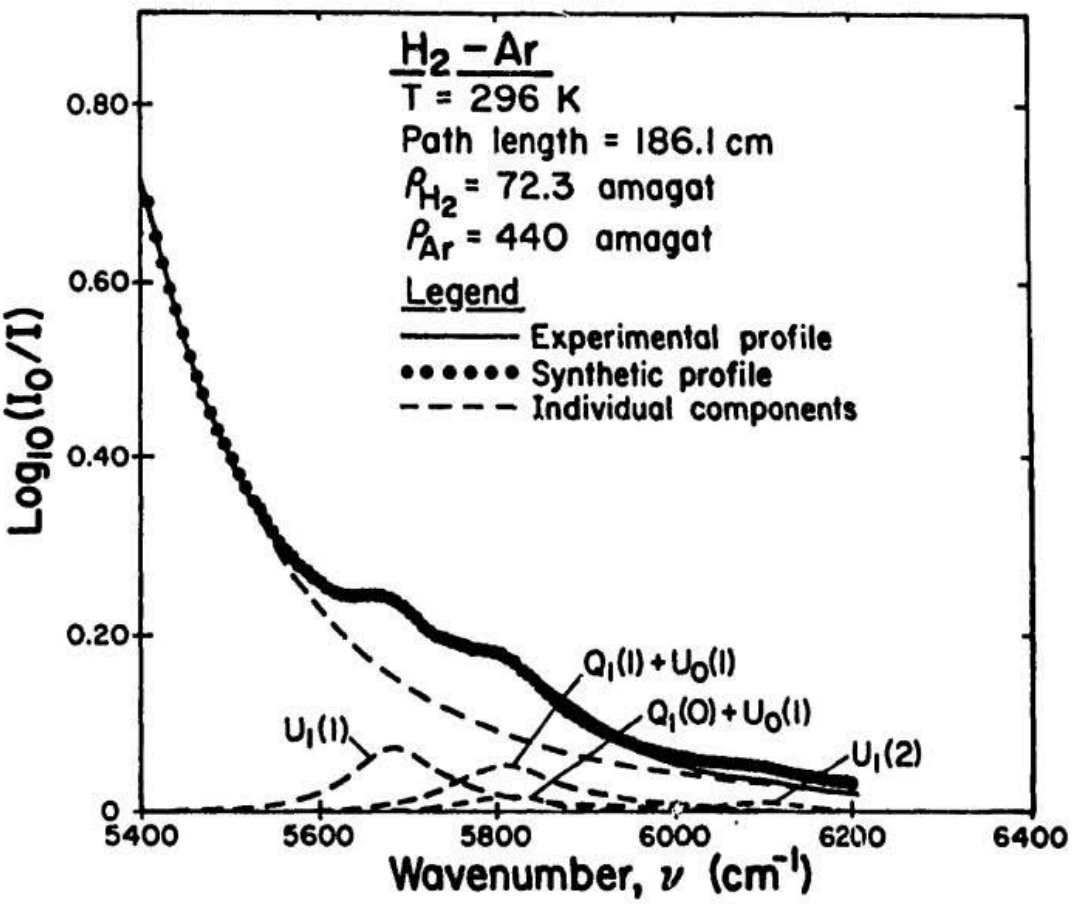

Figure 5.3: Analysis of a collision-induced enhancement absorption profile of the fundamental band of H_2 in $H_2 - Ar$ mixture at 296 K.

Table 5.2: Results of the profile analysis of the enhancement $U_1(1)$ transition of H_2 in $H_2 - Ar$ mixtures at 296 K.

	Half-width (cm^{-1})	Collision duration (10^{-14} s)
Single transition	60 ± 2	8.8
Double transition	75 ± 4	7.1

and synthetic profiles is good except in the region beyond $\sim$ 6000 cm^{-1}. The characteristic half-width parameters δ_u for single and double transitions obtained from the analysis are 60 $\pm$ 2 cm^{-1} and 75 $\pm$ 4 cm^{-1}, repectively. The corresponding collision durations $\tau(= 1/2\pi c\delta)$ are 8.8×10^{-14} s and 7.1×10^{-14} s, respectively. These results are presented in Table 5.2.

From the results of the analyses of the experimental profiles one can calculate the integrated absorption ceofficients $\int \alpha_{en}(\nu)d\nu$ of the $U_1(1)$ transition from the areas under its band profile.

$$\int \alpha_{en}(\nu)d\nu = (ln10/l)\int [log_{10}I_1(\nu)/I_2(\nu)]d\nu \tag{5.7}$$

$$= (ln10/l)(area\ under\ the\ curve) \tag{5.8}$$

The integrated absorption coefficient can be expanded in terms of powers of the densities of H_2 (ρ_a) and Ar (ρ_b) as the following

$$\int \alpha_{en}(\nu)d\nu = \alpha_{1b}\rho_a\rho_b + \alpha_{2b}\rho_a\rho_b^2 \tag{5.9}$$

or

$$(1/\rho_a\rho_b)\int \alpha_{en}(\nu)d\nu = \alpha_{1b} + \alpha_{2b}\rho_b \tag{5.10}$$

where α_{1b} and α_{2b} are the binary and ternary absorption coefficient respectively.

Table 5.3: Absorption coefficient of the enhancement $U_1(1)$ transition of H_2 by Ar at 296 K.

Binary absorption coefficient		Ternary absorption coefficient
α_{1b}	$\tilde{\alpha}_{1b}$	α_{2b}
$(10^{-7} cm^{-2} amagat^{-2})$	$(10^{-39} cm^6 s^{-1})$	$(10^{-9} cm^{-2} amagat^{-3})$
6.9 ± 0.6	5.0 ± 0.4	9.2 ± 0.4

These two quantities can be obtained from the intercept and the slope, respectively, of the plot of $(1/\rho_a\rho_b)\int \alpha_{en}(\nu)d\nu$ *vs.* ρ_b.

This plot is shown in Fig. 5.4. The numerical values of α_{1b} and α_{2b} were obtained from the linear least-squares fit of the data points. These results are given in Table 5.3.

The binary absorption coefficient $\tilde{\alpha}_{1b}$ expressed in $cm^6 s^{-1}$ is related to α_{1b} by the relation $\tilde{\alpha}_{1b} = (c/n_0^2)\alpha_{1b}/\bar{\nu}$, where n_0 is the Loschmidt's number $(2.687 \times 10^{19} cm^{-3})$ and $\bar{\nu}$ is the center of absorption of the $U_1(1)$ transition at 296 K. The quantity $\bar{\nu}$ is defined as $\int \alpha_{en}(\nu)d\nu / \int(\alpha_{en}(\nu)/\nu)d\nu$ and was found to be equal to 5722 cm^{-1} for the enhancement $U_1(1)$ transition of H_2 by Ar at 296 K. The value of $\tilde{\alpha}_{1b}$ for $U_1(1)$ is also given in Table 5.3. The experimental value of $\alpha_{1b}/\bar{\nu}$ is $(6.9 \pm 0.6) \times 10^{-7}/5722 = (1.2 \pm 0.1) \times 10^{-10} cm^{-1} amagat^{-2}$. The theoretical binary absorption coefficient of the enhancement $U_1(1)$ transition of H_2 by Ar at 296 K was calculated previously (see section 5.3 (b) and Table 5.1) to be $1.30 \times 10^{-10} cm^{-1} amagat^{-2}$. Thus the experimental value of $\alpha_{1b}/\bar{\nu}$ agrees well with the theoretical value.

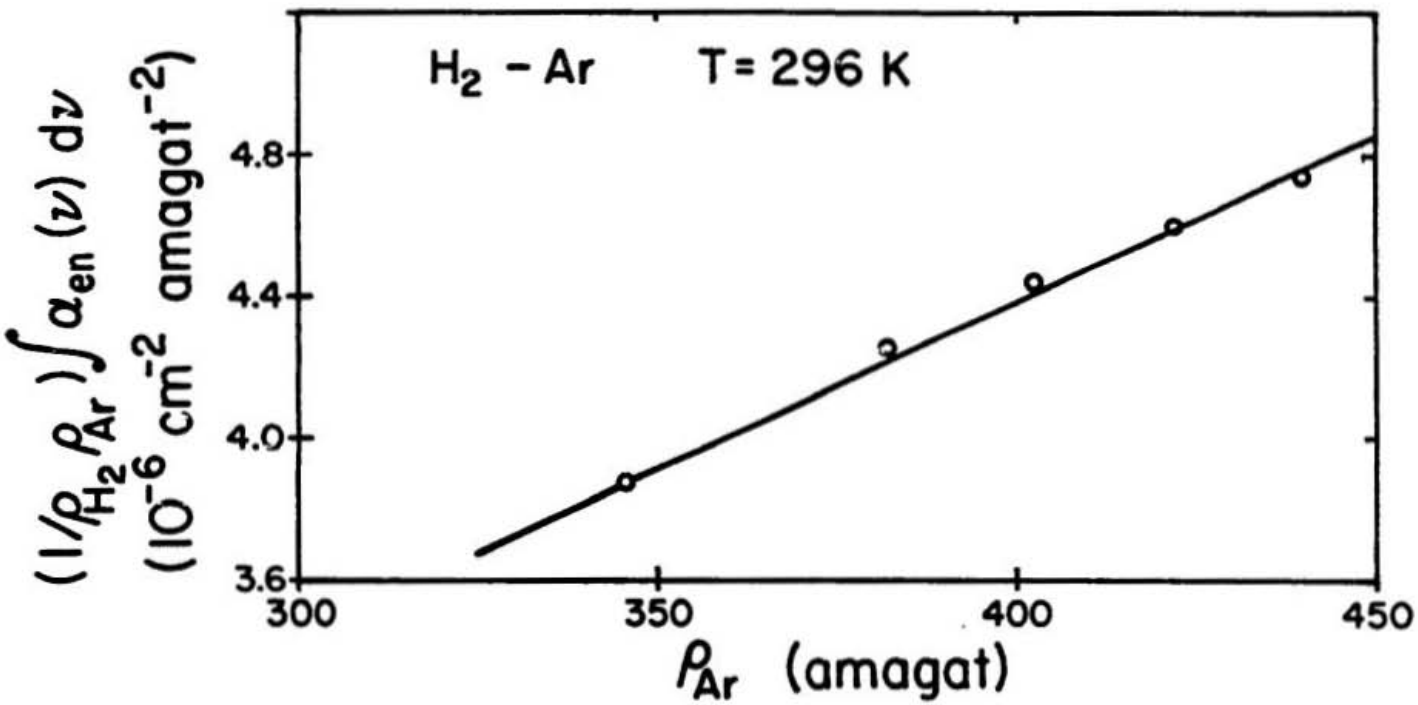

Figure 5.4: Plot of $(1/\rho_{H_2}\rho_{Ar})\int \alpha_{en}(\nu)d\nu$ versus ρ_{Ar} for collision-induced enhancement absorption of the fundamental band of H_2 in $H_2 - Ar$ mixtures of ρ_{H_2}=72.3 amagat at 296 K.

Chapter 6

Collision-Induced Absorption Spectra of HD in the First Overtone Region

6.1 Introduction

The collision-induced absorption spectrum of H_2 in its first overtone region was first observed by Welsh et al. (1951). Since then Hare and Welsh (1958), Watanabe et al. (1971), Watanabe (1971), McKellar and Welsh (1971), Silvaggio et al. (1981), and Van Nostrand (1983) have studied this spectrum at various temperatures and densities. The collision-induced absorption spectrum of D_2 in its first overtone region was first studied by Reddy and Kuo (1971) at room temperature in the pure gas and in binary mixtures of D_2 with argon and nitrogen. Gillard (1983) studied this spectrum in pure D_2 in more detail at various temperatures and densities.

The present chapter is devoted to the study of the collision-induced absorption spectrum of HD in its first overtone region at 77 K. This spectrum was observed for the first time in the present work. The absorption profiles were analyzed and results were compared with those of H_2 and D_2 to investigate the differences be-

tween the spectra of the heteronuclear and the homonuclear diatomic molecules. For the purpose of comparison, three collision-induced absorption profiles of H_2 in the first overtone region at three different densities at 77 K (Van Nostrand, 1983) are reproduced in Fig. 6.1. Similarly, three profiles of D_2 also at 77 K (Gillard, 1983) are reproduced in Fig. 6.2. An absorption spectrum of the collision-induced fundamental band of HD at 298 K (Reddy and Prasad, 1977) is also shown in Fig. 6.3 where the analysis of the spectrum is also shown. Here the analysis shows a large contribution to the absorption intensity of the fundamental band of HD comes from the isotropic overlap induction mechanism and the presence of a prominent inter-collisional dip in the Q branch.

6.2 The Experimental Absorption Profiles

The apparatus and experimental technique described in detail in Chapter 2 were used to obtain the collision-induced absorption spectra of HD in the first overtone region at 77 K. The densities of the gas studied were in the range 130–320 amagat. Three representative CIA profiles of HD in the first overtone region at 77 K for densities 191, 250, and 311 amagat are presented in Fig. 6.4. The assignments of the observed absorption peaks are also shown in the same figure. The transitions include the allowed transitions $P_2(1), R_2(0)$, and $R_2(1)$ and the collision-induced transitions $Q_2(J)+Q_0(J), Q_1(J)+Q_1(J), Q_2(J)+S_0(J), S_2(J)+Q_0(J), Q_1(J)+S_1(J), S_2(J)+S_0(J)$, and $S_1(J)+S_1(J)$. The measured wavenumbers of the absorption peaks in the region of the first overtone band of HD and their assignments are presented in Table 6.1.

The peak at $\sim 8080\ cm^{-1}$ corresponds to the collision-induced absorption of H_2

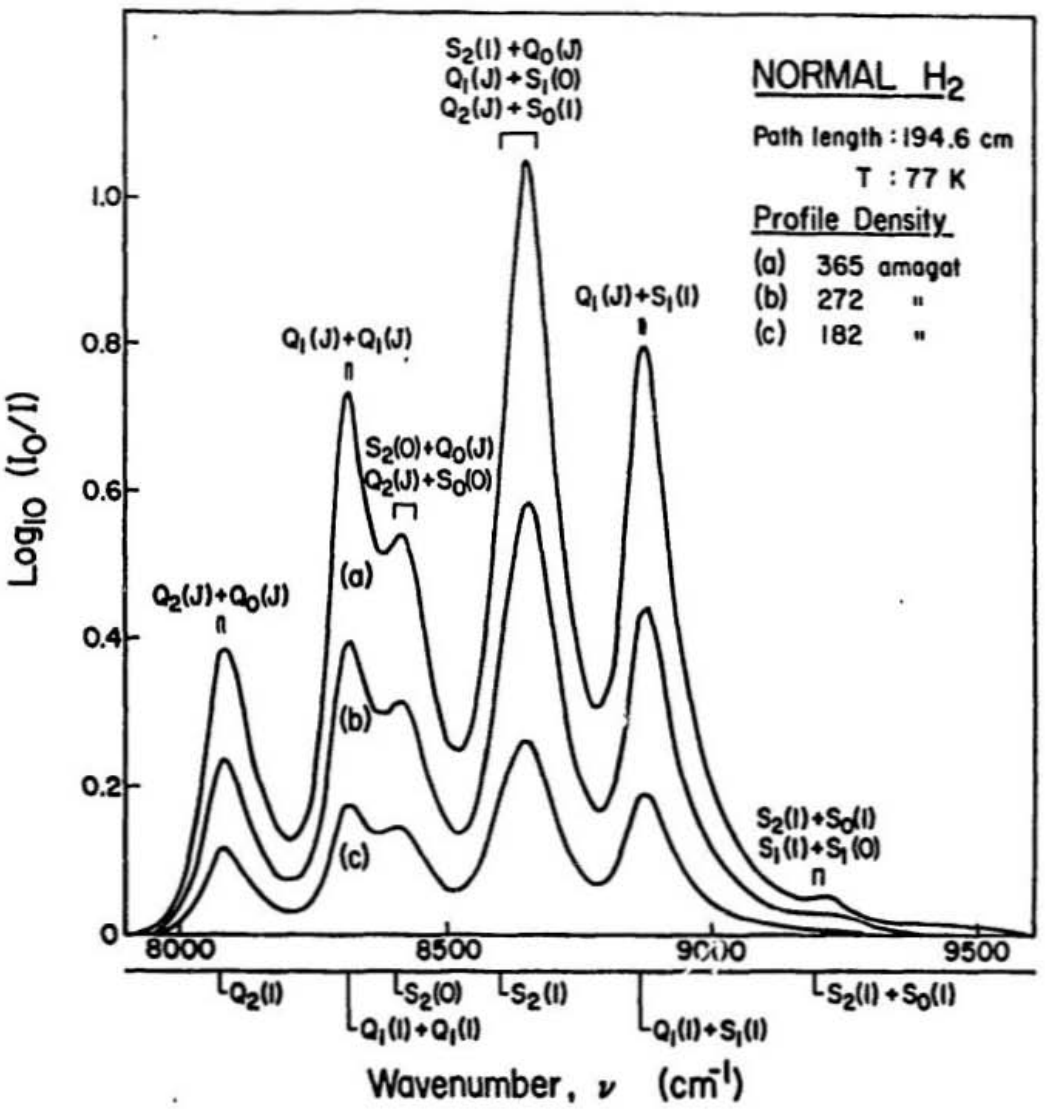

Figure 6.1: Collision-induced absorption profiles of H_2 in the first overtone region at three different densities of the gas at 77 K (adopted from van Nostrand, 1983).

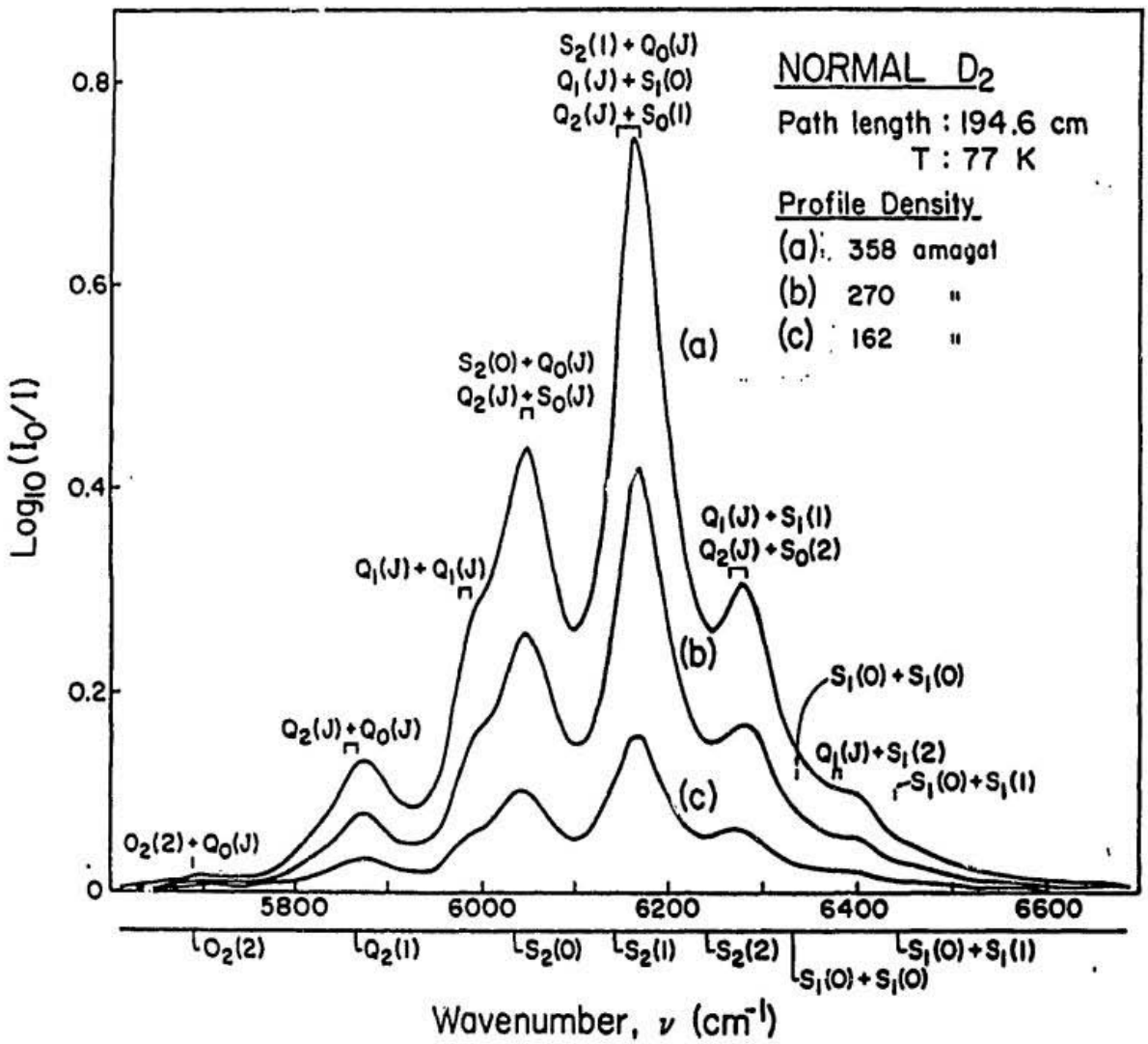

Figure 6.2: Collision-induced absorption profiles of D_2 in the first overtone region at three different densities of the gas at 77 K (adopted from Gillard, 1983).

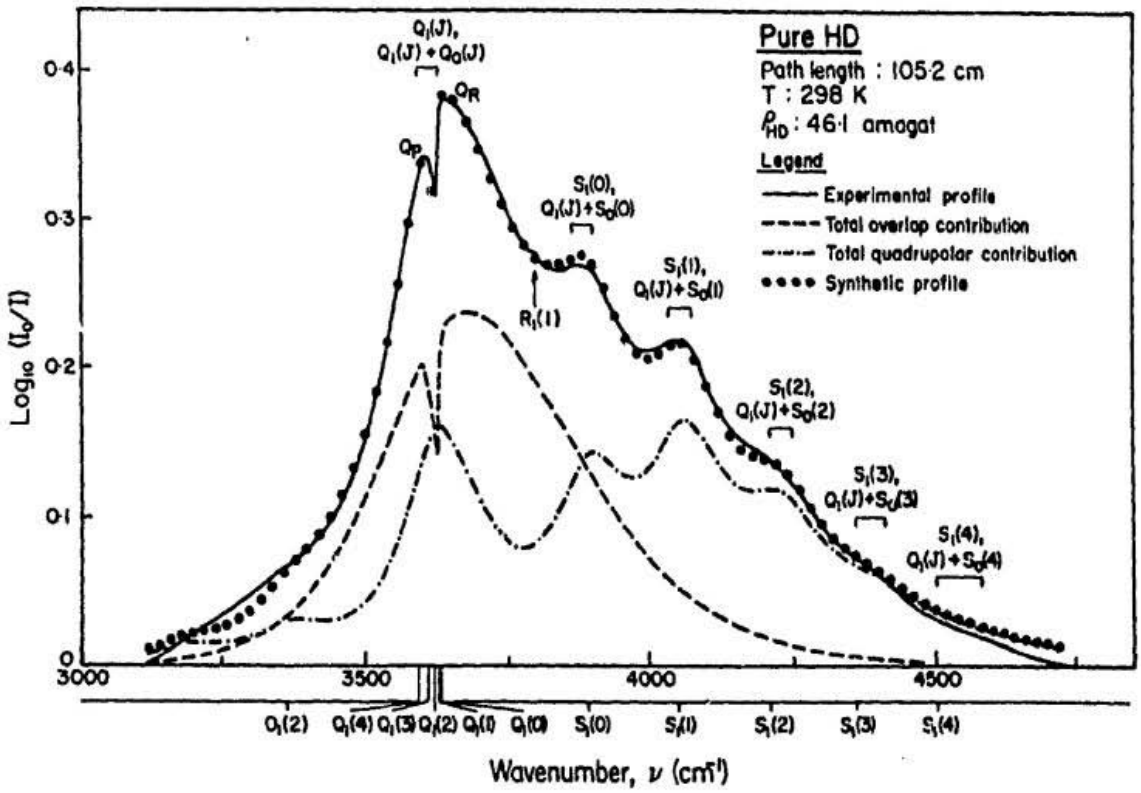

Figure 6.3: An absorption profile of the collision-induced fundamental band of HD at 298 K. The solid curve is the experimental profile. The computed contributions of the overlap and quadrupolar interactions to the total absorption intensity of the band are shown by the dashed- and dot-dashed curves, respectively. The dots represent the summation of these (adopted from Reddy and Prasad, 1977).

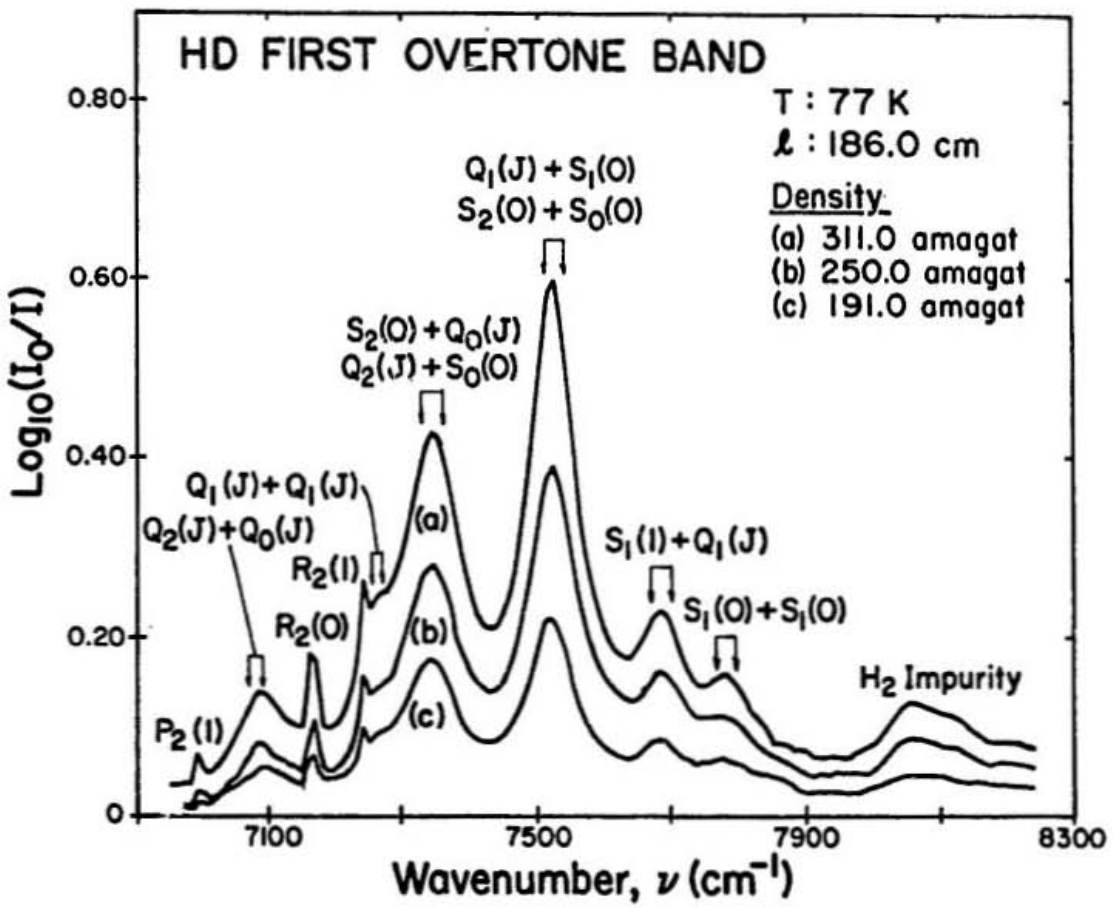

Figure 6.4: Absorption profiles of HD in the first overtone region at three different densities of the gas at 77 K.

Table 6.1: Assignments of the observed absorption peaks of the first overtone transitions of HD at 77 K.

Transition	Calculated wavenumber (cm^{-1})	Measured wavenumber (cm^{-1})
$P_2(1)$	6997.7	6997
$Q_2(1) + Q_0(2)$	7079.2	
$Q_2(0) + Q_0(2)$	7086.9	7089
$R_2(0)$	7168.5	7168
$R_2(1)$	7241.8	7241
$Q_2(2) + S_0(0)$	7331.1	
$S_2(0) + Q_0(0)$	7331.1	7333
$S_2(0) + Q_0(1)$	7331.1	
$S_2(0) + Q_0(2)$	7331.1	
$Q_1(2) + S_1(0)$	7508.3	
$Q_1(1) + S_1(0)$	7516.0	7517
$Q_1(0) + S_1(0)$	7519.8	
$Q_1(2) + S_1(1)$	7672.8	
$Q_1(1) + S_1(1)$	7680.5	7678
$Q_1(0) + S_1(1)$	7684.3	
$S_2(1) + S_0(0)$	7751.4	
$S_2(0) + S_0(1)$	7774.2	
$S_1(0) + S_1(0)$	7775.4	7776

which is present as an impurity in the HD gas and is assigned to the $Q_2(J) + Q_0(J)$ transitions of H_2.

The most obvious difference between the absorption spectra of the heteronuclear HD and the homonuclear H_2 and D_2 is, of course, the presence of the allowed transitions $P_2(1)$, $R_2(0)$, and $R_2(1)$ in the HD spectra . The similarity among these three absorption spectra is that none of them has the characteristic inter-collisional dip in the Q branch. As pointed out earlier the collision-induced fundamental bands have, in contrast, a large contribution from the isotropic overlap induction with characteristic dips in the Q branch (for example, see Fig. 6.3). Therefore in calculating the transition intensities of the collision-induced first overtone band of HD, the contribution of the isotropic overlap induction to the absorption intensity of the band can be neglected and those from the quadrupolar induction and the $\mathcal{L}$=3 anisotropic overlap induction (see Chapter 3, Section 3.2) should be taken into account.

6.3 Profile Analysis

As shown in Fig. 6.4, the absorption spectra of HD in the first overtone region have contribution to the absorption intensity from the allowed transitions in the low wavenumber end (below 7300 cm^{-1}), and from the first overtone transitions of H_2 impurity in the high wavenumber end (above 7800 cm^{-1}). Thus the synthetic profile in the spectral region 7300–7800 cm^{-1} where collision-induced first overtone transitions of HD only are present is fitted to the experimental profile. Once a satisfactory fit was obtained in this region, the resulting half-width parameter and the relative intensities of individual transitions were then used to obtain the synthetic profile in the entire spectral region of the first overtone band of HD.

(a) The line shapes

The absorption coefficient $\tilde{\alpha}(\nu)$ at a given wavenumber ν is given by (Eq. (3.43))

$$\tilde{\alpha}(\nu) = \sum_{m,n} \frac{\tilde{\alpha}^0_{nm} W_n(\Delta\nu)}{1 + exp(-hc\Delta\nu/kT)} \cdot \tag{6.1}$$

For the collision-induced first overtone transitions of HD, the lineshape function $W_n(\Delta\nu)$ is replaced by $W_q(\Delta\nu)$. Thus Eq. (6.1) simplifies to

$$\tilde{\alpha}(\nu) = \sum_{m} \frac{\tilde{\alpha}^0_{qm} W_q(\Delta\nu)}{1 + exp(-hc\Delta\nu/kT)} \cdot \tag{6.2}$$

In fitting the synthetic profiles to the observed profiles of the HD first overtone spectra, the Lorentzian line-shape function $W^L_q(\Delta\nu)$ (Eq. (3.47)) was found to give satisfactory results. It is represented as

$$W^L_q(\Delta\nu) = \frac{1}{1 + (\Delta\nu/\delta_q)^2} \cdot \tag{6.3}$$

(b) Transition intensities

Using the general expression for the integrated binary absorption coefficient of the Lth order multipole-induced transition given in Chapter 3, the integrated binary absorption coefficient of the mth quadrupole-induced first overtone transition of the HD molecule is written as

$$\begin{aligned} \tilde{\alpha}_{2m} &= (1/\rho^2) \int \frac{\alpha_m(\nu)}{\nu} d\nu \\ &= \frac{4\pi^3 e^2}{3hc} n_0^2 a_0^5 (a_0/\sigma)^5 \tilde{J}_2 X_{2m} \ , \end{aligned} \tag{6.4}$$

where

$$\begin{aligned} \tilde{J}_2 &= 12\pi \int_0^\infty x^{-8} g_0(x) x^2 dx \\ &= 12\pi J_8 \ , \end{aligned} \tag{6.5}$$

and J_8 is given by

$$J_8 = J_8^{cl} + (\Lambda^*)^2 J_8^{(1)} + (\Lambda^*)^4 J_8^{(2)} \,. \tag{6.6}$$

The collision-induced absorption intensities of the quadrupole-induced first overtone transitions of HD at 77 K were calculated using these formulas and the matrix elements of the quadrupole moment $<|\ Q\ |>$ and the polarizability $<|\ \alpha\ |>$ of the HD molecule available in the literature (Hunt et al., 1984). The calculated intensities are given in Table 6.2.

(c) Method of computation

The absorption profiles of the collision-induced first overtone band of HD at 77 K were analyzed using a computer program similar to the first program of Chapter 4 (see Appendix A). The Lorentzian lineshape function is used in this program. As mentioned earlier, the fitting of the synthetic profiles to the observed profiles was performed in the spectral region 7300–7800 cm^{-1} where the allowed first overtone P and R transitions of HD are not present and the contribution to the absorption intensity from the collision-induced first overtone transitions of H_2 (the impurity in the HD gas) is insignificant.

(d) Results of the profile analysis

When the calculated intensities of the HD first overtone band at 77 K in Table 6.2 were used in the above mentioned computer program to fit the synthetic to the experimental profiles, the result was found to be rather poor. The problem lies in the fact that the calculated intensities of the transitions involving $\Delta v = 2$ were consistently too high relative to the other transitions. Van Nostrand (1983) and Gillard (1983) encountered the same problems in the collision-induced first overtone bands of H_2 ar ' D_2, respectively (see also McKellar, 1988). Van Nostrand and

Table 6.2: Absorption intensities of the first overtone transitions of HD at 77 K.

Transition	Wavenumber (cm^{-1})	$\bar{\alpha}$ (cm^{-1})
$Q_2(0) + Q_0(1)$	7086.9	0.2396e-10
$Q_2(0) + Q_0(2)$	7086.9	0.0104e-10
$Q_2(1) + Q_0(0)$	7079.2	0.7459e-10
$Q_2(1) + Q_0(1)$	7079.2	0.5638e-10
$Q_2(1) + Q_0(2)$	7079.2	0.0316e-10
$Q_2(2) + Q_0(0)$	7064.0	0.0323e-10
$Q_2(2) + Q_0(1)$	7064.0	0.0268e-10
$Q_2(2) + Q_0(2)$	7064.0	0.0015e-10
$Q_2(0) + S_0(0)$	7354.0	1.0594e-10
$Q_2(0) + S_0(1)$	7530.0	0.3623e-10
$Q_2(0) + S_0(2)$	7703.0	0.0188e-10
$Q_2(1) + S_0(0)$	7346.3	0.6205e-10
$Q_2(1) + S_0(1)$	7522.3	0.2123e-10
$Q_2(1) + S_0(2)$	7695.3	0.0110e-10
$Q_2(2) + S_0(0)$	7331.1	0.0373e-10
$Q_2(2) + S_0(1)$	7507.1	0.0128e-10
$Q_2(2) + S_0(2)$	7680.1	0.0007e-10
$S_2(0) + Q_0(0)$	7331.1	3.5338e-10
$S_2(0) + Q_0(1)$	7331.1	2.0232e-10
$S_2(0) + Q_0(2)$	7331.1	0.1219e-10
$S_2(1) + Q_0(0)$	7484.3	1.2418e-10
$S_2(1) + Q_0(1)$	7484.3	0.7107e-10
$S_2(1) + Q_0(2)$	7484.3	0.0428e-10
$S_2(2) + Q_0(0)$	7627.2	0.0653e-10
$S_2(2) + Q_0(1)$	7627.2	0.0374e-10
$S_2(2) + Q_0(2)$	7627.2	0.0023e-10
$S_2(0) + S_0(0)$	7598.1	0.0747e-10
$S_2(0) + S_0(1)$	7774.2	0.0257e-10
$S_2(0) + S_0(2)$	7947.2	0.0014e-10
$S_2(1) + S_0(0)$	7751.4	0.0250e-10

Table 6.2 (Continued)

Transition	Wavenumber (cm^{-1})	$\tilde{\alpha}$ (cm^{-1})
$S_2(1) + S_0(1)$	7927.4	0.0086e-10
$S_2(2) + S_0(0)$	7894.2	0.0013e-10
$O_2(2) + Q_0(0)$	6819.8	0.0202e-10
$O_2(2) + Q_0(1)$	6819.8	0.0116e-10
$O_2(2) + Q_0(2)$	6819.8	0.0007e-10
$O_2(2) + S_0(0)$	7086.9	0.0006e-10
$O_2(2) + S_0(1)$	7262.9	0.0002e-10
$Q_1(0) + Q_1(1)$	7260.5	0.8826e-10
$Q_1(0) + Q_1(2)$	7252.8	0.0380e-10
$Q_1(1) + Q_1(1)$	7256.6	0.5127e-10
$Q_1(1) + Q_1(2)$	7248.9	0.0528e-10
$Q_1(2) + Q_1(2)$	7241.2	0.0013e-10
$Q_1(0) + S_1(0)$	7519.8	3.1988e-10
$Q_1(0) + S_1(1)$	7684.3	0.9443e-10
$Q_1(0) + S_1(2)$	7842.1	0.0419e-10
$Q_1(1) + S_1(0)$	7516.0	1.9054e-10
$Q_1(1) + S_1(1)$	7680.5	0.5635e-10
$Q_1(1) + S_1(2)$	7838.3	0.0250e-10
$Q_1(2) + S_1(0)$	7508.3	0.1134e-10
$Q_1(2) + S_1(1)$	7672.8	0.0335e-10
$Q_1(2) + S_1(2)$	7830.6	0.0015e-10
$Q_1(0) + O_1(2)$	6997.2	0.0318e-10
$Q_1(1) + O_1(2)$	6993.4	0.0189e-10
$Q_1(2) + O_1(2)$	6985.7	0.0011e-10
$S_1(0) + S_1(0)$	7775.4	0.1701e-10
$S_1(0) + S_1(1)$	7939.9	0.1039e-10
$S_1(0) + S_1(2)$	8097.6	0.0048e-10
$S_1(1) + S_1(1)$	8104.4	0.0158e-10
$S_1(0) + O_1(2)$	7252.8	0.0033e-10
$S_1(1) + O_1(2)$	7417.3	0.0010e-10

Gillard used an improvement factor of 0.68 to reduce all the matrix elements of the quadrupole moment of H_2 and D_2 involving $\Delta v = 2$ transitions and found that the reduced intensities led to very good agreement between the synthetic and the observed profiles.

Guided by this idea of improvement factor, the profile analysis was carried out with different improvement factors but found that a value of 0.68 for this factor gave the best fit between the synthetic and the observed profiles. An example of the profile analysis of the first overtone band of HD for a density of 311 amagat at 77 K , with an improvement factor of 0.68 for the reduction of the quadrupole matrix elements of HD for Δv=2 transitions is shown in Fig. 6.5. The large discrepancy between the synthetic and the experimental profiles near 7800 cm^{-1} is due to the transitions $Q_1(J)(HD) + Q_1(J)(H_2)$ resulting from the presence of the H_2 gas as the impurity in the HD gas. Within the density range 130–320 amagat in the present experiments for the collision-induced first overtone band of HD, the half-width δ_q obtained from the profile analysis has a value of 45±2 cm^{-1}, and no pressure narrowing has been detected. The value of the δ_q of the HD molecule falls between those of H_2 (49±2 cm^{-1}, Van Nostrand, 1983) and D_2 (39±3 cm^{-1}, Gillard, 1983). This is what one would expect since the half-width $\delta_q = 1/2\pi c\tau_q$, where τ_q is the collision duration which is smaller for the lighter H_2 molecules. The value of δ_q for the induced transitions of HD falls between those of H_2 and D_2 at the same temperature, as expected.

For each of the analyzed experimental absorption profiles the area under the synthetic profile was calculated to obtain the integrated absorption coefficient $\int \alpha(\nu)d\nu$ (see Eq. (4.12)). Values of $(1/\rho^2)\int \alpha(\nu)d\nu$ against ρ were plotted in Fig. 6.6.

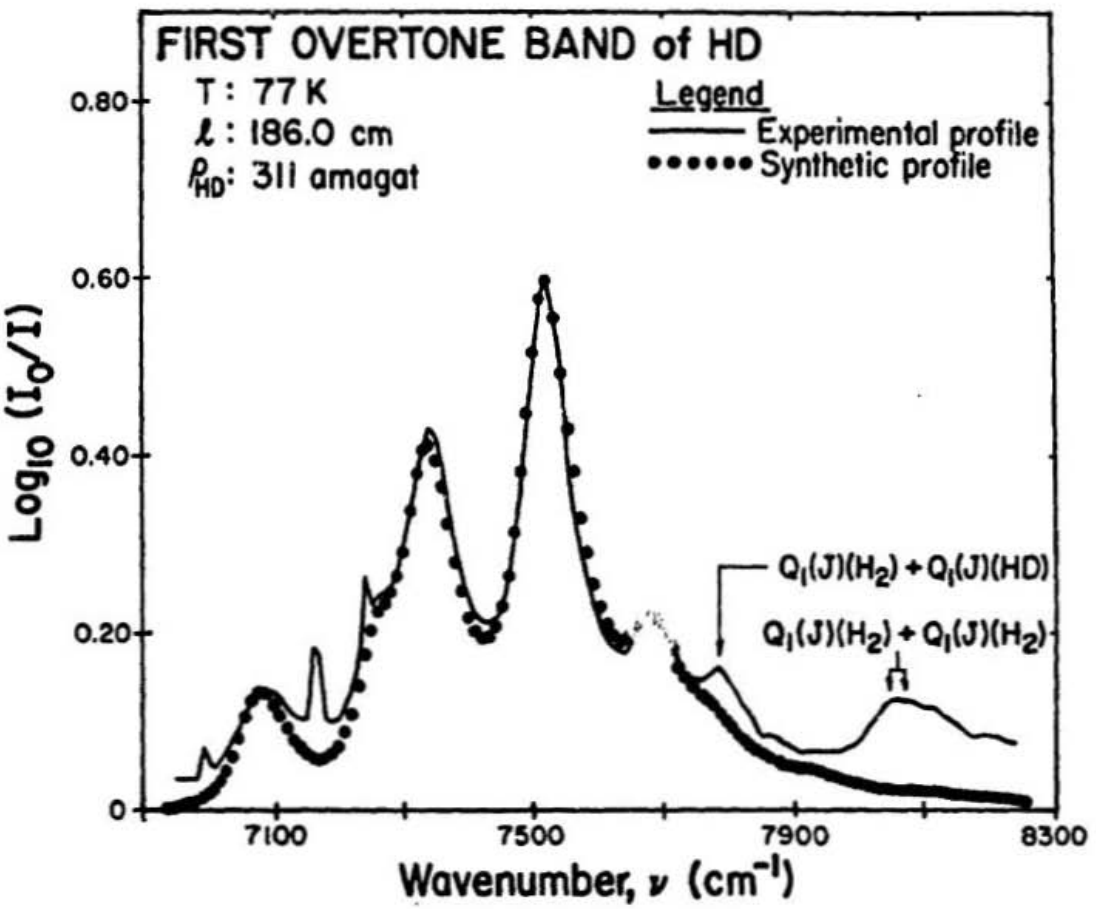

Figure 6.5: Analysis of an absorption profile of HD at a gas density of 311 amagat at 77 K.

Table 6.3: Absorption coefficients* of H_2, HD, and D_2 in the first overtone region at 77 K.

Gas	Binary absorption coefficient α_1 ($10^{-5} cm^{-2} amagat^{-2}$)	Ternary absorption coefficient α_2 ($10^{-9} cm^{-2} amagat^{-3}$)	Reference
H_2	4.31 ±0.09	-0.3±0.3	Van Nostrand (1983)
HD	2.73 ±0.07	-9.0±3.0	Present work
D_2	1.51 ±0.05	0.5±2.0	Gillard (1983)

* The errors quoted are standard errors.

The binary and ternary absorption coefficients α_1 and α_2 were determined from the ordinate-intercept and the slope of the graph, respectively (see Eq. (4.14)). The results are presented in Table 6.3 and compared with those of H_2 and D_2. As can be seen clearly from this table, the values of α_1 and α_2 for HD fall between corresponding values of H_2 and D_2.

(e) Discussion

An improvement factor of 0.68 applied to reduce the values of the matrix elements of the quadrupole moment of HD for all transitions involving $\Delta v = 2$ would make the synthetic profile to agree well with the experimental profile. Theoretically this is not allowed since the theoretically calculated matrix elements of the quadrupole moment of the H_2, HD, and D_2 molecules are considered to be quite accurate. To understand this puzzle, one should examine the B matrix elements given in Chapter 3. The square of the term $B_{32}(R)/ea_0$ represents the intensity contribution to the O, Q, and S branches of the collision-induced absorption band arising from the $\mathcal{L}$=3 anisotropic overlap induction term and the quadrupolar induction term. This is

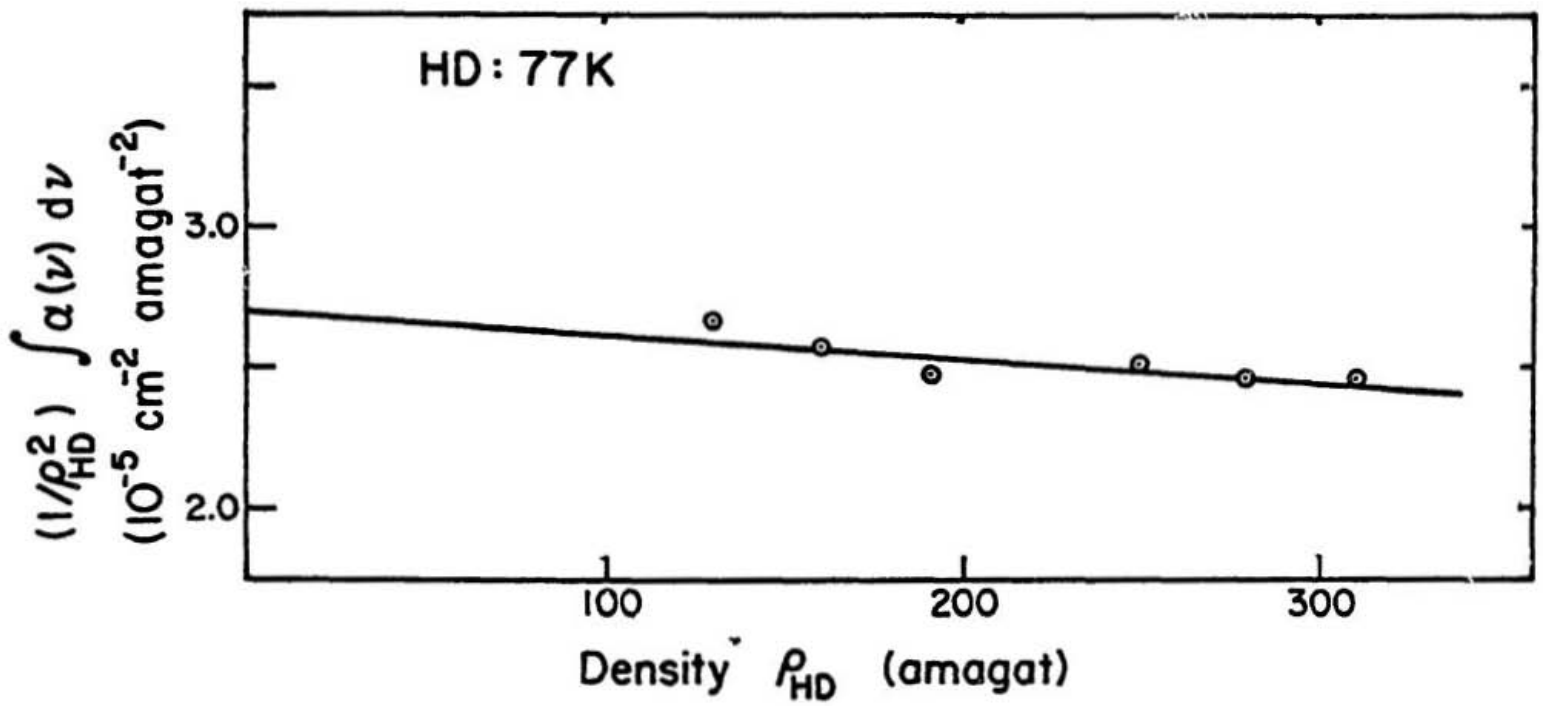

Figure 6.6: A plot of $(1/\rho_{HD}^2) \int \alpha(\nu) d\nu$ versus ρ_{HD} for the profiles of HD at 77 K for the collision-induced first overtone transitions of HD.

given by Eq. (3.23),

$$
\begin{aligned}
B_{12}(R)/ea_0{}^2 \;=\; & \lambda_{12}^2 exp[-2(R-\sigma)/\rho_{12}] \\
& +3 < vJ \;\; \alpha \;\; v'J' >^2 < vJ \mid Q \mid v'J' >^2 (R/a_0)^{-8} \\
& +2\sqrt{3}\lambda_{32} exp[-(R-\sigma)/\rho_{32}] \\
& \times < vJ \mid \alpha \mid v'J' >< vJ \mid Q \mid v'J' > (R/a_0)^{-4} . \qquad (6.7)
\end{aligned}
$$

The first term of this equation is very small; the second term is the major term for the intensity; and the third term is a mixed term which contributes negatively to the intensity of the transitions involving $\Delta v = 2$. Thus the apparent reduction of the matrix elements of the quadrupole moment involving transitions with $\Delta v = 2$ by a factor of 0.68 accounts for the *negative* contribution to the intensity of the band due to the mixed term $2\sqrt{3}\lambda_{32} exp[-(R-\sigma)/\rho_{32}] \times < vJ \mid \alpha \mid v'J' >< vJ \mid Q \mid v'J' > (R/a_0)^{-4}$. Recently Xiang (1992) also found the same effect in the collision-induced second overtone band ($\Delta v = 3$) of H_2, investigated at 77, 201, and 298 K.

Chapter 7

Collision-Induced Absorption of the Fundamental Band of HD in the Pure Gas at 77 K

7.1 Introduction

Homonuclear diatomic molecules such as H_2 and D_2 only possess 2^L-multipoles with L = *evennumber*, i.e., quadrupole (2^2-pole), hexadecapole (2^4-pole), etc. On the contrary, heteronuclear diatomic molecules such as HD possess 2^L-multipoles without any restrictions to the L. Thus HD possesses dipole (2^1), quadrupole (2^2), octopole (2^3), hexadecapole (2^4), 32-pole (2^5), etc. Because of the existing of the odd L multipoles in the HD, one expects its collision-induced absorption spectrum to contain T transitions ($\Delta J = 3$) and V transitions ($\Delta J = 5$) induced by the octopole ($L = 3$) and the 32-pole ($L = 5$) in addition to the usual U transitions ($\Delta J = 4$) induced by the hexadecapole ($L = 4$) in H_2 and D_2.

Spectra of collision-induced fundamental band of HD in the pure gas at moderate densities at three different temperatures have been studied by Reddy and Prasad (1977). Absorption profiles of the fundamental band of HD in the pure

gas at three different densities at 77 K are reproduced in Fig. 7.1. For these moderate densities of pure HD, the transitions in the fundamental band include the allowed transitions $R_1(0)$ and $R_1(1)$ and the collision-induced single and double transitions $Q_1(J), S_1(1), Q_1(J) + Q_0(J)$, and $Q_1(J) + S_0(1)$. Collision-induced $T(\Delta J = 3), U(\Delta J = 4)$, and $V(\Delta J = 5)$ transitions were not present in these absorption profiles because the gas densities were not high enough.

The present work was an attempt to obtain the T, U, and V transitions in the collision-induced fundamental band of HD in the pure gas at high gas densities.

7.2 Absorption Profiles

Collision-induced absorption spectra of the fundamental band of HD in the pure gas at 77 K were obtained using the apparatus and experimental technique described in Chapter 2. The gas densities are in the range 40–310 amagat. Three representative absorption profiles at densities 120, 160, and 200 amagat are shown in Fig. 7.2. Collision-induced T, U, and V transitions occur on the high wavenumber tail of the main fundamental band of HD which approaches infinite absorption because of the high gas densities. The measured wavenumbers of the absorption peaks of the collision-induced T, U, and V transitions are presented in Table 7.1.

The strong peak at ~4720 cm^{-1} is due to the collision-induced $S_1(1)$ and $Q_1(1) + S_0(1)$ transitions of H_2 which is present in the HD gas as an impurity. The collision-induced $U_1(1)$ transition of HD at 4803.0 cm^{-1} is completely masked by this strong peak of H_2 and can not be observed. The collision-induced double transitions of HD $Q_1(1) + U_0(1)$ at 4856.4 cm^{-1} and $Q_1(0) + U_0(1)$ at 4860.2 cm^{-1} are also difficult to observe due to their low intensity and closeness to this strong peak of H_2.

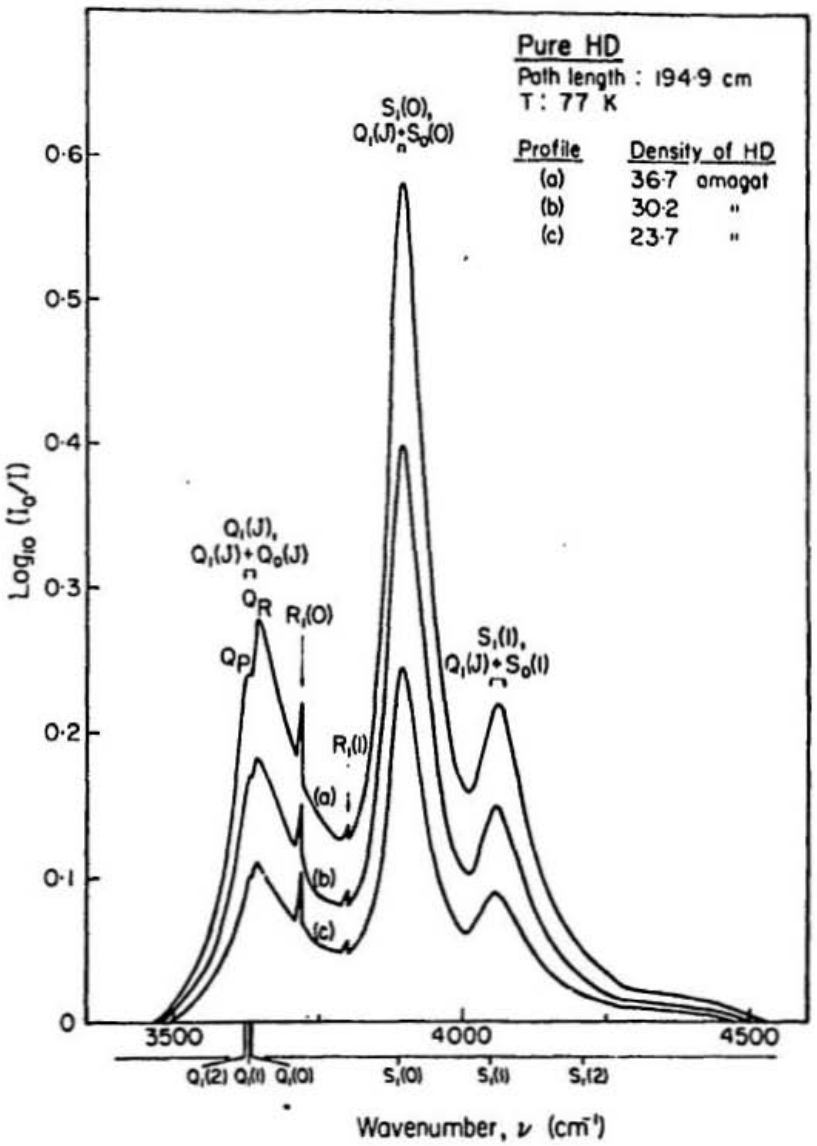

Figure 7.1: Absorption profiles of the fundamental band of HD in the pure gas at three different low densities at 77 K (adopted from Reddy and Prasad, 1977).

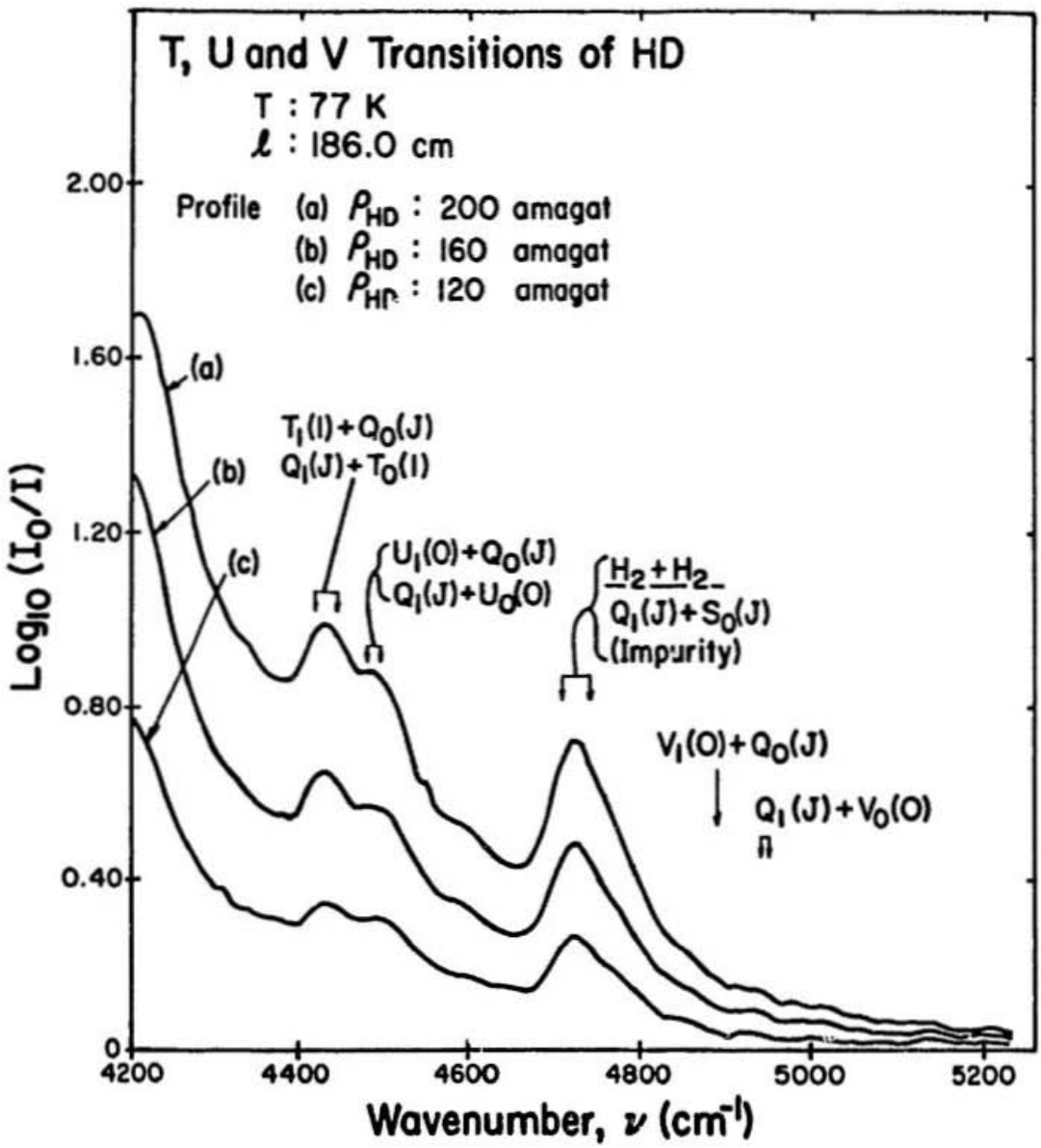

Figure 7.2: Absorption profiles of the fundamental band of HD in the pure gas at three different high densities at 77 K.

Table 7.1: Assignments of the observed absorption peaks of the T, U, and V transitions of the fundamental band of HD.

Transition	Calculated wavenumber (cm^{-1})	Measured wavenumber (cm^{-1})
$T_1(1) + Q_0(0)$	4387.8	
$T_1(1) + Q_0(1)$	4387.8	
$Q_1(1) + T_0(1)$	4422.2	
$Q_1(0) + T_0(1)$	4426.1	4428
$U_1(0) + Q_0(0)$	4477.0	
$U_1(0) + Q_0(1)$	4477.0	4493
$Q_1(1) + U_0(0)$	4511.5	
$Q_1(0) + U_0(0)$	4515.3	
$V_1(0) + Q_0(0)$	4892.2	
$V_1(0) + Q_0(1)$	4892.2	
$Q_1(1) + V_0(0)$	4945.6	4941
$Q_1(0) + V_0(0)$	4949.5	

Chapter 8

Conclusion

An experimental investigation of the collision-induced absorption spectra of binary mixtures of H_2 with D_2 and Ar and of pure HD was carried out using a 2 m absorption cell at 77, 201, and 296 K for total gas densities up to 550 amagat.

Using binary mixtures of normal H_2 with normal D_2 of equal partial densities, collision-induced absorption spectra of the double fundamental transitions of $H_2(v = 1 \leftarrow 0)+D_2(v = 1 \leftarrow 0)$ have been observed at 77 and 201 K in the spectral region 7000-8000 cm^{-1}. Double transitions of the type $Q_1(J)(H_2) + Q_1(J)(D_2)$, $Q_1(J)(H_2) + S_1(J)(D_2)$, $S_1(J)(H_2) + Q_1(D_2)$, and $S_1(J)(H_2) + S_1(J)(D_2)$ have been identified. The expeimental absorption profiles have been analyzed using the Lorentzian and the Birnbaum-Cohen lineshape functions in two separate computer programs. It was found that the half-width δ_q decreases with the total gas densities greater than 350 amagat (the pressure narrowing effect). The wavenumber shift $\delta\nu$ was found to increase linearly with the total gas density. The binary and ternary absorption coefficients for the double vibrational band of $H_2 + D_2$ have been determined.

Hexadecapole-induced U transitions of the type $U_1(1), U_1(2), Q_1(0) + U_0(1)$, and

$Q_1(1) + U_0(1)$ have been observed in the CIA enhancement spectra of the fundamental band of H_2 in $H_2 - Ar$ mixtures at room temperature for a base density of 72 amagat of H_2 and several partial densities of Ar up to 440 amagat. To explain the occurrence of the double transitions $Q_1(0) + U_0(1)$ and $Q_1(1) + U_0(1)$ in the enhancement spectra, a *cage* model has been proposed. The experimental binary absorption coefficient of the enhancement $U_1(1)$ transition obtained from the profile analysis was found to be in good agreement with the theoretical value.

The CIA spectra of the first overtone band of HD in the pure gas were observed at 77 K for gas densities up to 320 amagat. Both allowed transitions $P_2(1)$, $R_2(0)$, and $R_2(1)$ and collision-induced transitions $Q_2(J)+Q_0(J)$, $Q_1(J)+Q_1(J)$, $Q_2(J)+S_0(J)$, $S_2(J)+Q_0(J)$, $Q_1(J)+S_1(J)$, $S_2(J)+S_0(J)$, and $S_1(J)+S_1(J)$ have been observed. From the analysis of the experimental profiles, it was found that the isotropic overlap induction mechanism does not contribute to the intensity of the band; in the analysis, the matrix elements of the quadrupole moment for the $\Delta v = 2$ transitions were reduced by an improvement factor of 0.68 to obtain a satisfactory fit. The necessity for this reduction is interpreted as due to a *negative* contribution to the intensity of the band from a mixed term in the expansion of the square of the term $B_{32}(R)/ea_0$.

The CIA spectrum of the fundamental band of HD in the pure gas was observed at 77 K for gas densities up to 310 amagat. For the first time the collision-induced transitions of HD of the type $T_1(1) + Q_0(J), Q_1(J) + T_0(1), U_1(0) + Q_0(J), Q_1(J) + U_0(0), V_1(0) + Q_0(J)$, and $Q_1(J) + V_0(0)$ have been identified.

Appendices

Appendix A

Fortran Program for Profile Analysis: Modified Lorentzian Lineshape

```
c       non-linear least squares fit to experimental profile of a
c       synthetic quadrupolar spectrum
c       using modified Lorentzian lineshape
c
        implicit real*8 (a-h,o-z)
        real *8 a,af,afqt,r
        common sq(250),sqf(250),a(10),
     1 afq(250),nlq,r,afqt,
     2 i1,i2,i3,i4
        real*8 x(2000),y(2000),dvp(10),dvn(10),vsep(10),vsen(10)
        character*20 calfil,obsfil
```

```
      character*60 head
   15 format (a20)
c
c     read relative intensities (sq) and frequencies (sqf)
c     of quad. lines
c
      write (0,*) 'enter filename for calculated data'
      read (5,15) calfil
      open (unit = 8,file = calfil,status = 'old')
      rewind (8)
      write (0,*) 'enter filename for observed data'
      read (5,15,end = 990) obsfil
      if ((obsfil .eq. 'none') .or. (obsfil .eq. 'q')) go to 990
      open (unit = 9,file = obsfil,status = 'old')
      rewind (9)
   51 format (a60)
   55 format (15x,f7.2,7x,e10.4)
      do 56 i = 1 , 6
      read (8,51) head
   56 continue
   59 format(8x,f9.4,7x,e10.4)
c
      t=77.
c
```

```
      r=1.438832042D0/t
c
      write (0,*) 'enter no. of lines'
      read *,nlq
      do 70 i = 1 , nlq
            read (8,*) sqf(i),sq(i)
   70 continue
c
  100 continue
c
      np = 0
c
c     the following assumes a(10) = 0.0
      i1 = 10
      i2 = 10
      i3 = 10
      i4 = 10
c
      write (0,*) 'q d2 ?'
      read *, xx
            np = np + 1
            i1 = np
            a(i1) = xx
c
```

```
      write (0,*) 'q d4 ?'
      read *, xx
          if (xx .ne. 0.0) then
            np = np + 1
            i2 = np
            a(i2) = xx
           end if
c
      write (0,*) 'q  int. ?'
      read *, xx
            np = np + 1
            i3 = np
            a(i3) = xx
c
      write (0,*) 'q shift ?'
      read *, xx
          if (xx .ne. 0.0) then
                np = np + 1
                i4 = np
                a(i4) = xx
          end if
c
      do 130 i = np + 1 , 10
           a(i) = 0.0
```

```
  130  continue
c
c
    2  continue
  101  format (14x,i4)
       write (0,*) 'enter no. of points'
       read *,n
       do 110 i=1,5
       read (9,51) head
  110  continue
       do 111 i = 1 , n
       read (9,*) iseq,x(i),y(i)
  111  continue
c
                vse = 0.
              do 200 i=1,n
                 xi=x(i)
                 call cal(xi,af)
            vse = vse + (y(i) - af*x(i))**2
  200  continue
          aerr = vse/(n - np)
          aerr = sqrt(aerr)
       write (0,134) (a(i),i=1,np)
       write (0,141) aerr
```

```
  134  format (1h ,2x,10g12.5)
  141  format (' standard error = ',e14.7/)
c
c
       vsem = vse
       write (0,*) 'h=?'
       read *,h
  121  h= 0.8*h
       if (h .ge. 0.00001) then
          go to 122
       else
          go to 990
       end if
  122  continue
       do 205 j = 1,np
           a(j) = a(j)*(1+h)
                vse = 0.
              do 201 i=1,n
                 xi=x(i)
                 call cal(xi,af)
             vse = vse + (y(i) - af*x(i))**2
  201  continue
          dvp(j) = vse - vsem
          a(j) = a(j)/(1+h)
```

```
        vsep(j) = vse
205  continue
      dvpm = dvp(1)
     ip = 1
     do 206 k = 2,np
               if ( dvp(k) .lt. dvpm ) then
             dvpm = dvp(k)
             ip = k
        end if
206  continue
     do 207 j = 1,np
         a(j) = a(j)*(1-h)
               vse = 0.
            do 208 i=1,n
              xi=x(i)
               call cal(xi,af)
          vse = vse + (y(i) - af*x(i))**2
208  continue
        dvn(j) = vse - vsem
        a(j) = a(j)/(1-h)
        vsen(j) = vse
207  continue
      dvnm = dvn(1)
     in = 1
```

```
      do 209 k = 2,np
                if ( dvn(k) .lt. dvnm ) then
               dvnm = dvn(k)
               in = k
           end if
209   continue
      if ( dvpm .le. dvnm ) then
           if ( dvpm .lt. 0. ) then
                a(ip) = a(ip)*(1+h)
                write(0,134) (a(i),i=1,np)
                aerr = vsep(ip)/(n-np)
                aerr = sqrt(aerr)
                write (0,141) aerr
               vsem = vsep(ip)
                go to 122
           else
               go to 121
           end if
      else
          if ( dvnm .lt. 0. ) then
                a(in) = a(in)*(1-h)
                write (0,134) (a(i),i=1,np)
                aerr = vsen(in)/(n-np)
                aerr = sqrt(aerr)
```

```
                write (0,141) aerr
               vsem = vsen(in)
                go to 122
           else
               go to 121
           end if
      end if
  990 stop
      end
c
c
      subroutine cal(xi,af)
      implicit real*8 (a-h,o-z)
      double precision a,xt,af,afqt,r
      common sq(250),sqf(250),a(10),
     1 afq(250),nlq,r,afqt,
     2 i1,i2,i3,i4
c
c     quadrupolar contribution
c
  850 afqt=0.d0
  851      do 220 j=1,nlq
               xt=xi-sqf(j) + a(i4)
            rn = a(i3) * sq(j) * quad(xt,r,a(i1),a(i2))
```

```
            afq(j)=rn
            afqt=afqt+rn
  220   continue
        af=afqt
 1000   return
        end
c
        real*8 function quad(dv,r,a1,a2)
        implicit real*8 (a-h,o-z)
        if (a2 .ne. 0.0) then
                rn=1.0/(1.+(dv/a1)**2+(dv/a2)**4)
        else
               rn=1.0/(1.+(dv/a1)**2)
        end if
        quad = rn/(1.+dexp(-r*dv))
        return
        end
```

Appendix B

Fortran Program for Profile Analysis: Birnbaum-Cohen Lineshape

```
c       non-linear least squares fit to experimental profile of a
c       synthetic quadrupolar spectrum
c       using Birnbaum-Cohen lineshape
c
        implicit real*8 (a-h,o-z)
        real *8 a,af,afqt
        common sq(250),sqf(250),a(10),afq(250),nlq,afqt,i1,i2,i3,i4
        real*8 x(2000),y(2000),dvp(10),dvn(10),vsep(10),vsen(10)
        character*20 calfil,obsfil
        character*60 head
c
```

```
c       pi=3.14159
c
c       pi/2=1.5708
c
c       c=2.99792*10**10 cm/sec
c
c       k=1.38054*10**-16 erg/K
c
c       h=6.6256*10-27 erg*sec
c
c       r=1.438832042D0/T
c
c       con=1/(2*pi**2*c)
c
c       d0=2kT/ch
c
c       T=77.
c
c       con=1.68986e-12
c
c       d0=107.035
c
   15   format (a20)
        write (0,*) 'enter filename for calculated data'
```

```
      read (5,15) calfil
      open (unit = 8,file = calfil,status = 'old')
      rewind (8)
      write (0,*) 'enter nlq'
      read *, nlq
      write (0,*) 'enter filename for observed data'
      read (5,15,end = 990) obsfil
      if ((obsfil .eq. 'none') .or. (obsfil .eq. 'q')) go to 990
      open (unit = 9,file = obsfil,status = 'old')
      rewind (9)
      write (0,*) 'enter n'
      read *, n
   51 format (a60)
   55 format (15x,f7.2,7x,e10.4)
      do 56 i = 1 , 5
            read (8,51) head
   56 continue
   59 format(8x,f9.4,7x,e10.4)
      t=77.
      r=1.438832042D0/t
      do 70 i = 1 , nlq
      read (8,*) sqf(i),sq(i)
   70 continue
c
```

```
  100  continue
c
       np = 0
c
c      the following assumes a(10) = 0.0
       i1 = 10
       i2 = 10
       i3 = 10
       i4 = 10
c
       write (0,*) 'h=? '
       read *,h
c
       write (0,*) 'q d2 ?'
       read *, xx
              np = np + 1
              i1 = np
              a(i1) = xx
c
       write (0,*) 'q d4 ?'
       read *, xx
           if (xx .ne. 0.0) then
              np = np + 1
              i2 = np
```

```
            a(i2) = xx
          end if
c
      write (0,*) 'q  int. ?'
      read *, xx
            np = np + 1
            i3 = np
            a(i3) = xx
c
      write (0,*) 'q shift ?'
      read *, xx
          if (xx .ne. 0.0) then
                np = np + 1
                i4 = np
                a(i4) = xx
          end if
c
      do 130 i = np + 1 , 10
            a(i) = 0.0
  130 continue
c
c
    2 continue
      do 110 i=1,5
```

```
            read (9,51) head
  110  continue
       do 111 i = 1 , n
            read (9,*) iseq,x(i),y(i)
  111  continue
c
               vse = 0.
             do 200 i=1,n
               xi=x(i)
               call cal(xi,af)
           vse = vse + (y(i) - af*x(i))**2
  200  continue
         aerr = vse/(n - np)
         aerr = sqrt(aerr)
       write (0,134) (a(i),i=1,np)
       write (0,141) aerr
  134  format (1h ,2x,10g12.5)
  141  format (' standard error = ',e14.7/)
c
c
       vsem = vse
  121  h= 0.8*h
       if (h .ge. 0.00001) then
         go to 122
```

```
      else
         go to 990
      end if
122   continue
      do 205 j = 1,np
          a(j) = a(j)*(1+h)
               vse = 0.
             do 201 i=1,n
                xi=x(i)
                call cal(xi,af)
           vse = vse + (y(i) - af*x(i))**2
201   continue
         dvp(j) = vse - vsem
         a(j) = a(j)/(1+h)
         vsep(j) = vse
205   continue
      dvpm = dvp(1)
      ip = 1
      do 206 k = 2,np
                if ( dvp(k) .lt. dvpm ) then
             dvpm = dvp(k)
             ip = k
         end if
206   continue
```

```
      do 207 j = 1,np
          a(j) = a(j)*(1-h)
                vse = 0.
              do 208 i=1,n
                 xi=x(i)
                 call cal(xi,af)
            vse = vse + (y(i) - af*x(i))**2
208   continue
         dvn(j) = vse - vsem
         a(j) = a(j)/(1-h)
         vsen(j) = vse
207   continue
      dvnm = dvn(1)
      in = 1
      do 209 k = 2,np
                if ( dvn(k) .lt. dvnm ) then
              dvnm = dvn(k)
              in = k
         end if
209   continue
      if ( dvpm .le. dvnm ) then
           if ( dvpm .lt. 0. ) then
                 a(ip) = a(ip)*(1+h)
                 write(0,134) (a(i),i=1,np)
```

```
                aerr = vsep(ip)/(n-np)
                aerr = sqrt(aerr)
                write (0,141) aerr
               vsem = vsep(ip)
                go to 122
           else
               go to 121
           end if
       else
           if ( dvnm .lt. 0. ) then
                a(in) = a(in)*(1-h)
                write (0,134) (a(i),i=1,np)
                aerr = vsen(in)/(n-np)
                aerr = sqrt(aerr)
                write (0,141) aerr
               vsem = vsen(in)
                go to 122
           else
               go to 121
           end if
       end if
 990   stop
       end
c
```

```
c
      subroutine cal(xi,af)
      implicit real*8 (a-h,o-z)
      double precision a,xt,af,afqt
      common sq(250),sqf(250),a(10),afq(250),nlq,afqt,i1,i2,i3,i4
c
c     quadrupolar contribution
c
  850 afqt=0.d0
  851      do 220 j=1,nlq
                xt=xi-sqf(j) + a(i4)
           rn = a(i3) * sq(j) * quad(xt,a(i1),a(i2))
            afq(j)=rn
           afqt=afqt+rn
  220 continue
      af=afqt
 1000 return
      end
c
      real*8 function quad(dv,a1,a2)
      implicit real*8 (a-h,o-z)
      za=1.+(dv/a1)**2
      zb=(a1/a2)**2+(a1/107.035)**2
      z=sqrt(za*zb)
```

```
      ra=1.68986d-12/a1/za
      rb=dexp(a1/a2+dv/107.035)
      quad = ra*rb*xK1(z)
      return
      end
c
      real*8 function xK1(x)
      implicit real*8 (a-h,o-z)
      real*8 I1,K1
      if (x .le. 2) then
      t = (x / 3.75)**2
      I1 = 0.5 + t * (0.87890594+t * (0.51498869 + t * (0.15084934
     1 + t * (0.02658733 + t * (0.00301532 + t * (0.00032411 ))))))
      I1 = I1 * x
      t = x*x / 4.0
      K1 = x * dlog(x/2.0) * I1 + 1.0
      xK1 = K1 + t * (0.15443144 + t * ( -.67278579 + t * (-.18156897
     1 + t * (-.01919402 + t * ( -.00110404 + t * (-.00004686 ))))))
      else
      t = (2.0 / x)
      K1 = 1.25331414 + t * ( .23498619 + t * ( -.03655620 + t *
     1 ( .01504268 + t * ( -.00780353 + t * (.00325614 + t *
     2 ( -.00068245 ))))))
      xK1 = K1 *dsqrt(x) / dexp(x)
```

```
end if
return
end
```

References

- Babu, Y.S., M.Sc. Thesis, Memorial University of Newfoundland (1986).
- Bejar, J. and Gush, H.P., Can. J. Phys. **52**, 1669 (1974).
- Birnbaum, G. and Cohen, E.R., Can. J. Phys. **54**, 593 (1976).
- Birnbaum, G., Guillot, B., and Bratos, S., Adv. Chem. Phys. **51**, 49 (1982).
- Bragg, S.L., Brault, J.W. and Smith, W.H., Astrophys. J. **263**, 999 (1982).
- Chang, K.S., Ph.D. Thesis, Memorial University of Newfoundland (1974).
- Crane, A. and Gush, H.P., Can. J. Phys. **44**, 373 (1966).
- Crawford, M.F., Welsh, H.L., and Locke, J.L., Phys. Rev. **75**, 1607 (1949).
- de Boer, J., Repts. Prog. Phys. **12**, 305 (1949).
- De Remigis, J., Mactaggart, J.W. and Welsh, H.L., Can. J. Phys. **49**, 381 (1971).
- Durie, R.A. and Herzberg, G., Can. J. Phys. **38**, 806 (1960).
- Gibbs, P.W., Gray, C.G., Hunt, J.L., Reddy, S.P., Tipping, R.H. and Chang, K.S., Phys. Rev. Lett. **33**, 256 (1974).
- Gillard, P.G., Ph.D. Thesis, Memorial University of Newfoundland (1983).
- Gillard, P.G., Prasad, R.d.G. and Reddy, S.P., J. Chem. Phys. **81**, 3458 (1984).
- Hare, W.F.J. and Welsh, H.L., Can.J. Phys. **36**, 88 (1958).
- Herzberg, G., Nature **166**, 563 (1950).
- Holleman, G.W. and Ewing, G.E., J. Chem. Phys. **44**, 3121 (1966).
- Holleman, G.W. and Ewing, G.E., J. Chem. Phys. **47**, 571 (1967).
- Humphreys, C.J., J. Opt. Soc. Amer. **43**, 1027 (1953).
- Hunt, J.L., Poll, J.D. and Wolniewicz, L., Can. J. Phys. **62**, 1719 (1984).
- Hunt, J.L. and Poll, J.D., Mol. Phys. **59**, 163 (1986).
- Karl, G., Poll, J.D. and Wolniewicz, L., Van. J. Phys. **19**, 1781 (1975).

- Levine, H.B. and Birnbaum, G., Phys. Rev. **154**, 72 (1967).
- Lewis, J.C. and Van Kranendonk, J., Can. J. Phys. **50**, 352 (1972).
- Lewis, J.C. and Tjon, J.A., Physica A **91**, 161 (1978).
- Lewis, J.C., Phenomena Induced by Intermolecular Interactions, edited by G. Birnbaum, Plenum Publishing Corporation, New York (1985).
- Mactaggart, J.W., Ph.D. Thesis, University of Toronto (1971).
- Mactaggart, J.W. and Welsh, H.L., Can. J. Phys. **51**, 158 (1973).
- Mactaggart, J.W., De Remigis, J. and Welsh, H.L., Can. J. Phys. **51**, 1971 (1973).
- McCarty, R. D., Hord, J. and Roder, H.M., Natl. Bur. Standards Monograph 168 (1981).
- McKellar, A.R.W. and Welsh, H.L., Proc. Roy. Soc. London A **322**, 421 (1971).
- McKellar, A.R.W., Can. J. Phys. **51**, 389 (1973).
- McKellar, A.R.W., Can. J. Phys. **52**, 1144 (1974).
- McKellar, A.R.W. and Oka, T., Can. J. Phys. **56**, 1315 (1978).
- McKellar, A.R.W., Can. J. Phys. **66**, 155 (1988).
- McKellar, A.R.W., J. Chem. Phys. **92**, 3261 (1990).
- Meyer, W., Borysow, A. and Frommhold, L., Phys. Rev. A **40**, 6931 (1989).
- Michels, A., Wijker, H. and Wijker, H., Physica **15**, 627 (1949).
- Michels, A., Levelt, J.M. and De Graaff, W., Physica **24**, 659 (1958).
- Okumura, M., Chan, M. and Oka, T., Phys. Rev. Lett. **62**, 32 (1989).
- Penney, R.J., Prasad, R.D.G. and Reddy, S.P., J. Chem. Phys. **77**, 131 (1982).
- Plyler, E.K., Blaine, L.R. and Tidwell, E.D., J. Res. Natl. Bur. Standards **55**, 279 (1955).
- Poll, J.D. and Van Kranendonk, J., Can. J. Phys. **39**, 189 (1961).
- Poll, J.D., Proceedings I.A.U. Symposium 40 on Planetary Atmospheres (Reidel, Dordrecht), 384 (1971).

- Poll, J.D. and Hunt, J.L., Can. J. Phys. **54**, 461 (1976).
- Poll, J.D., Tipping, R.H., Prasad, R.D.G. and Reddy, S.P., Phys. Rev. Lett. **36**, 248 (1976).
- Poll, J.D., Proceedings of the International School of Physics Enrico Fermi, Course LXXV, Intermolecular Spectroscopy and Dynamical Properties of Dense Systems, edited by J. Van Kranendonk (North-Holland Publishing Company, New York) (1980).
- Prasad, R.D.G., Ph.D. Thesis, memorial University of Newfoundland (1976).
- Prasad, R.D.G., Clouter, M.J. and Reddy, S.P., Phys. Rev. **A 17**, 1690 (1978).
- Reddy, S.P. and Cho, C.W., Can. J. Phys. **43**, 2331 (1965).
- Reddy, S.P. and Kuo, C.Z., J. Mol. Spectrosc. **37**, 327 (1971).
- Reddy, S.P., Varghese, G. and Prasad, R.D.G., Phys. Rev. **A 15**, 975 (1977).
- Reddy, S.P. and Prasad, R.D.G., J. Chem. Phys. **66**, 5259 (1977).
- Reddy, S.P., Sen, A. and Prasad, R.D.G., J. Chem. Phys. **72**, 6102 (1980).
- Reddy, S.P., Phenomena Induced by Intermolecular Interactions, edited by G. Birnbaum (Plenum Publishing Corporation, New York) (1985).
- Rich, N.H. and McKellar, A.R.W., Can. J. Phys. **54**, 486 (1976).
- Rose, M.E., Elementary Theory of Angular Momentum, John Wiley & Sons, Inc., New York (1957).
- Silvaggio, P.M., Goorvitch, D. and Boese, R.W., J. Quant. Spectrosc. Radiat. Transfer. **26**, 103 (1981).
- Trefler, M. and Gush, H.P., Phys. Rev. Lett. **20**, 703 (1968).
- Van Kranendonk, J. and Bird, R.B., Physica **17**, 953 (1951a).
- Van Kranendonk, J. and bird, R.B., Physica **17**, 968 (1951b).
- Van Kranendonk, J., Physica **23**, 825 (1957).
- Van Kranendonk, J., Physica **24**, 347 (1958).
- Van Kranendonk, J., Physica **25**, 337 (1959).
- Van Kranendonk, J., Can. J. Phys. **46**, 1173 (1968).

- Van Kranendonk, J., Physica **73**, 156 (1974).
- van Nostrand, E., M.Sc. Thesis, Memorial University of Newfoundland (1983).
- Varghese, G., Prasad, R.D.G. and Reddy, S.P., Phys. Rev. **A 35**, 701 (1987).
- Watanabe, A., Can. J. Phys. **49**, 1320 (1971).
- Watanabe, A., Hunt, J.L. and Welsh, H.L., can J. Phys. **49**, 860 (1971).
- Welsh, H.L., Crawford, M.F., and Locke, J.L., Phys. Rev. **76**, 580 (1949).
- Welsh, H.L., Crawford, M.F., MacDonald, J.C.F. and Chishom, D.A., Phys. Rev. **83**, 1264 (1951).
- Welsh, H.L., MTP International Review of Science, Physical Chemistry, Vol. 3, Spectroscopy, edited by D.A. Ramsay (Butterworths, London) (1972).
- Wick, G.C., Atti. R. Acad. Naz. Lincei (Ser. 6) **21**, 708 (1935).
- Woolley, H.W., Scott, R.B. and Brickwedde, F.G., J. Res. Nat. Bur. Stand. **41**, 416 (1948).
- Xiang, F., M.Sc. Thesis, Memorial University of Newfoundland (1992).
- Zaidel, A.N., Prokofer, V.K., Raisku, S.M., Slavnyl, V.a. and Shreider, E.Ya., Tables of Spectral Lines (IFI/Plenum, New York-London) (1970).
- Zaidi, H.R. and Van Kranendonk, J., Can. J. Phys. **49**, 385 (1971).